SAINT-PETERSBURG UNIVERSITY

Manuscript

Alina Malysheva

MESOSCALE VORTEX DYNAMICS OF THE SOUTH ATLANTIC OCEAN BASED ON ALTIMETRY, IN SITU AND MODEL DATA

Scientific specialty 1.6.17. Oceanology

DISSERTATION

Dissertation is submitted for the degree of the candidate of geographical sciences

Translation from Russian

Supervisor:

D.Sc. in Geographical Sciences,

Belonenko T.V.

Saint Petersburg

2024

TABLE OF CONTENTS

INTRODUCTION

The relevance of the research topic

Ocean eddies have been known for a long time, but due to the development of measurement technologies, direct and indirect measurement of eddies only began in the 20th century. Vortices with horizontal dimensions of tens to hundreds of kilometers are of great interest. This type of vortices is called synoptic vortices. In other literature such vortices are also called mesoscale vortices (Zhmur, 2011).

"Synoptic eddies of the open ocean, discovered in the Soviet experiments "Poligon-67" (by mapping by calculation of currents using the dynamic method from two months of hydrological measurements in the Arabian Sea) and "Poligon-70" (by direct measurement of currents for 6 months at a network of 17 buoy stations in the northern tropics of the Atlantic) and studied in the experiments MODE (1973), POLYMODE (1977-78) and MEGAPOLIGON (1986), are eddy currents with typical horizontal dimensions (distance from the center to the zone of maximum velocities) on the order of 100 km, rotational velocities in the upper ocean of 20 - 80 cm/s, and velocities of their centers of 1 - 10 cm/s. Sometimes they can be detected on the ocean surface by the temperature front at their periphery: in intense eddies, the temperature difference in the frontal zone is 0.5 - 2.0°C with its width of 2 - 30 km" (Kamenkovich et al., 1982).

The monograph by Monin and Krasitsky (1985) gave a very precise and detailed description of what should be understood by the concept of ***synoptic eddies***: "...baroclinic quasigeostrophic eddies or Rossby waves in the ocean with horizontal scales of the order of the Rossby strain radius, formed apparently mainly due to baroclinic instability of large-scale currents and producing a maximum of the kinetic energy spectrum, in full analogy with the atmosphere...".

Fedorov in his article (Fedorov, 1986) also described a separate type of vortices - intrathermocline vortices: "An intrathermocline vortex is a limited volume of water rotating in the anticyclonic or cyclonic direction with a thickness of several hundred meters and a diameter of several tens of kilometers, the maximum azimuthal velocity of which is located in a thermocline (pycnocline) at the level of the core containing a local anomaly of the potential vortex. Orbital (azimuthal) velocities and anomalous dynamic and hydrophysical characteristics decrease from the vortex core in all directions, while they can remain

practically unchanged in time at horizontal movement of the vortex with the core for long distances exceeding many thousands of kilometers...", "...It should be noted, however, that the name "intra-thermocline" is rather conventional. At high latitudes, where water density is determined mainly by salinity and temperature can play the role of a passive tracer, it is better to speak of intra-picocline vortices or lenses" (Fedorov, 1986).

According Monin (1985), synoptic phenomena should include such phenomena whose horizontal scale is comparable or slightly larger than the deformation radius. "The results obtained give grounds to assert that although quasi-homogeneous anticyclonic intrathermocline lenses have a length usually less than the typical internal radius of deformation for a given region of the ocean, they cannot be smaller than the local (i.e., calculated from the characteristics of the lens itself) radius of deformation. Therefore, they should be considered as a type of synoptic phenomena".

Thus, against the background of large-scale currents, intense synoptic-scale motions develop in the ocean - eddies moving together with the water contained in them, as well as larger ones - Rossby waves. These synoptic processes are in many ways analogous to atmospheric processes, although there are significant quantitative differences, beginning with the fact that large-scale currents in the ocean have a different origin. Thus, while in the atmosphere the trade wind circulation and the west-east transport of temperate latitudes are created by heating from below (decreasing from the equator to the poles), in the ocean their main cause is the wind stress on the ocean surface combined with the influence of the coasts (absent in the atmosphere) and the Earth's rotation (more precisely, the change of the Coriolis parameter with latitude due to its sphericity).

The analogs of Rossby waves at the atmospheric jet currents in the ocean are meanders at the jet currents and the formations in the form of frontal synoptic vortices - rings - formed at their loss of stability and cutoff. Although rings are eddies, their motions are characterized by a systematic westward displacement, which is typical of Rossby waves.

More than 4 million studies and observations are known, which show that the largest number of eddies (vortex density is maximum) is observed in the areas of western boundary currents (Zhmur, 2011). Before it was considered that the most powerful sources of energy for synoptic disturbances were the Gulf Stream and the Kurosio, at present the list of ocean areas with the highest vortex energy intensity is as follows (in descending order): the

Agulhas Current reversal area, the Kurosio, the Gulf Stream, the Brazilian-Falkland Current confluence area, the Antarctic Circumpolar Current, and the East Australian Current (Koshlyakov & Belokopytov, 2020).

It is also known that the cause of vortex generation is baroclinic instability of large-mesh flows (Zhmur, 2011). Here is what Belyakov and Volkov (1985) wrote: "...The main cause of vortex generation in the World Ocean is most probably barotropic and baroclinic instability...". And also: "...An evaluation of the contributions of barotropic and baroclinic instability energies has shown that the barotropic perturbation energy is much smaller than the baroclinic energy and cannot and does not have much significance for the generation of vortices in the ocean...". Kamenkovich et al in their paper (1982) noted: "The main conclusion is that real ocean currents produced by external forces should apparently turn out to be unstable under very broad conditions. Moreover, since the characteristic spatial scales of the growing perturbations are of the same order of magnitude as the corresponding scales for the actually observed synoptic eddies in the ocean, it seems very plausible that baroclinic instability is one of the most important processes generating the synoptic variability of the ocean. The results of processing of observations of the expeditions "Polygon-70" and POLYMODE" are also in favor of this. The same authors believe that it is baroclinic instability that makes the greatest contribution to the formation of synoptic eddies: "Nevertheless, baroclinic instability remains the main recognized mechanism of cyclogenesis, irrespective of how fast the emerged disturbance develops" (Shakina, 1990).

"...It should be assumed that vortices are generated by baroclinic instability, as evidenced by the good agreement between the observed and calculated values of L. Vortices with smaller scales should not exist, vortices with larger scales should be determined by the size of the forcing force. It is characteristic that Arctic subsurface vortices have a core with water mass of another region. It seems that Arctic eddies are formed similarly to frontal eddies, but this occurs in the subsurface layer of the ocean" (Belyakov & Volkov, 1985).

The surge of interest in the vortex subject was caused by the discovery of the so-called coherent structures about half a century ago. Their numerous natural manifestations in "pure" form (cyclones and anticyclones in the atmosphere, Gulf Stream rings and synoptic eddies of the open ocean, mushroom and tripolar structures, intrathermocline lenses, topographic eddies), as well as in the form of the effects caused by them (bimodal

structure of zonal current flows, deep-water convection in the ocean) served as a breeding ground for the creation of appropriate mathematical models based on vortex theory. As a result, at present, there is a significant progress in understanding the mechanisms and essence of physical phenomena caused by the interaction of vortex structures (Borisov and Mamaev (ed.), 2003).

Let us consider synoptic disturbances in more detail. As mentioned above, jet currents meander, resulting in meanders. Meanders are capable of separating from the current, resulting in the formation of rings (Monin & Krasickij, 1985). Initially (e.g., Stommel, (1965)), meanders of the Gulf Stream were most extensively studied. Then meanders of the Kuroshio and other jet currents attracted attention (Monin & Krasickij, 1985). Rings and meanders are synoptic disturbances of frontal origin (western boundary currents) and rings are solitary eddies (Monin & Krasickij, 1985). However, this type of disturbance is also known to occur in the open ocean away from any jet currents (Zhmur, 2011). These synoptic open ocean eddies are widespread and also contain most of the kinetic energy of ocean currents (Monin & Krasickij, 1985). The discovery of this fact is the largest in ocean hydrodynamics in the post-war years. This type of eddies was considered, for example, by Richardson (1989), Olson, Evans (1986) and many others. The horizontal sizes of open-ocean eddies in earlier studies had a rather wide range of values, on average equal to the local baroclinic Rossby radius. Based on modern satellite data, the horizontal sizes of synoptic eddies of the open ocean are in the range of 50-150 km (Koshlyakov & Belokopytov, 2020).

Here are some more definitions of mesoscale (synoptic) eddies. "Mesoscale eddies are turbulent or rotating structures with scales of several hundred kilometers" (Stewart, 2006). Zhmur, V.V. (2011) defines a mesoscale vortex as a rotating core ("bag of water") together with a mass of water rotating around the core (Zhmur, 2011). Cushman-Roisin (1994) provides another definition of a vortex: "a vortex is a closed circulation that is relatively constant. What is meant by constant is that the circulation time of the fluid is shorter than the time during which the structure remains identifiable".

Mesoscale eddies play an important role in ocean circulation. They have their own dynamics dominated by nonlinear effects. A more detailed study of eddies has suggested that most of the energy of water movement is contained in eddies rather than in the general ocean circulation (Zhmur, 2011). A cyclone is a vortex where the rotary motion is in the

same sense as the earth's rotation, counter clockwise in the Northern Hemisphere and clockwise in the Southern Hemisphere. An anticyclone rotates the other way, clockwise in the Northern Hemisphere and counter clockwise in the Southern Hemisphere (Cushman-Roisin, 1994). Eddies are capable of transporting heat, mass, kinetic energy, and biogeochemical characteristics from the region of their formation across large distances, influencing climate (Gordon et al., 1992; Biastoch et al., 2008; Donners et al., 2004; Belonenko et al., 2020). They are formed almost ubiquitously throughout the ocean (Chelton et al., 2007, 2011) and are one of the main mechanisms of horizontal and vertical mixing. Eddies, depending on water temperature, determine coastal weather locally. Also eddies influence optical, hydrochemical, hydrophysical and acoustic characteristics of the ocean (Zhmur, 2011). Thus, a detailed study of mesoscale eddies in the global ocean is urgently needed, as it allows us to improve the understanding of dynamic, climatic, and biological oceanic processes.

The development of Earth remote sensing methods, the main advantages of which include spatial representativeness for providing regional and global studies, efficiency in obtaining information, and the possibility of organizing operational integrated monitoring at any point in the World Ocean, has opened a new era of ocean research in the synoptic frequency range. The capabilities of satellite altimetry can now be highly appreciated: measurements of global sea level are available with a spatial resolution of 1/12°. In recent years, many efforts have been made to achieve 1-2 cm accuracy of sea surface height measurements (Marcos et al., 2015). Research on mesoscale eddies includes the study of eddy structure, evolution and dynamics, their influence on weather, climate and global ocean circulation, and the development of methods and models to investigate and predict them. Existing research has resulted in a better understanding of the processes occurring in mesoscale eddies, their importance for the formation of weather events and their influence on climate. Nevertheless, this field of science is still an active area of research. Modern achievements in the fields of computer technologies and models have made it possible to maintain the relevance of studies of synoptic (mesoscale) ocean dynamics for a long time, posing new challenges. This work is a **part** of this global research.

Generally, vortex activity regions are somehow confined to regions with large-scale currents due to the presence of baroclinic and barotropic instability, which is one of the main conditions for the generation of mesoscale vortices (Monin and Zhiharev, 1990). In each region mesoscale eddies have their specific features, characteristic only for a particular

region and determined by many factors, among which the main one is the existing system of currents. In the Southern Hemisphere, one of the most dynamically active currents is the Agulhas Current. Agulhas eddies are capable of travelling hundreds (and even thousands) of kilometres, which indicates their high water exchange potential; therefore, they can be considered special natural tracers of water exchange between the Indian and Atlantic Oceans and have a significant influence on the structure of the global climate (Gordon et al, 1993; Donners et al, 2004). The influence of Agulhas eddies on the general circulation in the Atlantic Ocean occurs through two main mechanisms: radiation by Rossby waves and advection by mesoscale eddies (Biastoch et al, 2008; van Sebille et al, 2007). This phenomenon is discussed in more detail in Chapter 3.

Thus, the object of the study is the mesoscale eddy dynamics in the region of the Agulhas Current, the Cape Basin and the South Atlantic Ocean. The subject of the study is mesoscale (synoptic) eddies in this region.

The objective of the research and the main tasks

The main **objective** of this work is to identify specific features of the mesoscale eddy dynamics of the South Atlantic Ocean based on satellite altimetry, the global ocean reanalysis dataset GLORYS12V1 and drifting Argo floats.

To achieve this goal, the following **tasks** have been defined:

1. Estimation of Agulhas transport and study of the vertical structure of eddies by an independent co-location method. Comparison of the obtained estimates with the estimates obtained earlier by other researchers using various but different methods.
2. Analysis of the structure of waters of different origins in eddies of the Cape Basin based on the Lagrangian method.
3. Estimates of the meridional displacement of mesoscale eddies when they move westwards based on altimetry data.
4. Estimation of kinematic and dynamic characteristics of Agulhas eddies of different polarity. Estimates of potential vorticity by the Ertel and Rossby approaches for two eddies of different polarities located in the Cape Basin.

5. Analysis of the evolution of kinetic and available potential energy of eddies during their transformation by elongating based on reanalysis data.

The scientific novelty of this research

1. For the first time, for the region under consideration, estimates of heat content and salt content in a separate Agulhas eddy, as well as estimates of heat and salt flow and transport, were obtained from GLORYS12V1 data.
2. The existing two-mode thermohaline structure of eddies in the Cape Basin is interpreted for the first time. This two-mode structure is explained by the interaction of the Agulhas eddies with the waters of the South Atlantic circulation and the Benguela Current in the Cape Basin.
3. For the first time, we obtained estimates of the zonal and meridional displacements of the Agulhas eddies based on META3.2 data. We obtained estimates of the travel distances and lifetimes of long-lived eddies, as well as average estimates of their parameters, amplitude, radius, and orbital velocity. A new interpretation of the meridional displacement of eddies is proposed.
4. For the first time, estimates of changes in the kinetic and available potential energy of eddies in the Cape Basin during their transformation by stretching were obtained.

The theoretical and practical significance of the research

The theoretical significance of these results consists of obtaining new insights into the mesoscale eddy dynamics of South Atlantic waters on the basis of a comprehensive analysis of altimetry, model and in situ data. This work reveals this problem from a new perspective, complements the existing knowledge on mesoscale eddy dynamics in this region and contributes to the development of sea dynamics theory.

The practical significance of these results contributes to the expansion of the body of knowledge about the eddy dynamics of the ocean and is rooted in the fact that the original

methods and approaches developed by the author can be used to study oceanologic fields in other regions of the World Ocean.

The validity of the results

The reliability of the results is determined by the representativeness of the arsenal of initial information used: altimetry measurements, model data and in situ measurements obtained using drifting Argo floats. The validity of the scientific provisions, conclusions and recommendations contained in this dissertation research is ensured by the approved methodology and application of modern methods of analysing empirical information and hydrodynamic models describing the processes under consideration.

The results of the dissertation were obtained under the following projects:

- RFBR № 17-05-00034: "Synoptic structure of sea water dynamics and its influence on average characteristics of hydrophysical and biotic fields using remotely sensed data";
- RFBR № 20-05-00066: "Characterization of Rossby waves in jet streams using remotely sensed data".

Publication and approbation of the results

Seven articles (4 in Russian, 3 in English) were published on the topic of this dissertation. All the articles were published in periodicals: 3 were periodicals included in the Web of Science/Scopus list, and 4 were periodicals included in the HAC list. List of published works on the subject of the dissertation:

1. **Malysheva A.A.,** Koldunov A.V., Belonenko T.V., Sandalyuk N.V. Agulhas leakage eddies based on altimetry data, Uchenye zapiski RGGMU. 2018. № 52. P. 154-170 (RISC, HAC).

2. **Malysheva A.A.**, Kubryakov A.A., Koldunov A.V., Belonenko T.V. Estimation of Agulhas leakage based on satellite altimetry and Argo floats, Issledovanie Zemli iz kosmosa. 2020a, №2, P. 24–34. (RISC, HAC, Scopus).

3. **Malysheva A.A**., Kubryakov A.A., Koldunov A.V. and Belonenko T.V. Estimating Agulhas Leakage by Means of Satellite Altimetry and Argo Data. Izv. Atmos. Ocean. Phys., 2020b, 56, 1581–1589. (HAC, WoS, Scopus)

4. Gnevyshev V.G., **Malysheva A.A**., Belonenko T.V., and Koldunov A.V. On Agulhas eddies and Rossby waves travelling by forcing effects, Russ. J. Earth Sci., 2021, 21, ES5003. (RISC, HAC, WoS, Scopus).
5. **Malysheva A.A**., Belonenko T.V., Yakovleva D. A. Characteristics of two Agulhas eddies of different polarity, Gidrometeorologiya i ekologiya, 2022, № 68, P. 478—493. (RISC, HAC).

6. Belonenko T.V., Budyansky M.V., **Malysheva A.A**. et al. Observing the Agulhas Leakage Source in the Water Mixing Area, Pure Appl. Geophys., 2023. (RISC, HAC, WoS, Scopus).

7. **Malysheva A. A.**, Belonenko T. V. Changes in available potential and kinetic energy of mesoscale eddies in the Cape Basin, Gidrometeorologiya i ekologiya, № 63, 2023. (RISC, HAC).

The results of this study were presented at various national and international conferences:

1. The 16th All-Russian Open Conference "Current problems in remote sensing of the Earth from space". November 12-16, 2018, Moscow. **Malysheva A.A.,** Koldunov A.V., Belonenko T.V., Sandalyuk N.V. Agulhas leakage eddies based on altimetry data. Oral presentation.
2. II All-Russian Conference "Hydrometeorology and Ecology: achievements and development prospects". December 19-20, 2018, Saint Petersburg. **Malysheva A.A.,** Koldunov A.V., Belonenko T.V. Influence of the Agulhas Current variability on the meridional thermohaline circulation. Oral presentation.
3. The 17th All-Russian Open Conference "Current problems in remote sensing of the Earth from space". November 11-15, 2019, Moscow. **Malysheva A.A**., Kubryakov

A.A., Koldunov A.V. and Belonenko T.V. Estimating Agulhas Leakage by Means of Satellite Altimetry and Argo Data. Poster presentation.

4. III All-Russian Conference "Hydrometeorology and Ecology: achievements and development prospects". December 18-19, 2019, Saint Petersburg. **Malysheva A.A**., Kubryakov A.A., Koldunov A.V. and Belonenko T.V. Estimating Agulhas Leakage by Means of Satellite Altimetry and Argo Data. Oral presentation.
5. IV All-Russian Scientific Conference of Young Scientists "Comprehensive Studies of the World Ocean" (CSWO/KIMO-2019). April 22-26, 2019, Sevastopol. **Malysheva A.A**., Belonenko T.V., Kubryakov A.A. Study of Agulhas leakage using altimetry and Argo floats data. Oral presentation.
6. The 18th All-Russian Open Conference "Current problems in remote sensing of the Earth from space". November 16-20, 2020, Moscow. **Malysheva A.A**., Gnevyshev V.G., Belonenko T.V., Koldunov A.V. Meridional and zonal distribution of mesoscale eddies in the South Atlantic. Oral presentation.
7. V All-Russian Scientific Conference of Young Scientists "Comprehensive Studies of the World Ocean" (CSWO/KIMO-2020). May 18-22, 2020, Kaliningrad. **Malysheva A.A**., Kubryakov A.A., Koldunov A.V., Belonenko T.V. Co-location method for the study of Agulhas leakage. Oral presentation.
8. VI All-Russian Scientific Conference of Young Scientists "Comprehensive Studies of the World Ocean" (CSWO/KIMO-2021). April 18-24, 2021, Sevastopol. **Malysheva A.A**., Gnevyshev V.G., Belonenko T.V., Koldunov A.V. On Agulhas eddies and Rossby waves propagating in the South Atlantic. Poster presentation.
9. The 19th All-Russian Open Conference "Current problems in remote sensing of the Earth from space". November 15-19, 2021, Moscow. **Malysheva A.A**., Gnevyshev V.G., Belonenko T.V., Koldunov A.V. Rossby waves, striations and mesoscale eddies of the South Atlantic. Poster presentation.
10. The 20th All-Russian Open Conference "Current problems in remote sensing of the Earth from space". November 14-18, 2022, Moscow. **Malysheva A.A**., Gnevyshev V.G., Belonenko T.V., Koldunov A.V. Rossby waves, striations and mesoscale eddies of the South Atlantic. Poster presentation.
11. VII All-Russian Scientific Conference of Young Scientists "Comprehensive Studies of the World Ocean" (CSWO/KIMO-2023). May 15-19, 2023, Saint-Petersburg. **Malysheva A.A**., Belonenko T.V., Budyansky M.V. Lagrangian method for the study of Agulhas leakage in a water mixing region. Poster presentation.

Selected results from this work have been recognized with awards:

1. **Diploma of the winner** in the Contest for the best oceanographic research among students and PhD students, Shirshov Institute of Oceanology of Russian Academy of Sciences, 2019.
2. **Diploma of the winner** in the Contest for the best student papers of the Ocean Physics Section at the V All-Russian Conference KIMO2020, Atlantic Branch of the Institute of Oceanology of the Russian Academy of Sciences, 2020.
3. **Diploma of the winner** in the Contest for the best oceanographic research among students and PhD students, Shirshov Institute of Oceanology of Russian Academy of Sciences, 2022.

The personal contribution of the author

The thesis statements and the results obtained from them are contained in the articles published in the WoS, Scopus and VAK journals. The author has made a significant contribution to the bulk of the research presented in the thesis and coauthored articles. In the joint publications, the author is responsible for the selection of the data, the determination of the methodology of their processing, the writing of the programs used to calculate the study characteristics, and their analysis and visualization. The author participated in the interpretation and physical analysis of the obtained results and preparation of the texts of the publications.

The structure of the dissertation

The dissertation consists of an introduction, 5 chapters, a conclusion and a list of references. The results of the dissertation work are presented on 113 pages and include 46 figures and 5 tables. The list of references consisted of 155 titles.

The **Introduction** formulates the goals and objectives of the research, presents the main thesis statements, describes the relevance and novelty, as well as the theoretical and practical significance of this work, and provides a list of publications and conferences as a result of the research approbation.

Chapter 1 provides a complete physical, geographical and oceanological description of the study area. Literature sources devoted to the study of the Agulhas Current

and the South Atlantic Ocean are analysed in detail. A brief overview of the eddy dynamics of the study area is presented.

Chapter 2 details the data used and the methods used to analyse them.

Chapter 3 takes a comprehensive look at the Agulhas leakage phenomenon based on altimetry, reanalysis data and Argo floats data.

Chapter 4 investigates the meridional displacement of Agulhas eddies and analyses theoretical approaches to this phenomenon.

Chapter 5 is devoted to the analysis of the dynamic and kinematic characteristics of eddies in the Cape Basin. Parameters such as relative and potential vorticity, spatial dimensions of eddies, orbital velocity and drift velocity, the Brunt–Vaisala frequency, and the available potential and kinetic energy of eddies are considered, and the behavior of eddies during interactions with barotropic flow is analysed.

The **conclusion** contains the main conclusions of the research.

Gratitude

The author expresses an extreme degree of appreciation and gratitude to her scientific supervisor D.Sc. in Geographical Sciences Belonenko T.V., for help at all stages of the thesis; to Koldunov A.V., Ph.D., for consulting during calculations; and to Gnevyshev V.G., Ph.D., leading employee of the Shirshov Institute of Oceanology of the Russian Academy of Sciences for attention on the work, useful recommendations and valuable advice in its realization. The author is grateful to all the teachers of the Department of Oceanology of SPbU for their support and participation throughout the years of study at the Department.

Main scientific results

1. It is shown that long-lived Agulhas eddies, moving westward, cross the Atlantic Ocean and thereby transfer the properties of the waters of the Indian Ocean to the shores of South America. (Malysheva et al., 2018, p. 158). It is shown that the estimate of Agulhas leakage (discharge) by one mesoscale eddy is on average 8.5 Sv. The transport

of heat and salt by one mesoscale Agulhas leakage eddy is $2.25 \cdot 10^9$ W and $5.36 \cdot 10^5$ $kg \cdot s^{-1}$, respectively. The heat content and salt content in one Agulhas leakage eddy are $2.03 \cdot 10^{15}$ J and $4.83 \cdot 10^{11}$ kg, respectively (Malysheva et al, 2020a, p. 31, Malysheva et al, 2020b, p. 1587);

2. It is shown that the main feature of the study area is the mixing of water particles of different origins. The waters of the South Atlantic Gyre interact with the waters of the Agulhas Current more actively than previously thought. The waters carried by the Agulhas leakage eddies originate not only from the Agulhas Current itself, but also from the South Atlantic Gyre and the Benguela Current. This effect may influence the formation of two-mode eddy structures described but unexplained in other studies (Belonenko et al, 2023, pp. 3412-3414);
3. Zonal displacement and, accordingly, the zonal component of the movement speed dominate, however, in certain sections of the track, the displacement of the eddy to the equator is comparable to the zonal displacement. The meridional displacement varies in the range of 9 – 895 km. It has been established that the greater the speed of the eddy, the greater its meridional displacement per unit time (Gnevyshev et al, 2021, pp. 9, 13);
4. The only theory about meridional displacement that is consistent with empirical observations is the theory of Lighthill (1967), but in a modified version. If in the formula proposed by Lighthill we use the first baroclinic radius instead of the barotropic one, then we see a good correspondence of the directions of movement of the Agulhas eddy tracks in the South Atlantic with the formula (Gnevyshev et al, 2021, pp. 7, 8);
5. It has been established that in the process of deformation of eddies by a barotropic flow, a decrease in energy occurs: over 7 days of vortex stretching, the potential energy decreases by 3 times for an anticyclone and by 1.5 for a cyclone, and the kinetic energy on average decreases by 1.3 times (Malysheva and Belonenko, 2023, p. 694).
6. The vertical structure of eddies was analyzed using the example of two opposite-polar eddies in the Cape Basin. It is shown that for a cyclone the anomalies of isotherms and isohalines extend up to 1000 m, and for an anticyclone - up to 1200 m. The core of the anticyclone extends to a depth of 800 m. The eddy cores are clearly visible on the Brunt–Vaisala frequency section. The cyclone core, which is characterized by homogeneous stratification, is characterized by maximum the Brunt–Vaisala frequency values ($4 \cdot 10^{-5}$ s^{-1}), in contrast to the anticyclone core, in which the Brunt–Vaisala frequency values are zero, therefore, there is no stratification. Relative vorticity is also clearly visible in the eddy cores, the maximum positive values ($4 \cdot 10^{-6}$ s^{-1}) are observed

in the cyclone region, the maximum negative ($–2·10^{–6}$ $s^{–1}$) - in the anticyclone region. An assessment of the vorticity potential (PV) is presented based on two approaches: the Ertel formula and the Rossby formula. It is shown that in the center of the anticyclone there is practically no stratification, which contributes to low values of potential vorticity according to Ertel ($0.6·10^{-10}$ – $0.8·10^{-10}$ $m^{-1}·s^{-1}$). And in the center of the cyclone, large values of the buoyancy frequency contribute to large PV values ($1.8·10^{–10}$ $–2·10^{–10}$ $m^{–1}·s^{–1}$). In addition, in the center of the anticyclone, where the negative relative vorticity is large, PV is close to zero. The minimum (negative) values of potential Rossby vorticity reach $–2·10^{–5}$ $s^{–1}$ and are observed in the region of the anticyclone core. The maximum values of $8·10^{–5}$ $s^{–1}$ are located in the region of the cyclone core. There is also an exchange of potential vorticity between vortices when they interact with each other (Malysheva et al., 2022, pp. 484-486, 488, 489).

Thesis statements

1. The heat and salt anomalies inside an individual Agulhas leakage eddy are 2.03×10^{15} J and 4.83×10^{11} kg, respectively. The mean Agulhas leakage transport by one mesoscale eddy is 8.5 Sv. The transport of heat and salt by the individual Agulhas leakage eddy is 2.25×10^{9} W and 5.36×10^{5} kg $s^{–1}$, respectively.

2. Agulhas eddies, formed as a result of the disintegration of Agulhas rings, transfer the properties of Indian Ocean waters with the transformation of the thermohaline structure of the eddies in the Cape Basin, in which particles are gradually replaced by particles from South Atlantic waters, forming a two-mode water structure in the eddies.

3. Based on altimetry data it was established, that anticyclones move westwards, and at the same time meridional displacement toward the equator occurs. Estimates of the meridional displacement vary in the range of 9-895 km. A possible physical mechanism explaining the meridional displacement of eddies is the directional angular emission of long Rossby waves by non-zonal currents.

4. When eddies interact with flow, mesoscale eddies are stretched into filaments, with the kinetic energy of the eddy decreasing from $3×10^{15}$ to $2{,}6×10^{15}$ J and the available potential energy decreasing from $4×10^{18}$ to $0{,}1×10^{18}$ J.

CHAPTER 1. PHYSIOGRAPHIC DESCRIPTION OF THE RESEARCH AREA

1.1 Agulhas Current

The Agulhas Current is a warm westerly boundary current in the southern Indian Ocean and is part of the westwards-directed South Equatorial Current that runs around the east coast of Africa between 27° and 40°S (Gordon, 1985) (Fig. 1.1). The current is narrow and fast (at the surface, velocities can reach 200 cm/s). According to synoptic measurements, the Agulhas Current covers the entire water column, but in a previous study (Boebel et al., 1998), it was shown that the current extends only 2300 meters. The depth of the current tends to increase with latitude, which compensates for the increase in planetary eddies.

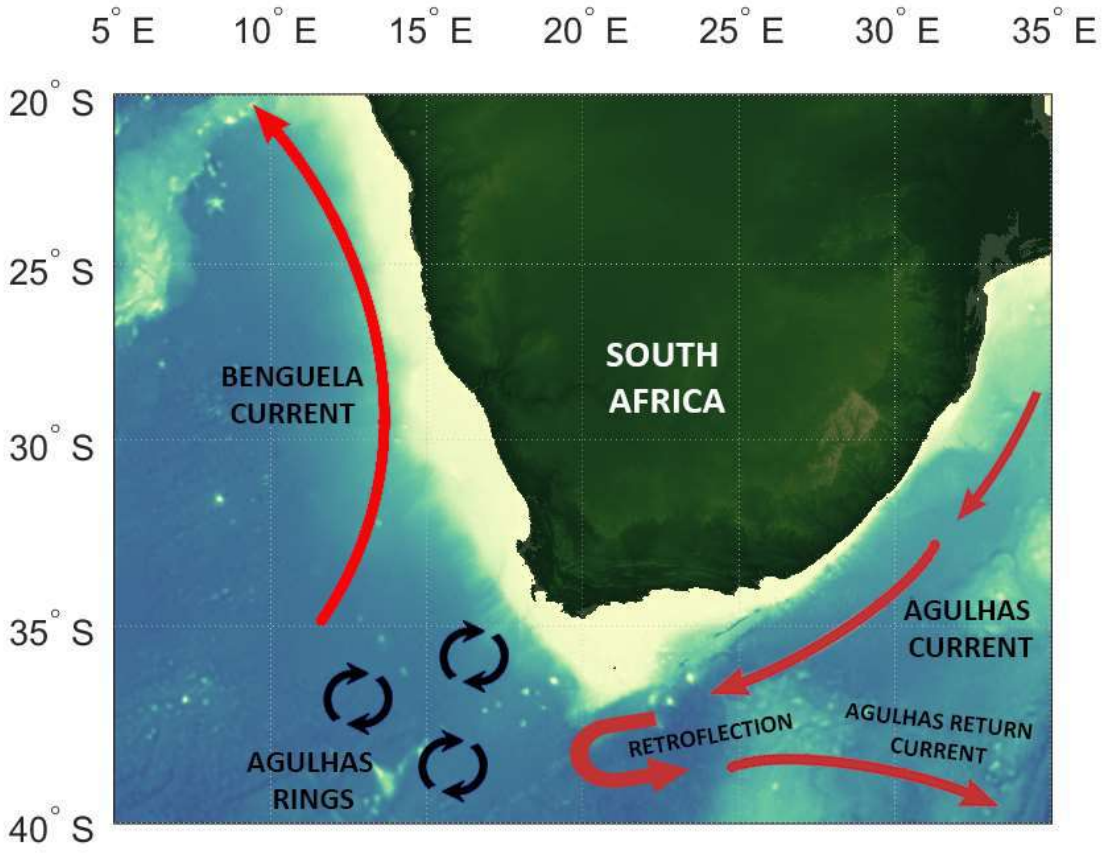

Figure 1.1. General scheme of the Agulhas Current.

As one of the major currents in the Southern Hemisphere, the Agulhas Current System transports large masses of water. One of the earliest estimates of the geostrophic

transport of the current was given in Gordon (1985) and was 67 Sv (1 Sv = 10^6 $m^3 \cdot s^{-1}$). A few years later, Toole and Warren (1993) obtained higher estimates: 85 Sv. However, some researchers noted that the no-movement level used by Toole and Warren did not take into account the countercurrent, the Lower Agulhas Current. Beal and Bryden (1999) determined a geostrophic transport of 73 Sv based on LADCP data, which was only 3% different from the direct transport calculation using LADCP. Donohue et al. (2000) attempted to refine previous calculations of transported water volume by removing barotropic tides and calculating instrumentation and measurement errors. They estimated the transport of waters southwards to be 78±3 and 76±2 Sv. The most recent estimates are from a group of scientists led by Bryden et al. (2003), who, in 2003, calculated the mean transported water volume to be 69.7±4.3 Sv based on annual measurements of flow velocities.

As the Agulhas Current approaches the southern edge of the African continental shelf, it begins to reverse direction. Approximately 36°S, the current separates from the continental shelf and turns eastwards in a large anticyclonic loop called the **Agulhas retroflection** (there is no analog for this term in the Russian-language scientific literature), forming **the Agulhas Return Current**. The width of the Agulhas Return Current is approximately 70 km, and the volume of transported water is 44±5 Sv in the upper thousand meters. The configuration of the current does not remain constant, and the loop formed is constantly moving toward the South Atlantic. After reaching a certain point in the extremum, the loop breaks off and closes into a ring (Gordon et al., 1987) that continues westwards. Further out in the Cape Basin, the Agulhas ring decomposes into smaller scale vortices. These eddies are filled with relatively warm and salty Indian Ocean water. The temperature of this water is more than 5°C warmer, and the salinity is 0.3 psu higher than that of waters at the surface of the South Atlantic Ocean, which are of equal density (Gordon et al., 1985). The eddies retain their characteristic thermal characteristics up to 5°E westwards and 46°S southwards and propagate in the South Atlantic Ocean at 12 cm/sec (Lutjeharms and van Ballegooyen, 1988). This transport between the Indian and Atlantic Oceans may have a significant influence on the structure of the global climate.

1.2. South Atlantic Ocean

The circulation of the South Atlantic is characterized by anticyclonic circulation, which consists of four main branches: the Brazil Current, the South Atlantic Current, the Benguela Current, and the South Equatorial Current (Fig. 1.2). The latter carry water from the Indian and Pacific Oceans toward the North Atlantic. As mentioned above, when moving westwards, namely, in the Cape Basin, the Agulhas Rings break up into smaller-scale eddies and interact with the surrounding waters. Thus, there is a basin off the southwest coast of South Africa where Agulhas eddies interact with the waters of the South Atlantic Gyre and the Benguela Current, which is also influenced by the Angola Current. This process is unique and has not been found in any other major eastern boundary current system.

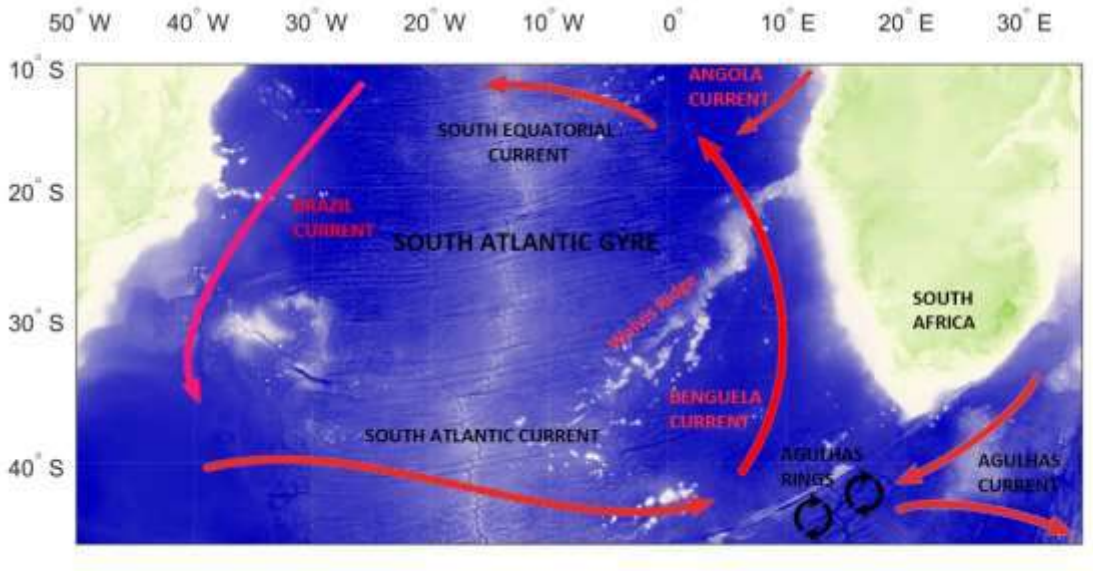

Fig. 1.2. General scheme of water circulation in the South Atlantic Ocean.

CHAPTER 2. DATA AND METHODS

2.1. Data

The main sources of data for this study are global ocean reanalysis and satellite altimetry data. The global model of the Earth surface relief ETOPO1 was also used. All calculations were performed using the MATLAB program environment. The TEOS-10 equation of state for seawater was used to calculate the thermodynamic properties of seawater. The Lagrangian method was used to model the water circulation, which describes the transport and mixing in the studied region by calculating the trajectories of a large number of artificial passive particles.

2.1.1. «Mesoscale Eddies in Altimeter Observations of SSH» data

We used "Mesoscale Eddies in Altimeter Observations of SSH" (META3.2 DT allsat) data available on the AVISO portal (https://www.aviso.altimetry.fr) supported by CNES in collaboration with IMEDEA. A specially developed vortex identification algorithm based on the analysis of altimetric images (Pegliasco et al., 2022) was used to create an array containing mesoscale eddies extracted by automatic identification and tracking. The essence of the original algorithm used to create this array was as follows. An individual mesoscale eddy identified by the automatic algorithm was extracted as a connected set of pixels that satisfied a certain number of criteria, such as the presence of a local maximum (minimum) in the sea level anomaly field for an anticyclonic (cyclonic) eddy and consistency of anomaly values within the contour of this cluster with the sign of its extremum. The maximum vortex size was limited to 1000 pixels, the minimum size was 8 pixels, and the minimum vortex amplitude was 1 cm. In the dataset, each vortex was assigned an identification number and the coordinates of its trajectory. The META3.2 product contains information on the polarity of vortices, their radius and amplitude, orbital velocity, and lifetime.

2.1.2. Argo floats data

Argo floats data (http://www.argo.net) were used. An important advantage of Argo floats surveys is the possibility of conducting measurements not only at the surface but also in the water column. In addition, contact measurements are still the most accurate information on the state of the marine environment. For example, Argo measures sea water temperature and salinity. Argo allows measurements up to depths of 1500 m with a frequency of once every 5 days.

2.1.3. GLORYS12V1

The Global Ocean Physics Reanalysis (GLORYS12V1), an eddy-resolving reanalysis of the World Ocean, is available on the Copernicus Marine Environment Monitoring Service (CMEMS) portal. The product includes parameters such as temperature, salinity, current velocity, and sea surface height. The reanalysis is based on the CMEMS global real-time forecasting system. GLORYS12V1 assimilates satellite and in situ data. The reanalysis is based on the NEMO model, where the ERA-Interim atmospheric reanalysis of the European Center for Medium-Range Weather Forecasts (ECMWF) is used as a forcing. The Boussinesq approximation is applied in the model equations. Since the simulation does not directly represent the global mean steric sea level variability, a globally diagnosed mean steric sea level trend is added to the simulated dynamic sea level at each time step to improve consistency with assimilated satellite observations. Different types of observations are assimilated using a Kalman filter (SEEK - Singular Evolutive Extended Kalman). Sea level anomalies (SLA) data are derived from a satellite altimeter, sea surface temperature (SST) data from the AVHRR satellite from NOAA, and in situ vertical profiles of temperature and salinity (T/S) from the CORA database with CMEMS quality control. A “hybrid” mean dynamic topography (MDT) based on the CNES-CLS13 MDT was also used as a reference for altimetry data assimilation.

The spatial resolution of the data is 1/12° at 50 levels when altimetric observations are available. The temporal discreteness is one day.

2.1.4. ETOPO1

The depth data for the study area were taken from the global surface elevation model ETOPO1 (https://www.ngdc.noaa.gov). The model was implemented on a grid with a spatial resolution of 1/60°.

2.1.5. WOA13

An updated version of the World Ocean Atlas (WOA13), which is a database of generalized climatological data, was used in the analysis of the thermohaline properties of eddies. The data are presented on a 1° grid.

2.1.6. TEOS-10

The international equation of state of seawater TEOS-10 (http://www.teos-10.org/) was used to calculate the thermodynamic properties of seawater. The characteristics of the waters, such as the Brunt–Vaisala frequency and density, were also calculated.

2.1.7. Algorithm AMEDA

We used an optimized algorithm, the angular momentum eddy detection and tracking algorithm (AMEDA), for detecting and tracking eddies from two-dimensional velocity fields. This eddy identification method uses a hybrid method based on physical parameters and is applied to the GLORYS12V1 reanalysis data. The main advantages of AMEDA are as follows: the algorithm is robust to the grid resolution, it uses a minimal number of tunable parameters, the dynamic features of the detected eddies are quantified, and the tracking procedure identifies the merging and splitting events. The proposed method provides the complete dynamic evolution of the detected eddies throughout their lifetime. This allows us to precisely identify the formation areas of long-lived eddies, the regions where eddy splitting or merging frequently occur, and where eddies interact with

currents (Le Vu et al., 2018). Using the AMEDA algorithm, we identified the inferred eddies from the GLORYS12V1 data.

2.2. Methods of data analysis

2.2.1. Co-location method

To study the vertical structure of mesoscale eddies, we used the so-called co-location approach, a joint analysis of mesoscale eddies and Argo profiles, as described below.

Of all the Agulhas leakage eddies, we chose those that satisfied the following conditions:

- A mesoscale eddy formed in the Agulhas Retroflection region.
- The mesoscale eddy was automatically identified using the Mesoscale Eddy Trajectory Atlas Product database throughout its entire life cycle.
- The mesoscale eddy had a life span longer than 6 months.
- The mesoscale eddy captured an Argo float, and the float itself moved with the eddy.
- The Argo float was located at the core of the mesoscale eddy.
- If at some point in time the Argo float was located at a distance exceeding the eddy radius, that eddy was rejected.

The last three conditions indicate that of all the Agulhas leakage eddies, only those that continuously moved westwards along with an Argo float profile were considered in the joint analysis. We were able to find six eddies that satisfied the selected conditions in the period 1993–2017, and their characteristics were subsequently analysed to obtain the necessary estimates. In particular, the geographical position of the float in the eddy at the time of capture was found. The mean eddy parameters and parameters at the moment of float capture by the eddy were obtained from the “Mesoscale Eddy Trajectory Atlas Product” dataset. WOA13 data were used to analyse the thermohaline structure of the eddies. Temperature and salinity anomalies were calculated relative to these mean climatic values for each time point at the corresponding points of the eddy trajectory. Thus, it is

possible to observe the variability in thermohaline characteristics from the moment of capture to the end of the float location in the eddy and to compare the T/S characteristics of eddies and surrounding waters.

2.2.2. Calculation of eddy transport

The heat and salt transport, as well as the heat and salt contents, of the eddies were calculated using average parameters from the "Mesoscale Eddy Trajectory Atlas Product" dataset. Following the approach proposed in Chaigneau et al. (2011), the heat content (AT) and salt content (AS) in the eddy volume V were estimated:

$$AT = \int \rho C_p T' dV , \tag{2.1}$$

$$AS = \int \rho S' dV , \tag{2.2}$$

along with mesoscale eddy heat transport (HT) and salt transport (ST):

$$HT = \int \rho C_p T' v dS , \tag{2.3}$$

$$ST = \int \rho S' v dS , \tag{2.4}$$

where $\rho = 1.025$ kg·m^{-3}, Cp = 4200 J·kg^{-1} (°C)$^{-1}$, T' is the mean temperature anomaly over depth, and S' is the mean salinity anomaly over depth (Yari et al., 2012). Note that these estimates are averages and characterize transport by only one eddy.

2.2.3. Calculation of potential vorticity

The main dynamic characteristic of eddies is the potential vorticity (PV). If the system in which eddies move was closed, the law of conservation of potential vorticity would be fulfilled for these eddies. This law is analogous to the law of conservation of quantity of motion in mechanical processes. However, in the real ocean, eddy processes cannot be expected to be isolated from all other processes; consequently, the system is not closed, so the potential vorticity of eddies may change during evolution along with changes in their thermohaline and kinematic characteristics.

Two main approaches for calculating the potential vortex vorticity are presented in this paper: the Ertel and Rossby approaches.

Calculation of potential vorticity PV eddies by Ertel's formula

The potential vorticity in the Ertel approach was calculated using formula (12) from Zhmur et al. (Zhmur et al., 2021):

$$PV = \frac{(-\frac{\partial v}{\partial z})\cdot\frac{\partial \rho}{\partial x} - (-\frac{\partial u}{\partial z} + f_h)\cdot\frac{\partial \rho}{\partial y} + (\frac{\partial v}{\partial x} - \frac{\partial u}{\partial y} + f)\cdot\frac{\partial \rho}{\partial z}}{\rho}, \quad (2.5)$$

where ρ is the flow density; *u* and *v* are the zonal and meridional components of the current velocity, respectively; $f = 2\omega\sin\varphi$ is the Coriolis parameter; $f_h = 2\omega\cos\varphi$ is the meridional component of the angular velocity of the Earth's rotation $2\boldsymbol{\Omega} = (0, f_h, f)$; and φ is the latitude. The right-hand coordinate axis is used, where the *x*-axis points east, the *y*-axis points north, and *z* is the vertical axis. Since the vertical velocity gradients and f_h are also negligible, the potential vorticity is calculated using a simpler formula:

$$PV = \frac{(\zeta + f)\cdot\frac{\partial \rho}{\partial z}}{\rho_0}, \quad (2.6)$$

where ρ_0 is the reference density of water; in calculations, ρ_0 = 1027 кг/м^3, and $\zeta = \frac{\partial v}{\partial x} - \frac{\partial u}{\partial y}$ is the relative vorticity.

Calculation of potential vorticity PV eddies by Rossby's formula

The calculation of σ in the Rossby approach was performed using formula (13) from Zhmur et al. (Zhmur et al., 2021):

$$\sigma = rot_z \mathbf{V} + \frac{\partial}{\partial z}\left(\frac{f^2}{N^2}\frac{\partial \psi}{\partial z}\right) = \nabla^2\psi + \frac{\partial}{\partial z}\left(\frac{f^2}{N^2}\frac{\partial \psi}{\partial z}\right), \quad (2.7)$$

where ψ is the stream function and *N* is the Brunt–Vaisala frequency.

The potential vorticity σ calculated by the Rossby formula differs in dimension from that calculated by the PV via the Ertel formula.

2.2.4. Lagrangian method

Water circulation in oceanic basins has been simulated within the natural framework using Lagrangian methods, which describe the transport and mixing in a study region by computing trajectories of a large number of artificial passive particles. The Lagrangian method is now available due to the development of numerical circulation models and the public availability of altimetric data. Consequently, tracking the origin, transport and mixing of different waters by calculating the trajectories of artificial particles back in time from a fixed date based on altimetric data is possible.

The field of a Lagrangian indicator is represented on a basin Lagrangian map for each day. The set of consecutive maps allows one to track the evolution of this field day by day. These maps often resemble patterns with patches, tendrils, and filaments with increased gradients of the indicator values. The lines with prominent horizontal gradients are Lagrangian fronts (Prants et al., 2014, 2017) separating water masses with a distinct history that often coincides with confluence lines and vortex boundaries. A large number of particles are distributed across the study area. The trajectories of Lagrangian particles are computed by solving the advection equations:

$$\frac{d\lambda}{dt} = u(\lambda, \varphi, t), \frac{d\varphi}{dt} = v(\lambda, \varphi, t), \tag{2.8}$$

where u and v are the angular zonal and meridional components of the GLORYS velocity field, respectively, and φ and λ are the latitude and longitude, respectively. The angular velocities are used because their equations have a maximally simple form on Earth's sphere. Bicubic spatial interpolation and smoothing of the temporal evolution by third-order Lagrangian polynomials are used to provide accurate numerical results. The Lagrangian trajectories are computed by integrating Eq. (2.8) using the fourth-order Runge–Kutta scheme with a constant time step of 0.001 days.

For each particle, the length of its trajectory is

$$S = \mathrm{R}_E \int_{t_1}^{t_2} \sqrt{(\lambda'(t))^2 \cos^2 \varphi(t) + (\varphi'(t))^2}\, dt \tag{2.9}$$

was calculated for a given period (30 days in the present study). The length of the curve is traced by the trajectory of the advected particle from its initial position ($\varphi(t_1)$, $\lambda(t_1)$) to the final position ($\varphi(t_2)$, $\lambda(t_2)$), where $\varphi'(t)$ and $\lambda'(t)$ are the derivatives over time and R_E = 6371 km is the Earth's radius (Budyansky et al., 2022).

To identify the eddy centers and track the motion of eddies and their impact on surrounding waters, we compute the locations of stationary points with zero velocity in all the model layers and record them every day. Standard stability analysis of the linearized advection equations is then performed to specify the stagnation points of the elliptic and hyperbolic types (for details, see Prants et al., 2017). The stable elliptic points (triangles on the maps) are located at the centers of eddies where rotation prevails over deformation. The birth of an eddy is manifested by the appearance of an elliptic point, whereas its disappearance signals the decay of the eddy. The hyperbolic points with associated stable and unstable manifolds organize the flow around eddies to cause water exchange with the surrounding waters. The hyperbolic points (orange crosses on the maps), where deformation prevails during rotation, are located mostly between eddies. Any hyperbolic point has directions in which water particles approach it and directions in which they move away. In the theory of dynamical systems, such geometric structures are known as stable (attracting) and unstable (repelling) manifolds.

CHAPTER 3. AGULHAS LEAKAGE

3.1. The term Agulhas leakage

The term "Agulhas leakage" refers to water exported by mesoscale eddies originating in the Agulhas Current System from the Indian Ocean through the Atlantic Ocean to the shores of South America. Agulhas leakage eddies are key links for water exchange in the Southern Hemisphere (Byrne et al., 1995; Doglioli et al., 2006) and affect the Atlantic meridional thermohaline circulation; therefore, obtaining numerical estimates of these phenomena is extremely important.

According to the literature, the influence of Agulhas leakage on the general circulation in the Atlantic Ocean is due to two main mechanisms: emission of Rossby waves and advection by mesoscale vortices (Biastoch et al., 2008; van Sebille et al., 2007). The authors refer to the first mechanism as linear processes and the second as nonlinear processes. However, at least one point does not allow one to unambiguously separate vortices from Rossby waves. When one speaks of Rossby waves, one usually considers a linear dispersion relation that allows one to theoretically estimate the phase velocity of the waves in the longwave approximation (Belonenko et al., 1998, 2004, 2016; Chelton et al., 2011; Belonenko and Kubryakov, 2014). However, in the nonlinear approach, the displacement velocity of displacement vortices is also taken from the linear problem (Chelton et al., 2011). In the framework of quasigeostrophic theory, Rossby waves and mesoscale eddies in the ocean are shown to constitute nonlinear processes that have common generation mechanisms (Le Blon and Majsek (1981), Nezlin (1986), Pedloski (1984), Gnevyshev et al. (2019)). Without further consideration of this theory, we note that Agulhas leakage eddies only move westwards, sometimes travelling thousands of kilometres, with their trajectories deviating to the equator by several degrees (Chelton et al., 2011).

Agulhas leakage eddies have been repeatedly investigated using satellite images of sea surface temperature together with altimeter data (Byrne et al., 1995; Beismann et al., 1999; Schouten et al, 2000; Garzoli et al., 2000; Doglioli et al., 2007), but eddy transport has not been estimated from these data. Estimates of Agulhas leakage have been derived by alternative methods, e.g., water mass analysis (Gordon et al., 1992), Eulerian model

flows (Reason et al., 2003), and numerical Lagrangian particle flows (Bryden et al., 2005), combining modelling and hydrographic estimates (Gordon et al., 1987) and drift buoys (Richardson et al., 2007). According to Gordon et al. (1990), based on GeoSat measurements and CTD profiles, the amount of Agulhas leakage is 20-30 Sv. Richardson (2007) estimated Agulhas transport to be approximately 15 Sv but noted that this estimate was obtained with a rather large uncertainty in the approach used. Van Sebille et al. (2009), based on linear regression of Lagrangian float data and determination of the position of the Agulhas flow front from altimetric data, obtained an estimate of Agulhas leakage of 13.2 Sv. In the literature, quantitative estimates of Agulhas leakage vary widely from 4 Sv (Schmitz, 1995) to 22 Sv (Donners et al, 2004), but most studies report values of 11-17 Sv.

Thus, in this chapter, we derive an estimate of Agulhas leakage using an independent method. We determined the number of long-lived mesoscale eddies that, originating in the Agulhas Current system, drift westwards, thereby transporting water with Indian Ocean characteristics to the shores of South America. We evaluated the characteristics of Agulhas leakage based on the co-location method, a joint analysis of altimetric data and Argo profiler measurements. This paper also analyses the spatial distribution of water particles of different origins in the Cape Basin using the Lagrangian method to evaluate the role of the South Atlantic circulation and the Benguela Current in Agulhas leakage.

3.2. Temporal variability in the number of Agulhas leakage eddies

In the first stage, eddy tracks and characteristics were analysed on the basis of the Mesoscale Eddy Trajectory Atlas Product archive. We were interested in the eddies that formed in the Agulhas Retroflection region and cross the South Atlantic. Figure 1 shows that long-lived eddies move in a westerly direction across the Atlantic Ocean and thus transfer the waters of the Indian Ocean to the shores of South America. It should be noted that the number of eddies with life spans of at least 3 years is much lower than that of eddies with life spans longer than 2 years, which is in turn less than the number of eddies with lifespans longer than 1 year. We next analysed the temporal variability in the number of Agulhas leakage eddies that originated in the Agulhas Retroflection region and crossed a certain meridian in the South Atlantic in the range of 35° W–10° E. Figure 3.2 provides

complete statistics on the number of eddies for each year, depending on longitude. The greater the distance from the place of generation is, the smaller the number of eddies that reach it. While the number of Agulhas leakage eddies at 10° E is normally greater than 20 in different years, no more than 4 eddies cross the prime meridian (depending on the year). Figure 3.2 shows that the South Atlantic Ridge (east of 20°W) is still crossed by a considerable number of Agulhas leakage eddies; however, only two of them reached 30°W in 2007 and 2016, and only one was recorded at 34°W in 2007. This contradicts the main conclusions drawn by Biastoch et al. (2008) and Weijer et al. (2014) that the waters of the Indian Ocean propagating northwards across the equator as Kelvin waves can have an appreciable impact on dynamic processes in the Northern Hemisphere. In Fig. 3.2, we can also distinguish the years when the Agulhas leakage was most intense: 2009–2010, along with 1996, 2014, and 2015. Nonetheless, in some years (1993, 1996, 1998, 2000–2003, 2005, 2008, 2011, 2012, 2017, 2018), Agulhas leakage did not reach beyond the South Atlantic Ridge.

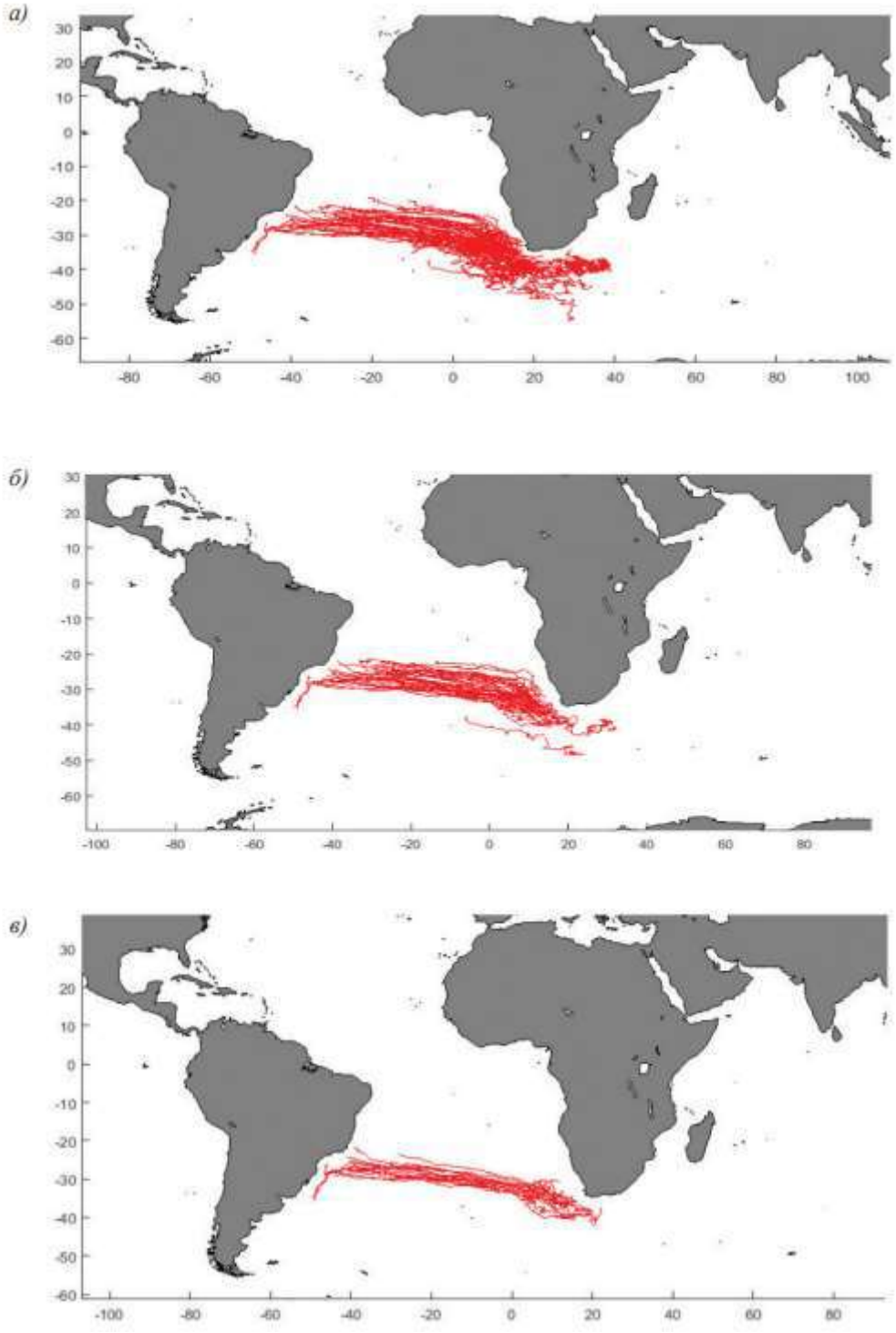

Figure 3.1. Tracks of mesoscale eddies with lifespans of at least (a) 1, (b) 2, and (c) 3 years for the period 1993–2017.

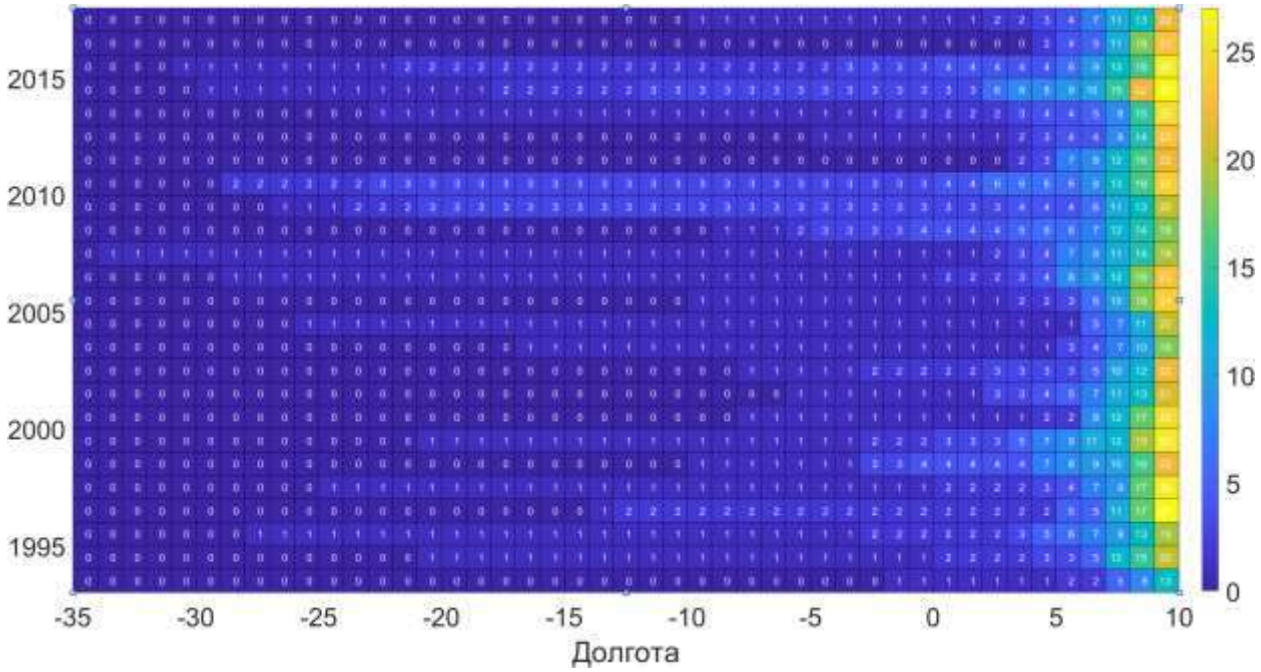

Figure 3.2. Eddy statistics for Agulhas leakage in the South Atlantic: values are shown on the scale and as numbers on the chart. The abscissa shows longitudes, and the ordinate shows time (1993–2017).

3.3. Co-location method

To study the vertical structure of mesoscale eddies, we used the co-location method described in Chapter 2. We managed to find six eddies that satisfied the selected conditions in the time interval 1993-2017, and their characteristics were further analysed to obtain the necessary estimates. The data for one mesoscale eddy that drifted westwards together with the Argo float (№. 6901635) are presented below as an example. The duration of the measurements of this Argo float was recorded during the period from 06.12.14 to 01.04.16 (482 days), and importantly, float №6901635 was captured by the eddy for the entire period, which allowed us to analyse the joint effects of the thermohaline characteristics of this eddy and its geometric and kinematic parameters. Figure 3.3 shows the geographical position of the float at the time of capture by the anticyclonic eddy (positive values of sea level anomalies).

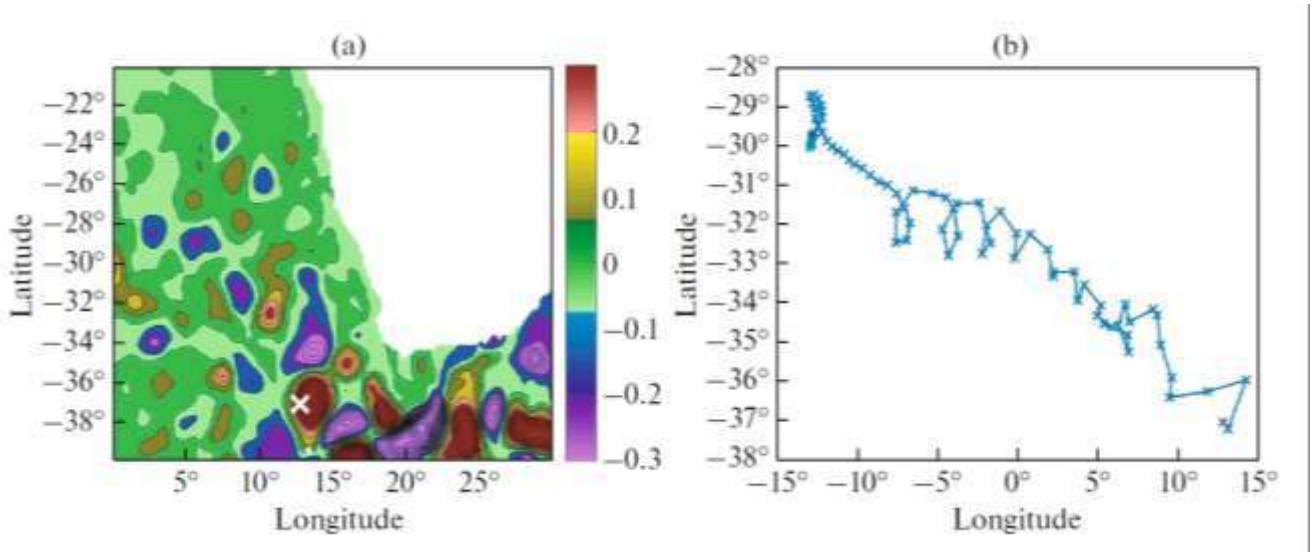

Figure 3.3. (a) Sea level anomalies (cm) according to satellite altimetry data as of December 6, 2014; the position of float no. 6901635 is shown with a cross. (b) The trajectory of the float's movement along the mesoscale eddy; the red cross marks the beginning of movement, and the black cross marks its end.

Table 1 shows the eddy parameters obtained from the Mesoscale Eddy Trajectory Atlas Product archive. Note that the mean values of the amplitude and velocity of the eddy movement are on average almost the same as at the initial moment the eddy was captured by the float, and the mean orbital velocity even exceeds the initial values. However, the radius of the eddy at the beginning of the period was slightly larger than average. This is not surprising since eddies generally lose their energy and gradually dissipate as they move.

Table 3.1. Parameters of the mesoscale eddy of the Agulhas leakage according to the "Mesoscale Eddy Trajectory Atlas Product" database

Characteristics	Average values for the period of existence	Values at the time the float was captured by the eddy
Time spent by the float in the eddy, days	482	482
Orbital velocity, cm/s	45	39
Amplitude, cm	15	14
Radius, km	98	112
Speed of travel, cm/s	8,5	8,5

Figure 3.4 shows the temporal variations in the salinity and temperature anomalies in the eddy. The anomalies were calculated using the WOA13 data for each point in time relative to the mean climatic values at the corresponding points of the eddy trajectory. The variability of the thermohaline characteristics from the moment of capture to the end of the float's presence in the eddy was nonstationary, and the values of the anomalies gradually decreased; however, it should be noted that in the given time interval, the mesoscale eddy was identified from both the "Mesoscale Eddy Trajectory Atlas Product" database and the anomalies of thermohaline characteristics. Figure 3.4 also shows that the eddy was approximately 1000 m deep, the maximum anomaly values occurred at depths of 500–700 m, and the salinity and temperature anomalies at these depths were greater than the mean climatic values by 0.6 and 5°C, respectively. The core of the eddy, which was located at depths of 300–700 m, was traced in the anomalies over the first two months when the float was captured by the eddy. It is important to note that the mesoscale eddy retained its characteristics for a long period of time (approximately 8 months), after which its intensity decreased and the eddy gradually dissipated.

Figure 3.4 shows the eddy anomalies, the positive values of which confirm that the thermohaline characteristics of the eddy are different from those of the surrounding water. Let us confirm this fact using T/S analysis. Figure 3.5 shows a comparison of the T/S characteristics of the Agulhas leakage eddy with the average T/S characteristics of the surrounding waters. All the profiles of the float have a homogeneous structure. This indicates that the same water mass was transported by the eddy that captured the float, and mixing with the surrounding waters was insignificant. The eddy has a temperature of 5°C and a salinity of 0.8-1.0 above the average background water temperature. This means that the considered eddy indeed transports warmer and saltier waters to the South Atlantic and maintains different properties from the environment for a long time.

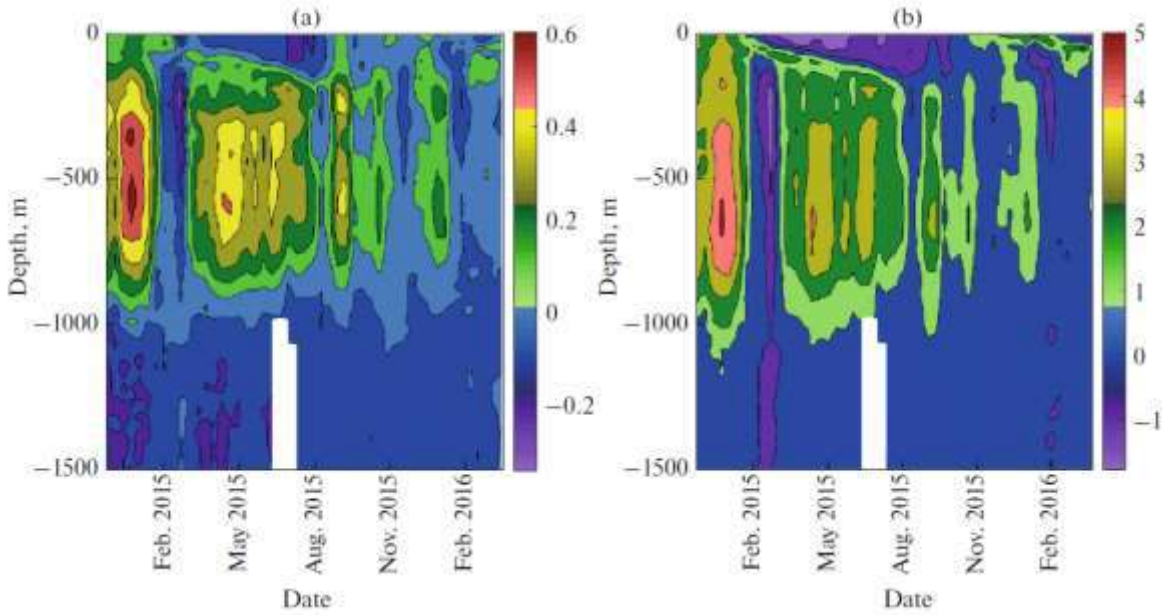

Figure 3.4. Temporal variability of (a) salinity and (b) temperature (°C) anomalies in the eddy, according to the data from float № 6901635.

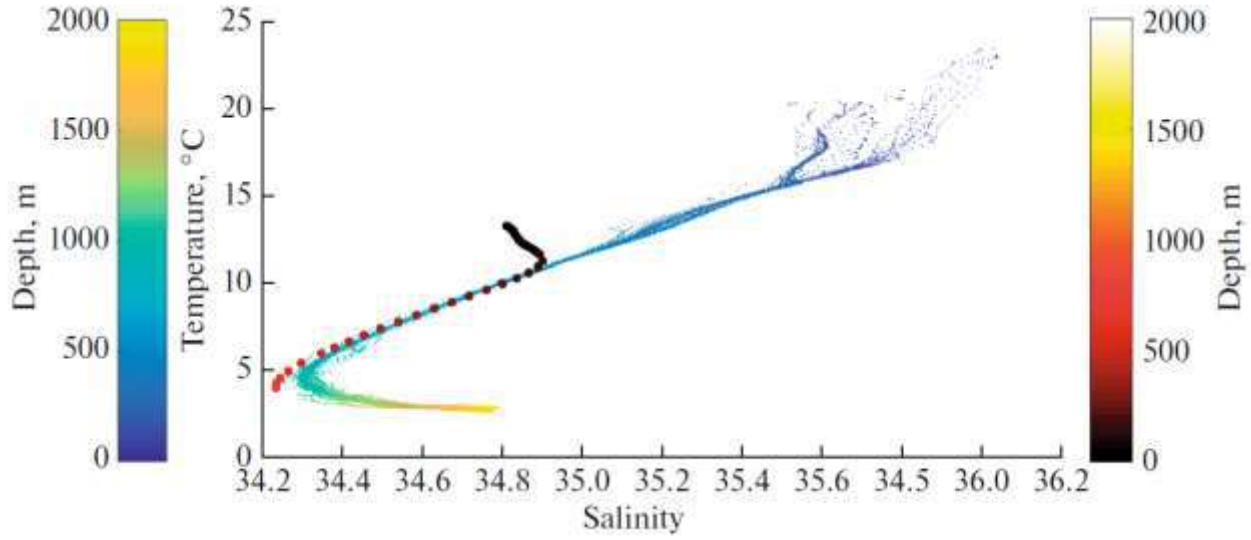

Figure 3.5. Comparison of the eddy T/S curves (i.e., profiles of float № 6901635 (blue) and surrounding waters (red)). The color marks the depth of the point on the profile with the corresponding characteristics.

The above analysis was performed for six selected Agulhas leakage eddies satisfying the joint analysis criteria. The values of the average characteristics necessary for calculating the eddy transport of heat and salt were obtained. Considering the average

parameters of the selected eddies (in the calculations, the eddy radius is 50 km, the depth is 1 km, and the transport velocity is 8.5 cm/s) and following the approach proposed in Chaigneau et al. (2011), the transport estimate (flow rate) is 8.5 Sv.

Next, we estimated the heat content (AT) and salt content (AS) in the eddy volume V (Chaigneau et al., 2011). The calculation of the heat and salt contents in a single Agulhas leakage eddy is described in Chapter 2. The resulting estimates are presented in Table 3.2. Note that these estimates are averages and characterize the eddy transport by a single eddy. Using the data in Table 3.2 and the eddy statistics presented in Figure 3.2, we can estimate the corresponding estimates of Agulhas leakage for each longitude of the South Atlantic by multiplying these estimates by the number of eddies. In particular, for 34°W, the Agulhas leakage estimates are the same as those presented in Table 3.2, and for 30°W, they are 2 times greater. We emphasize once again that we are discussing the average Agulhas leakage estimates of heat and salt transport by mesoscale eddies.

Table 3.2. Estimates of the heat and salt contents in the volume of a mesoscale eddy and the corresponding heat and salt transport associated with Agulhas leakage by one eddy

Eddy characteristics	Values
Heat content, *AT*, J	2.03×10^{15}
Salt content, *AS*, kg	4.83×10^{11}
Heat transport, *HT*, W	2.25×10^{9}
Salt transport, *ST*, kg s^{-1}	5.36×10^{5}

3.4. Lagrangian analysis of Agulhas leakage in the mixing zone of three water types

In the Cape Basin, after leaving the area of formation, the Agulhas rings rapidly disintegrated to form smaller-scale eddies (mesoscale eddies) (Duncombe Rae, 1991; Gordon & Haxby, 1990; Lutjeharms & van Ballegooyen, 1988; Olson & Evans, 1986a, 1986b), which are the main contributors to Agulhas leakage. As a result of ring collapse, Agulhas waters mix with those of the South Atlantic Gyre and the Benguela Current, which extends northwards along the west coast of South Africa (Hutchings et al., 2009). Although

there is no consensus on the exact contribution of Agulhas waters to the Benguela Current, there is a correlation between the strength of the Benguela Current and the eddy transport of the Agulhas Current (Garzoli & Gordon, 1996). Moreover, Matano and Beier (2003) found that most of the energy of the Benguela Current is provided by Agulhas eddies; i.e., the Benguela Current can be considered a vehicle for the transport of Agulhas eddies into the Atlantic Ocean. However, it cannot be denied that the structure of eddies that formed in the Cape Basin is also significantly influenced by the waters of the South Atlantic circulation (Fig. 1.2).

Thus, there is a basin off the southwestern coast of South Africa where the Agulhas eddies interact with the waters of the South Atlantic Gyre and the Benguela Current. Guerra et al. (2022) considered temperature and salinity profiles from 1993 to 2016; moreover, they analysed more than 3200 temperature profiles and 2400 salinity profiles from historical databases and compared them with 52 long-lived Agulhas eddies. This analysis revealed that in 88% of the cases, all the profiles could be attributed to two types of water: type I, temperature 16.2 ± 0.6° C, salinity 35.6 ± 0.1; and type II, temperature 12.9 ± 0.7°C, salinity 35.2 ± 0.1. We believe that the first type of water is formed by the warm and salty waters of the Agulhas Current, which carry the properties of the Indian Ocean, while the second type is formed by the cold and fresher waters of the South Atlantic Gyre and the Benguela Current. However, both types of water were simultaneously detected inside the majority of eddies that formed in the Cape Basin (67%) (Guerra et al., 2022).

Thus, not only the Agulhas Current eddies but also the eddies directly formed in the Cape Basin transport the waters of the Agulhas leakage to the Atlantic (Fig. 3.6). They play an important role in the interoceanic transfer of heat, salt, and mass. The interaction of the Agulhas eddies with the waters of the South Atlantic Gyre and the Benguela Current is a unique process and is not found in any other major system of eastern boundary currents.

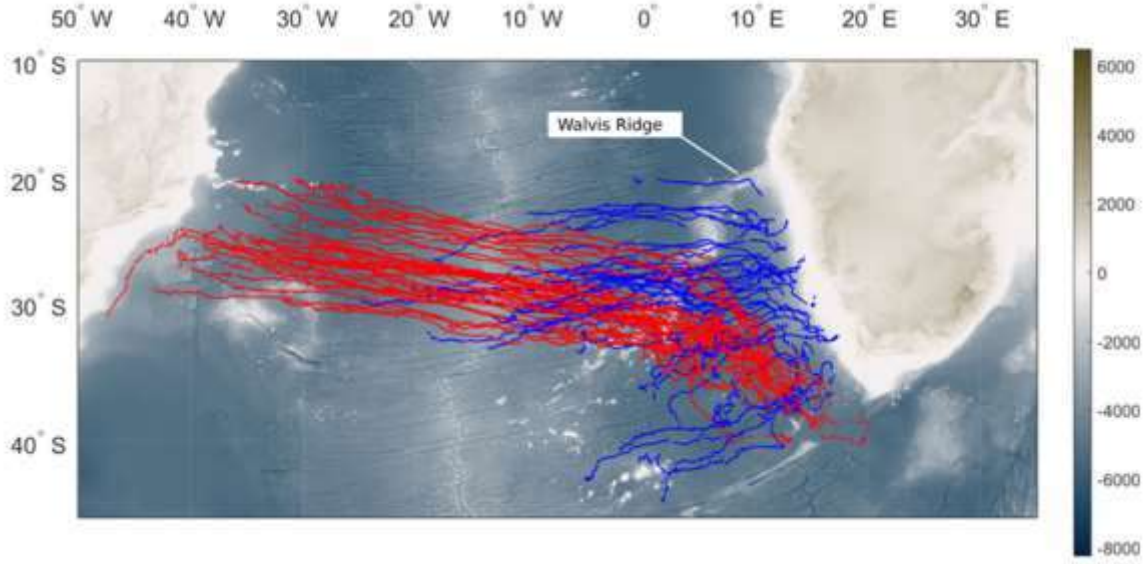

Figure 3.6. Tracks of 40 long-lived individual anticyclones (red) and 40 long-lived cyclones (blue) identified by META3.2 for 1993–2021. The color scale shows the depth (m).

3.4.1. Statistical analysis of mesoscale eddies

Using META3.2 for the study region (20–46° S, 0–24° E), we detected 54,496 eddies in the Agulhas Current from 1993–2017, 28,018 of which were cyclones and 26,478 were anticyclonic. Only anticyclones are long-lived eddied of the Agulhas Current, with lifetimes exceeding one year. The tracks of Agulhas anticyclones with lifespans > 2.5 years in the South Atlantic were analysed by Gnevyshev et al. (2021). Tracks of 40 long-lived individual anticyclones and 40 long-lived cyclones identified by the automatic identification method are shown in Fig. 3.6. It can be seen that the eddies move to the west, but the tracks of the anticyclones tend to deviate to the equator, while the cyclones turn to the south. The physical mechanisms of this phenomenon are discussed by Gnevyshev et al. (2021).

We divided the region under consideration into three zones: (I) 34-45° S, 0-13° E; (II) 34-45° S, 13-24° E; and (III) 20-34° S, 0-24° E (Fig. 3.7), considering different places of eddy generation and providing statistical analysis for each individual zone. We consider only long-lived eddies with lifetimes > 60 days.

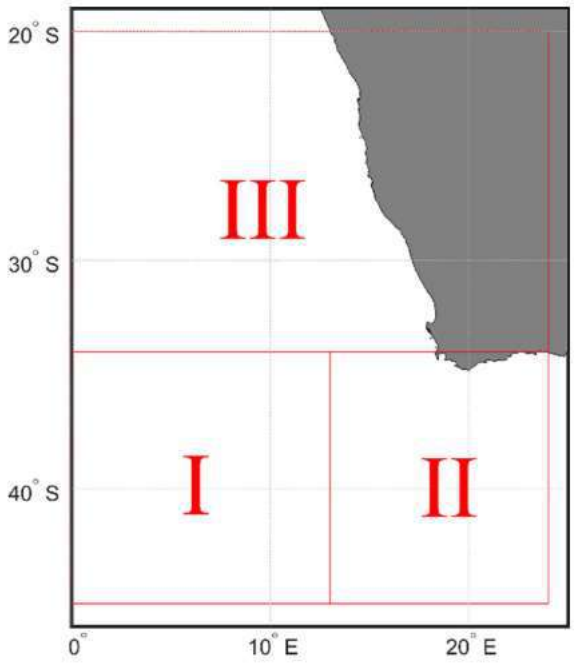

Figure 3.7. Zones under consideration.

Note that eddies in the three zones differ in terms of their generation mechanisms. In Zone I, located in the southwest part of the region, eddies are generated due to the barotropic and baroclinic instability of the branches of the South Atlantic Gyre. The places at which eddies are generated and dissipated are mainly limited by the area boundaries. In Zone II, located in the southeastern part of the region, eddies are generated due to the decay and destruction of the Agulhas rings and are associated with Agulhas leakage. The trajectories of these eddies extend to the northwest and are much longer than those in Zone I. Finally, Zone III is located in the northwestern part of the region. The trajectories of the eddies generated there are directed mainly to the west. These eddies contain Indian Ocean waters due to mixing with waters from Agulhas leakage. Figure 3.8 shows the main features of these groups of eddies. Note that the zonal eddy displacement and, accordingly, the zonal component of the velocity dominate since this is facilitated by the influence of the β-effect. Eddies propagate almost rectilinearly. Under the influence of topography, especially when crossing the Walvis Ridge, the paths change the propagation azimuth, after which eddies propagate rectlinearly again. We also indicate the tendency of anticyclone tracks to shift to the equator and cyclones to the south. The effect shown in Fig. 1 was reported earlier by Gnevyshev et al. (2021).

The numbers of anticyclones (*Ac*) and cyclones (*Cyc*) for the period 2009-05-31 to 2020-05-30 in the three zones are shown in Table 3.3. Then, we performed a statistical analysis.

Table 3.3. The numbers (N) of anticyclones (*Ac*) and cyclones (*Cyc*) with lifetimes > 60 days in the three zones with area S and the ratio of N to area S (see Fig. 3.7)

Areas (S, km2) of Zones I-III	N (*Ac*)	N\S (*Ac*) × 10^{-4}	N (*Cyc*)	N\S (*Cyc*) × 10^{-4}
I (1356 ×10^3)	259	1.91003	267	1.96903
II (1147.3 ×10^3)	159	1.38586	156	1.35971
III (2468.1 ×10^3)	390	1.58016	424	1.71792

Note that Zone III contains the largest number of both *Ac* and *Cyc* individuals. However, Zone III also exceeded zones I and II. The largest number of eddies per unit area occurs in Zone I, where the waters of the South Atlantic Gyre interact with the waters of Agulhas leakage.

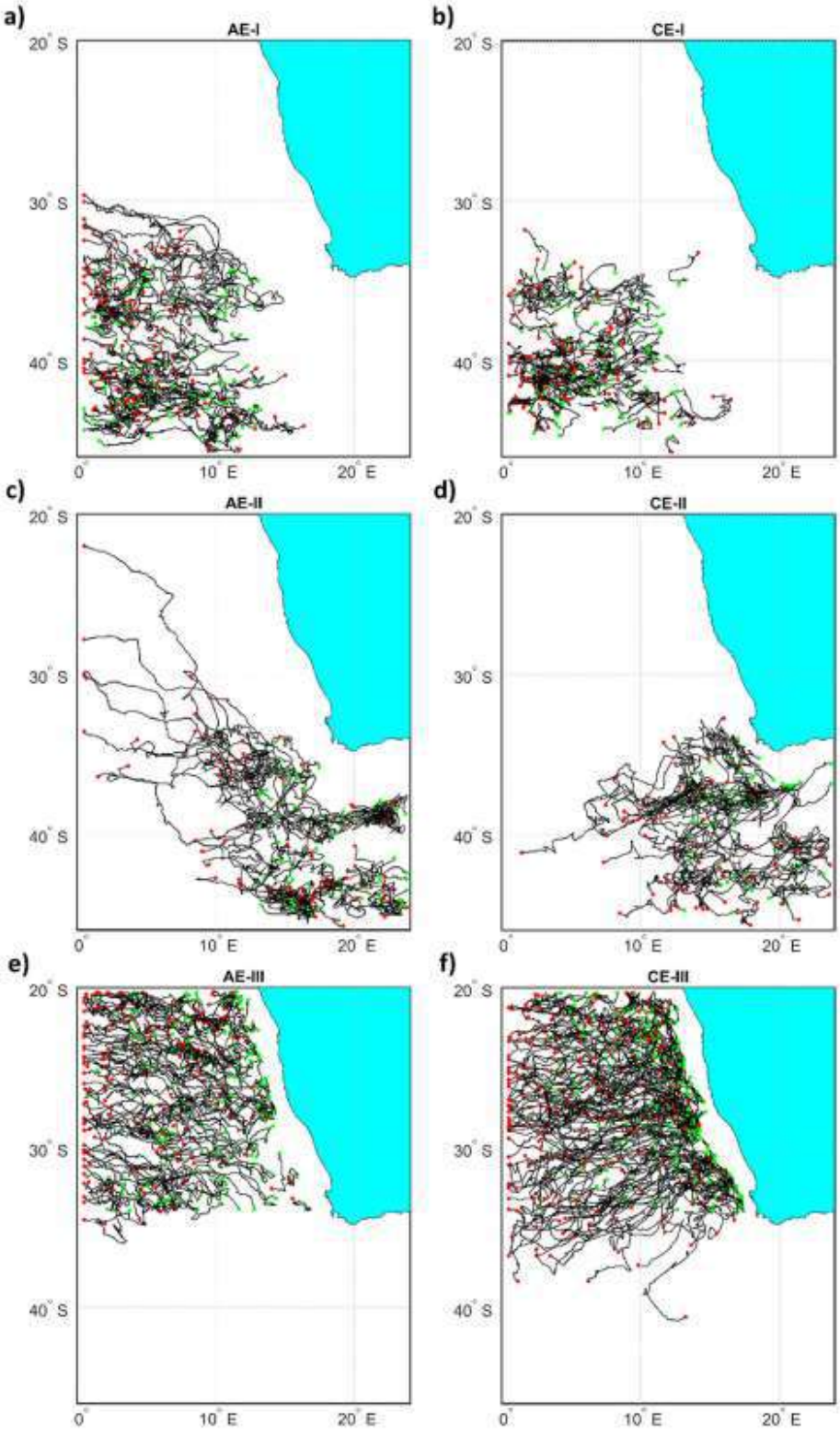

Figure 3.8. Trajectories of the individual eddies in Zones I (a, b), II (c, d), and III (e, f). Anticyclones are shown on the left, and cyclones are shown on the right. The places at which eddies are generated are shown by green points, and red points indicate the places at which eddies are dissipated. Only eddies with lifetimes greater than 60 days are considered.

Since AMEDA allows one to detect eddy centers and their characteristic contours as well as dynamical features associated with eddies, we can estimate the integral square (km^2) of eddy contours. Using AMEDA, we provide the distributions of various characteristics for eddies generated in Zones I–III. In Fig. 3.9, we consider contours for individual eddies with a time step for the data used, i.e., one day of the GLORYS12V1 data. A contour is a daily image of an eddy. If an eddy lives for 100 days, then we have 100 contours; if 10 eddies have a lifetime of 100 days, we have 1000 contours. We estimate an eddy contour area. Figure 3.9 indicates that the integral area for *Ac* is much larger than the integral area for *Cyc* despite the number of individual *Cyc* having a lifetime of more than 60 days exceeding the number of long-lived *Ac*. This illustrates that the number of contours of *Ac* significantly exceeds the number of contours of *Cyc*; hence, the integral area of *Ac* contours is larger than the integral area of *Cyc* contours.

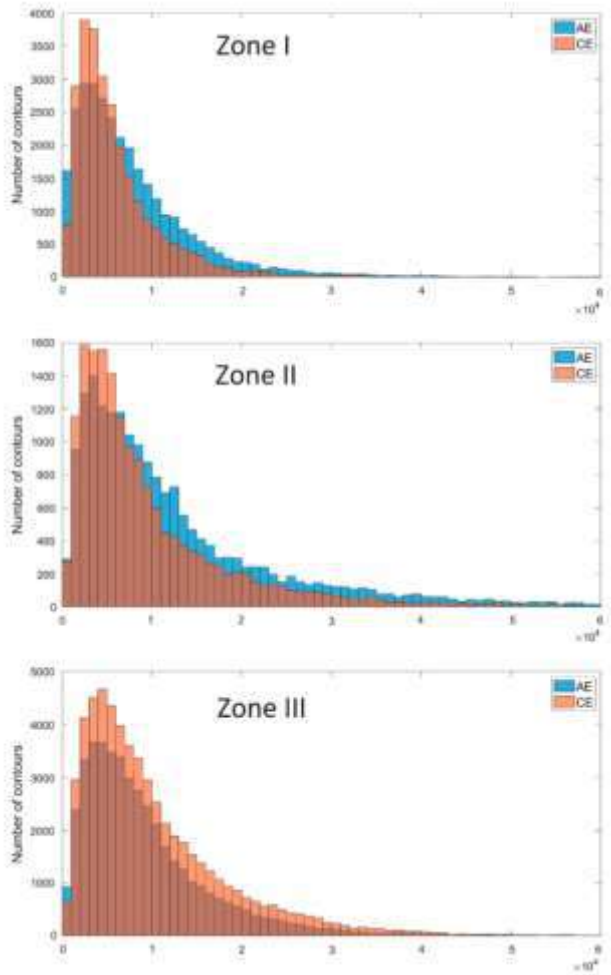

Figure 3.9. Distribution of the integral area (km^2) of eddy contours for *Ac* and *Cyc* in Zones I–III. The dark brown color corresponds to the combination of light brown (for *Cyc*) with blue (for *Ac*).

The other characteristics of the eddies in Zones I-III are shown in Figures 3.10-3.15. The scales (diameters) of *Ac* in Zone I are slightly larger than those of *Cyc*, but in general, the scales are comparable for *Ac* and *Cyc*. The radii of most of the eddy contours are 40–50 km (see Fig. 3.10).

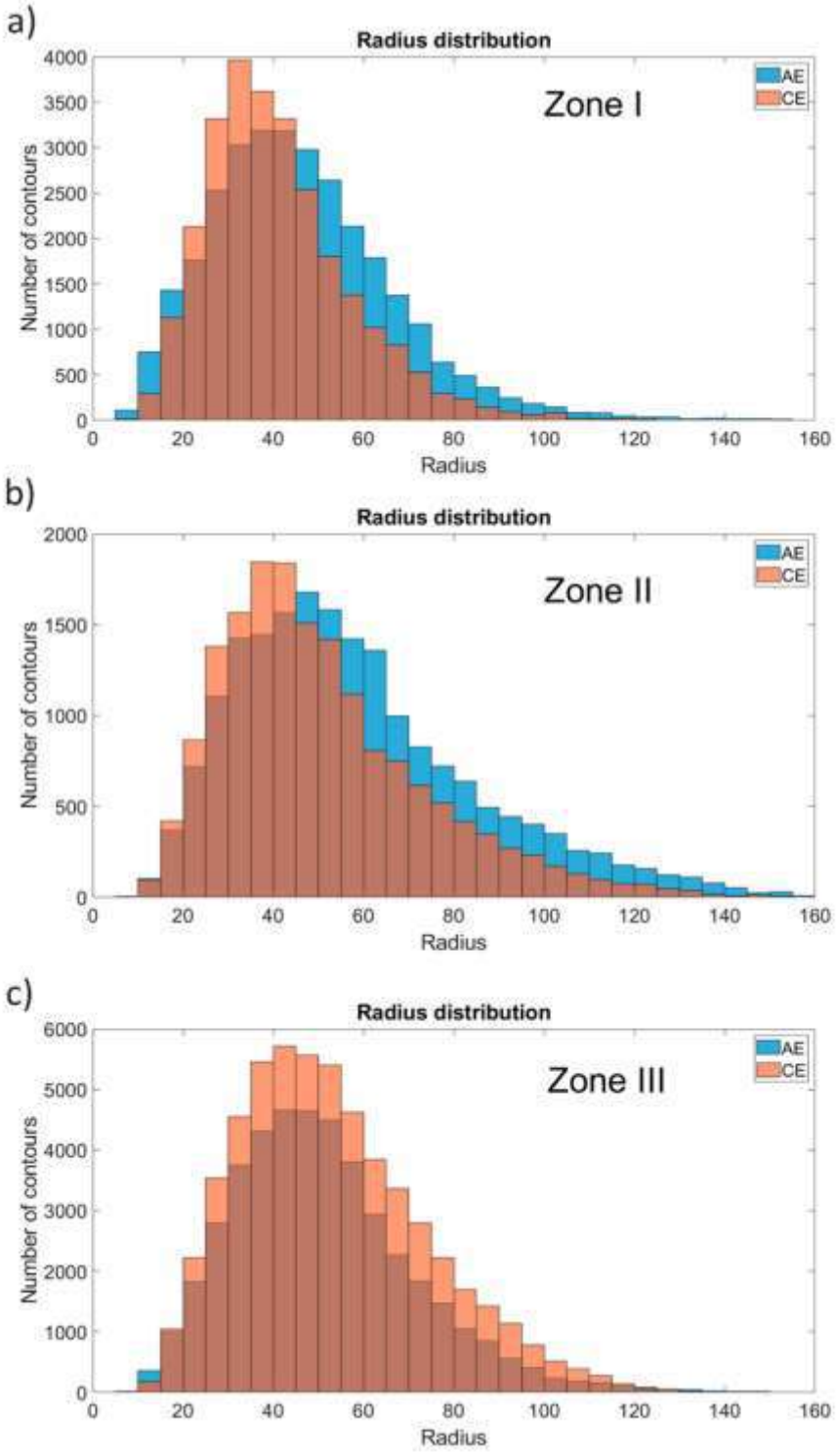

Figure 3.10. Distributions of eddy radii (km) for *Ac* (blue) and *Cyc* (light brown).

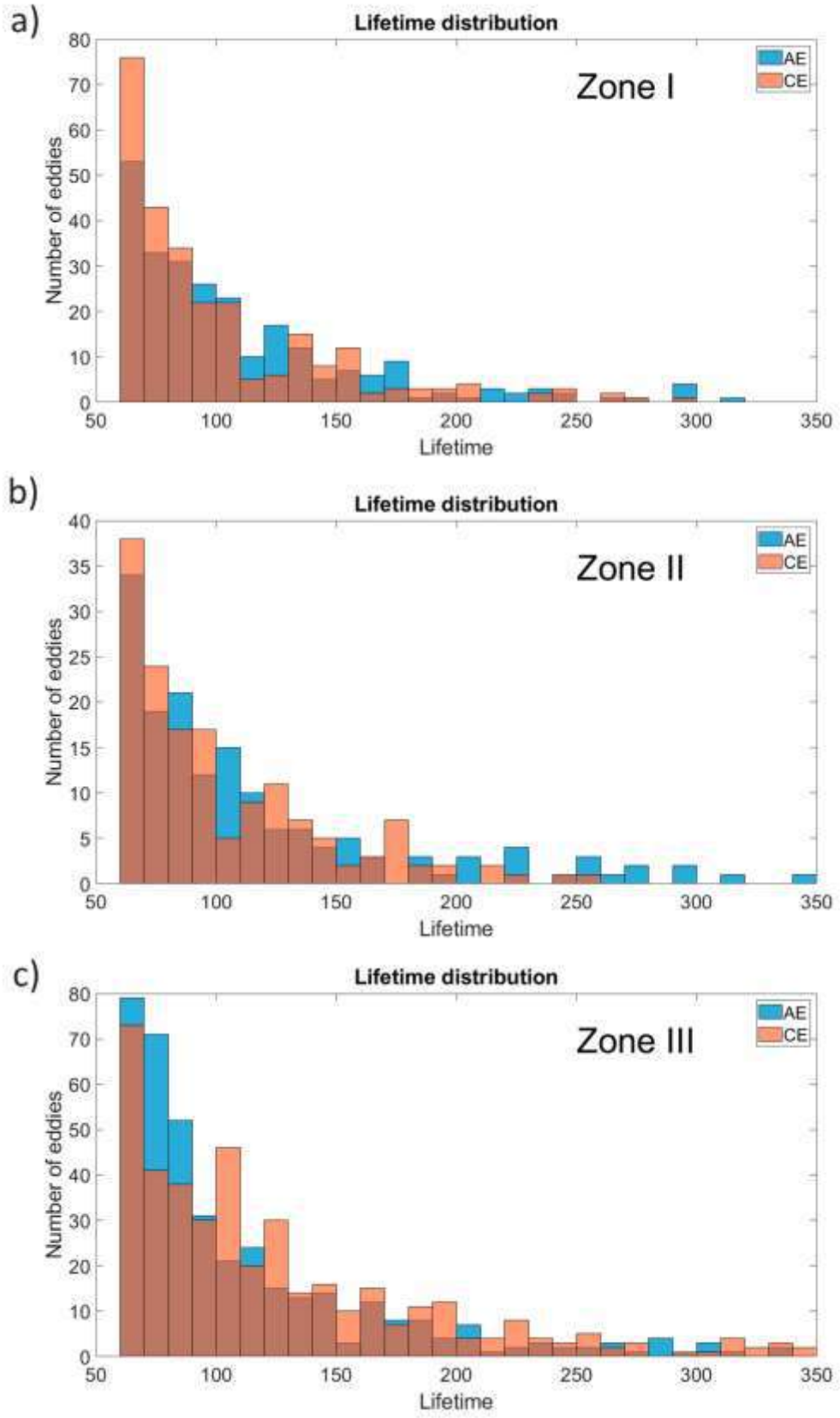

Figure 3.11. Distribution of lifetime (days) for *Ac* (blue) and *Cyc* (light brown).

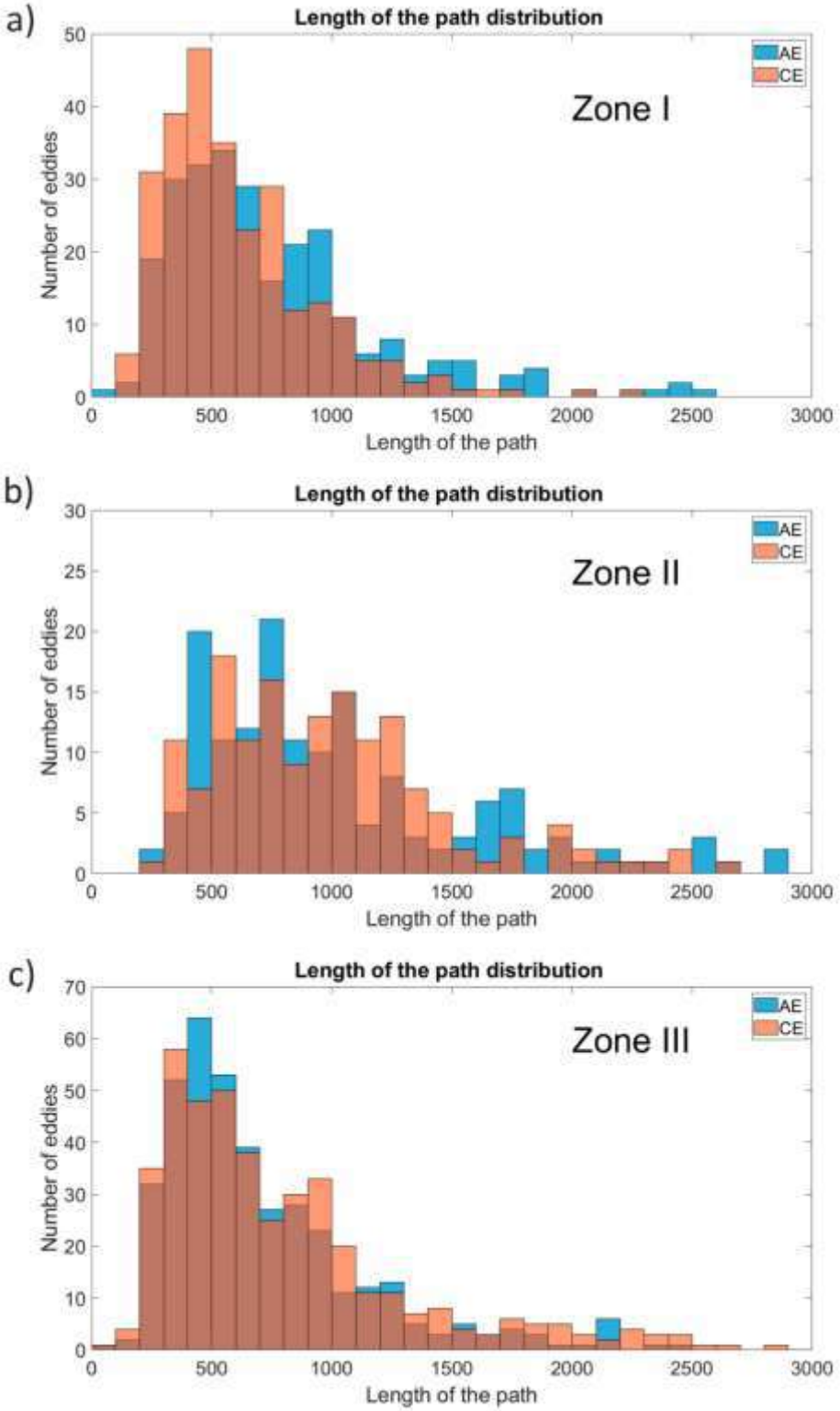

Figure 3.12. Distribution of path lengths of individual eddies (km) for *Ac* (blue) and *Cyc* (light brown).

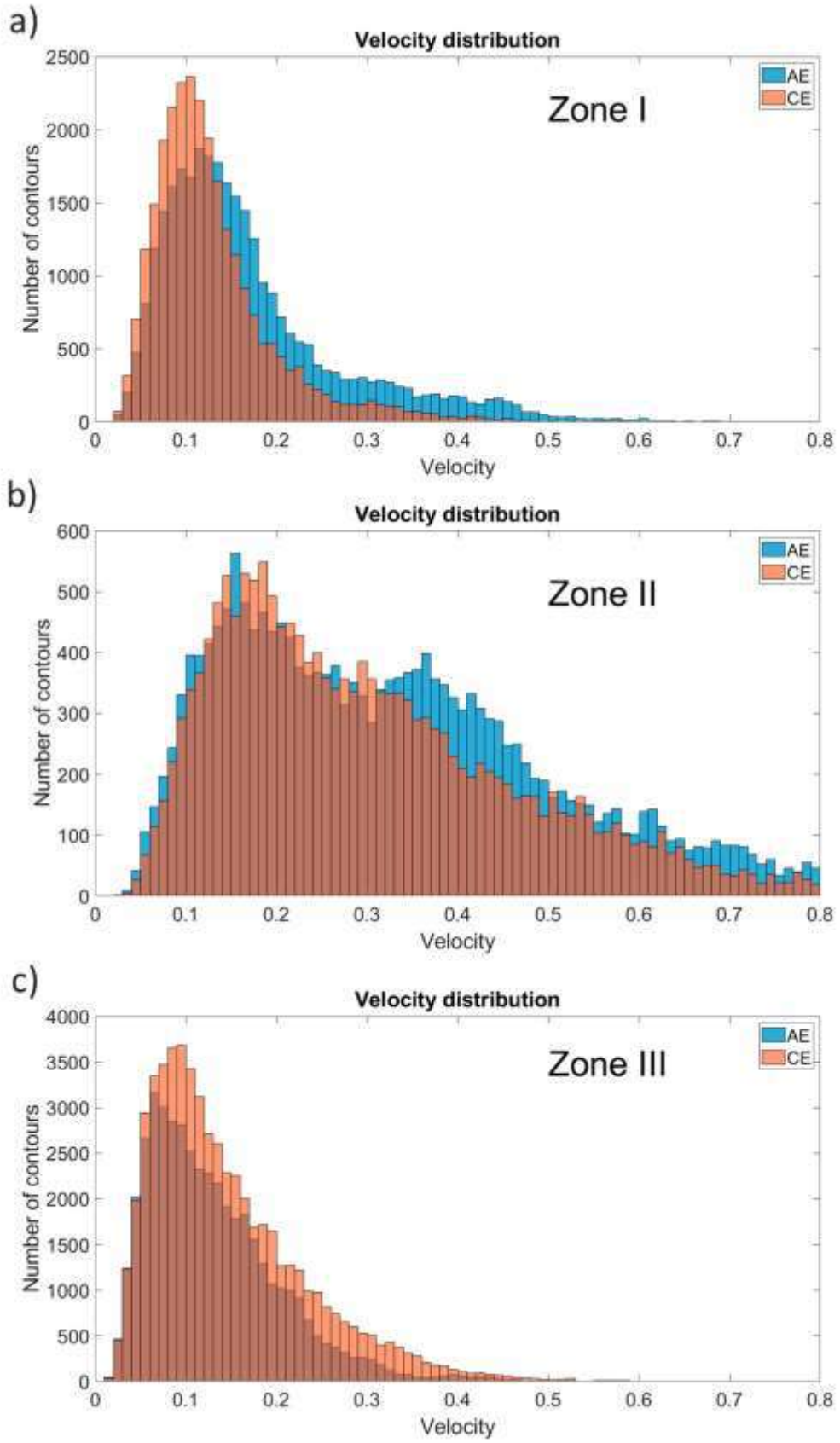

Figure 3.13. Orbital velocity distributions (m/s) for *Ac* (blue) and *Cyc* (light brown).

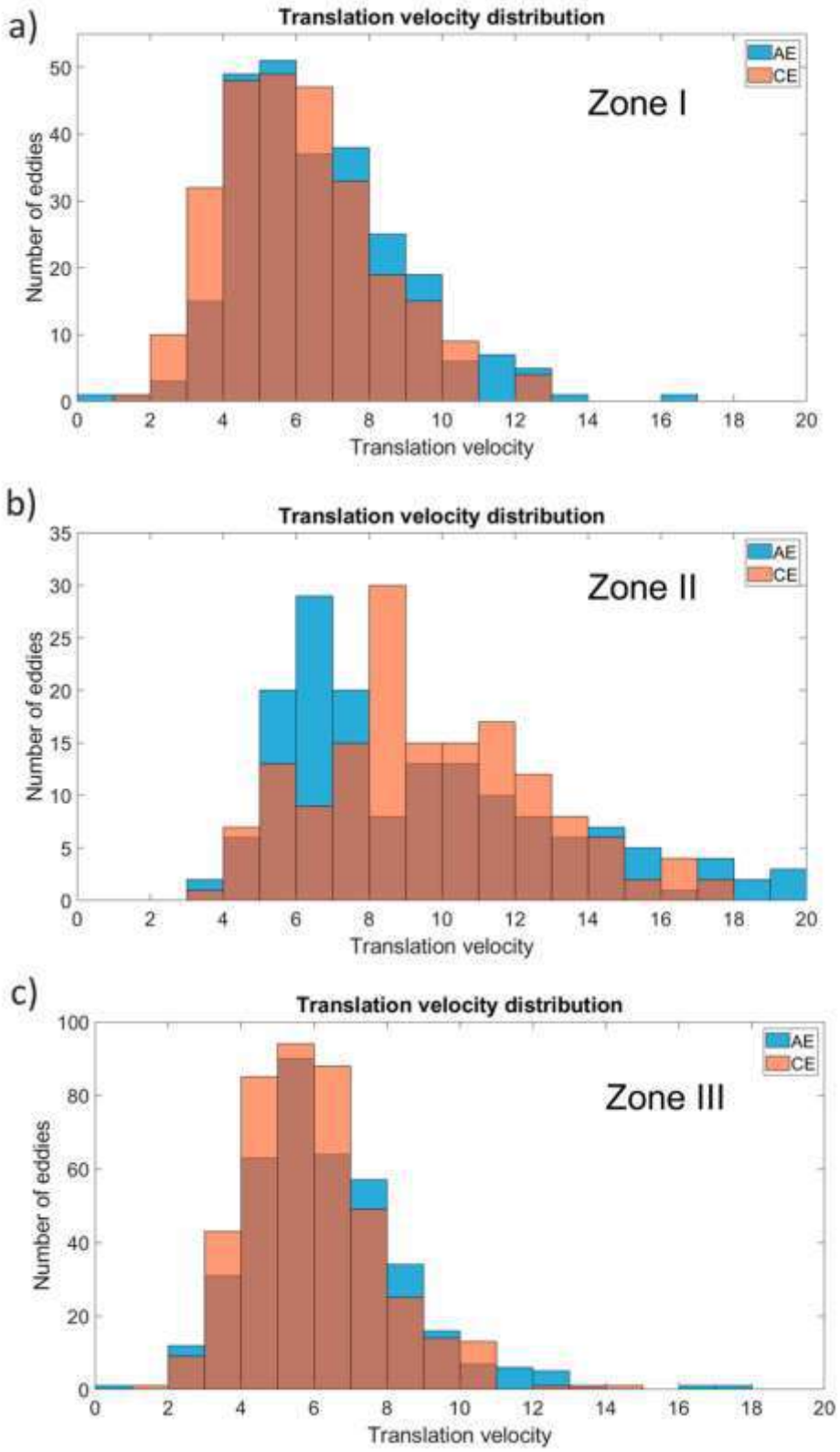

Figure 3.14. Drift rate distributions (km/day) for *Ac* (blue) and *Cyc* (light brown).

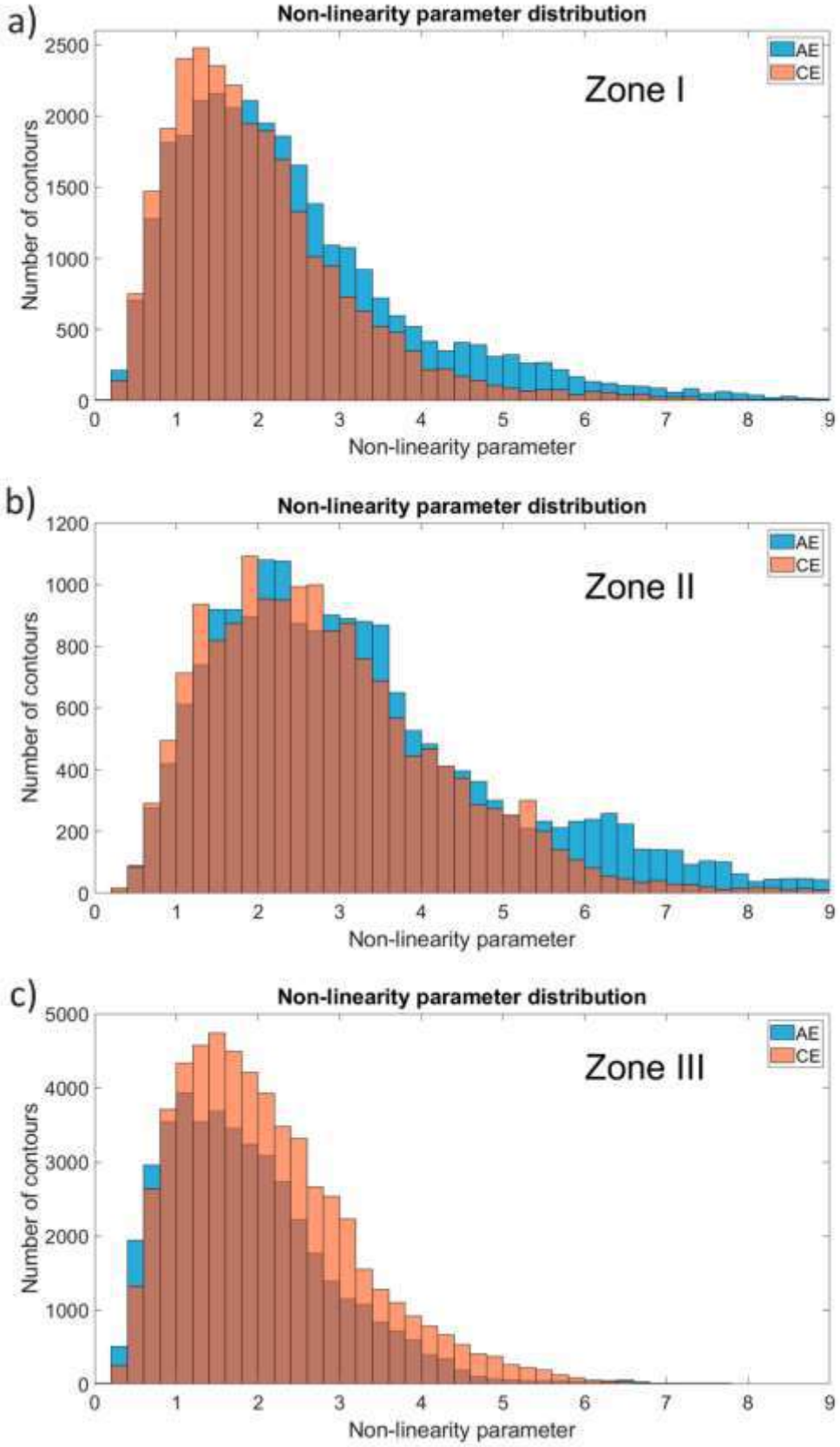

Figure 3.15. Distribution of the nonlinearity parameter for *Ac* (blue) and *Cyc* (light brown).

The distribution of eddy lifetimes confirmed that *Ac* was longer than *Cyc*. Note that we considered the eddy lifetimes only within the considered zones. Most eddies located in these zones have lifetimes of less than 100 days. However, some eddies in zones II and III have lifetimes longer than 500 days (Figure 3.11). Accordingly, these individual eddies have the longest path lengths (Figure 3.12). The mean orbital velocities range mainly from 0.05 to 0.5 m/s for both *Ac* and *Cyc*. However, the mean orbital velocities are greater in zone II, where many eddies are formed due to the destruction of large Agulhas rings (Fig. 3.13). The drift velocities are 3-13 km/d (3-15 cm/s) for both *Ac* and *Cyc*. The drift velocities of *Ac* are slightly greater than those of *Cyc* in all three zones (Fig. 3.14). Finally, the distribution of the nonlinearity parameter (the ratio of the orbital velocity of the eddy to its velocity of motion) shows significant nonlinearity (Fig. 3.15).

3.4.2. Lagrangian analysis of water particles

Based on the GLORYS12V1 data, we provide a Lagrangian analysis of the water particles. We consider a region limited by 20-46°S, 0-20°E, which includes the Cape Basin. We perform an analysis of Lagrangian maps at a depth of 266 m. This depth makes it possible to exclude the influence of wind and other surface effects, but at the same time, this depth makes it possible to identify the cores of mesoscale eddies located within a layer of 150–800 m (Malysheva et al., 2022; Sandalyuk & Belonenko, 2021). We analysed 7 types of daily Lagrangian maps for the period from May 2010 to April 2020. Furthermore, we consider the main Lagrangian indicators calculated for the region under consideration. Below, we present Lagrangian maps for only certain dates.

Figure 3.16 shows the map of particle motion (S-map) for 2013-09-04. The Lagrangian modelling method identifies many cyclones and anticyclones in the region under consideration on the current date. Those eddies that are characterized by large lengths of particle trajectories are highlighted in black. These particles rotate relative to the centers with significant orbital velocities. In other words, a large trajectory length (and the black color of the points) corresponds to the particles that rotate in an eddy or are carried by a jet stream. According to the scale, the maximum saturated black color corresponds to a trajectory length of 700 km. Figure 3.16 shows a band of eddies, mainly anticyclones, that

extend from the southern tip of Africa in the direction of the northwest. This phenomenon is a manifestation of Agulhas leakage on the presented S-map.

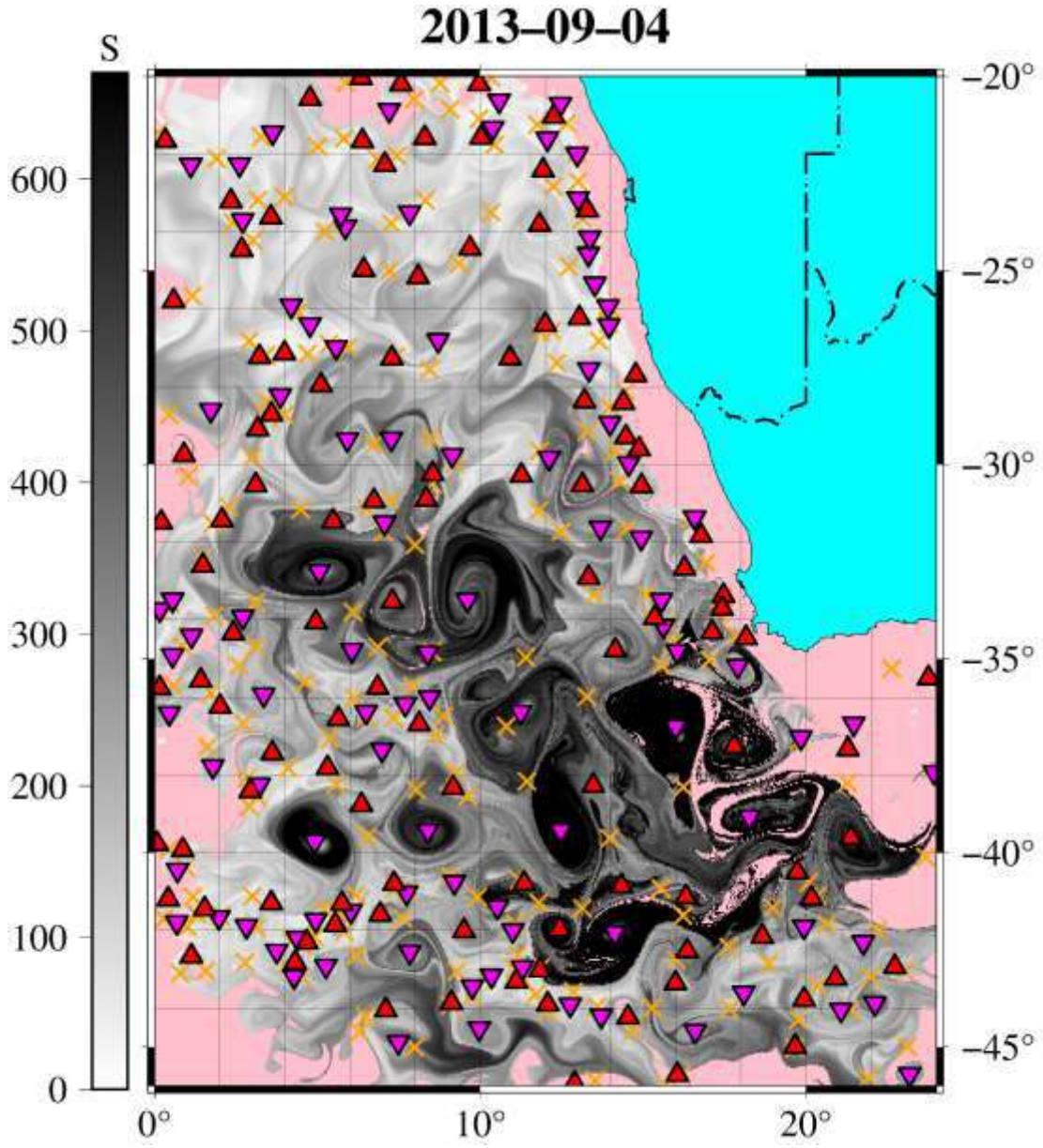

Figure 3.16. A map of particle motions (Lagrangian S-map) on September 4, 2013, at a depth of 266 m. The black color corresponds to the length of the trajectory that each point (water particle) passed in km 30 days earlier than the date indicated in the title. The pink colour corresponds to points belonging to one of two types of water: the first are those points that touched the mask of the shore (or the contour of the shelf), and the second are those points that reached the edges of the selected box of the velocity field in the past. The triangles represent elliptical points: red triangles represent the centers of cyclones shown as filled upwards triangles, and crimson triangles represent the centers of anticyclones

shown as filled downwards triangles. The orange crosses show the hyperbolic points, which are points of instability.

Figure 3.17 shows the origin map (O-map) for the region under consideration. The O-map shows the Lagrangian particles, which are distributed at a depth of 266 m. The green color corresponds to the water particles associated with Agulhas leakage. This band of points on the western side of Africa extended to the northwest. These waters of the Agulhas Current formed in the Indian Ocean and subsequently crossed 24°E. The yellow color characterizes the particles that crossed 46°S during the last year. These particles can reveal the southern part of the South Atlantic Gyre where south-easterly winds cause currents to flow to the east, which is difficult to distinguish from the northern boundary of the Antarctic Circumpolar Current. The influence of the Antarctic Circumpolar Current is limited to the southern part of the region. The red color characterizes the particles that crossed the prime meridian during the last year. These water particles arrived from the west and may have originated from the South Atlantic Gyre and affected both the Agulhas leakage and the Benguela Current. The blue color refers to the particles of the Angola Current. Figure 3.17 shows that the influence of the Angola Current is limited to only the northern part of the region. There are many white points distributed throughout the region in Fig. 3.17. These values correspond to the particles that for 1 year of counting in reverse time could not reach any of the boundaries of the region or coastline.

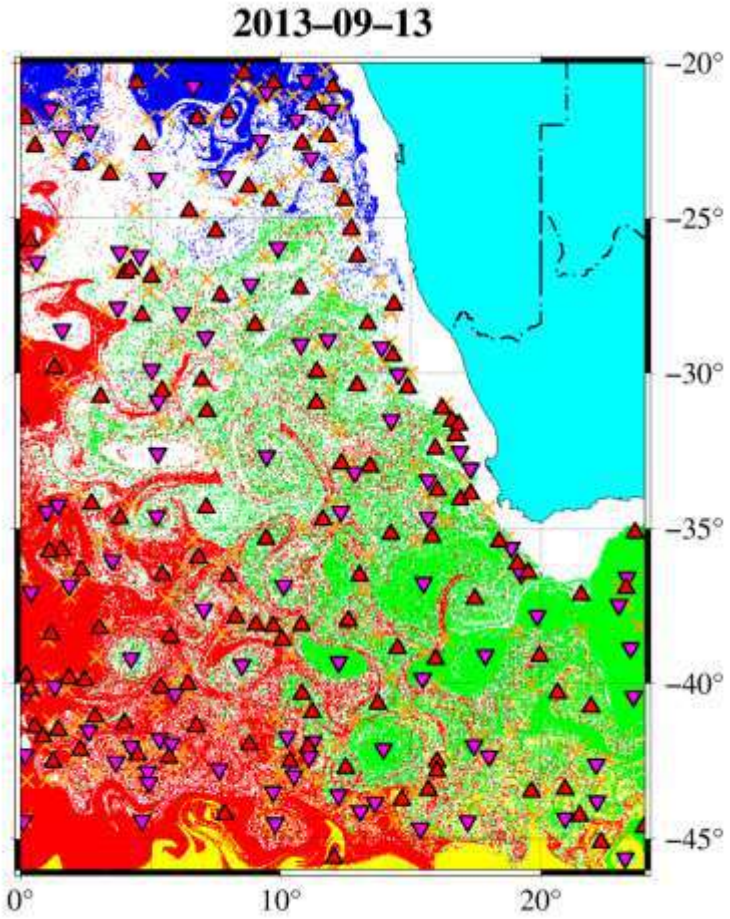

Figure 3.17. The map of the origin of water masses (Lagrangian O-map) on September 13, 2013, at a depth of 266 m. The points are colored green for the water particles that crossed the meridian 20°E 365 days ago from this date; yellow is for the particles that crossed 46°S within a year ago from this date; red is for the particles that crossed the 0 meridian; and blue is for the particles that crossed 20°S. The white colour represents the mask of the shelf from the boundaries of the intersection of the bottom at a depth of 266 m and the coastline on the surface and represents the particles that have not crossed any of the boxing borders. The triangles represent elliptical points: red triangles represent the centers of cyclones shown as filled upwards triangles, and crimson triangles represent the centers of anticyclones shown as filled downwards triangles. The orange crosses show the hyperbolic points, which are points of instability.

Figure 3.18 complements the O-map showing ‘‘the age’’ of the water particles. The T-map shows the period when the particle crosses one of the borders of the area. On the scale, black represents water particles that crossed the border of the region 1–30 days ago, gray represents those that crossed 100–200 days ago, and white represents those that crossed

200–365 days ago from the given date. This means that the waters shown in black are ‘‘young waters’’ that recently arrived in the region. In contrast, white indicates ‘‘old waters’’. A large number of water particles have not left the region during the past year. Figure 3.18 shows that ‘‘young waters’’, i.e., particles with short residence times in the region, correspond to the main circulation elements, which include the Agulhas leakage, Antarctic Circumpolar Current, Benguela Current, and Angola Current. Moreover, a large number of particles in the region do not differ in any significant mobility, and they are painted white in Fig. 3.18.

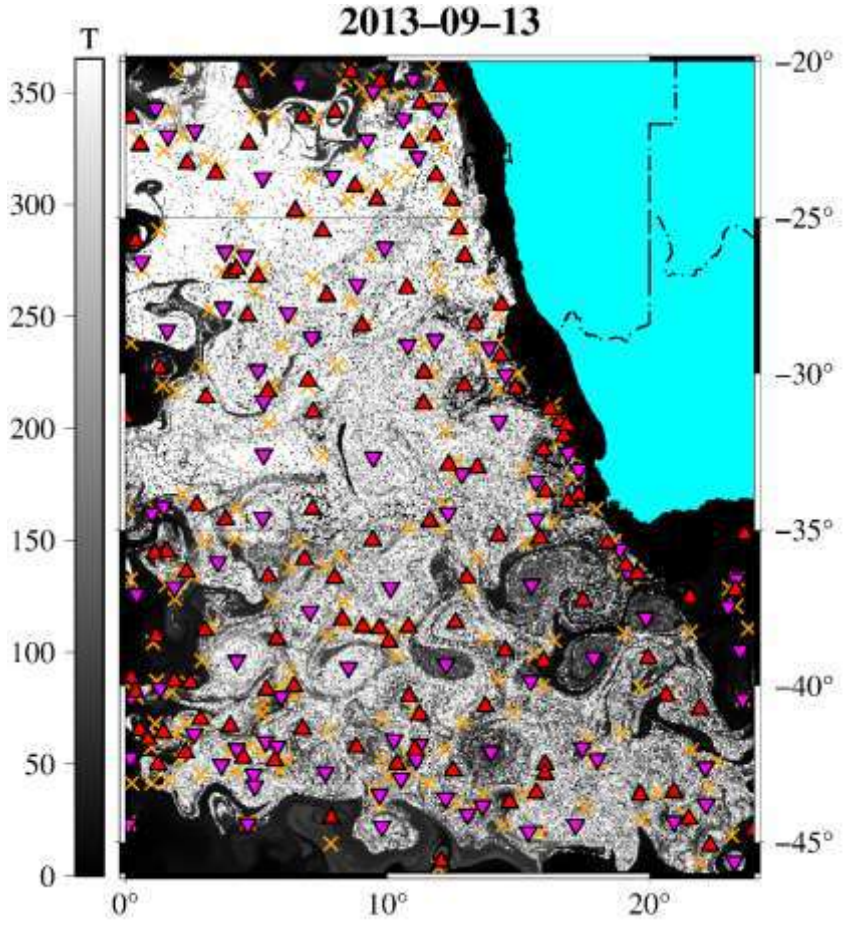

Figure 3.18. Particle ‘age’ map (Lagrangian T-map) on September 13, 2013, at a depth of 266 m. The color shows the time interval between the launch of particles on the specified date and the moment when one of the boundaries of the area is reached. In other words, the scale shows the time T at which the corresponding border of the region was reached within a year ago from the date indicated on each frame map. The white color indicates the points that were within the borders of this region during the year from this date or at the time of the launch of the markers on the shelf. The triangles and crosses are the same as in the previous figures.

Figures 3.19 and 3.20 demonstrate the zonal and meridional displacement of the water particles, respectively. These figures show that the main and most important element of circulation in the area under consideration is Agulhas leakage, but it is influenced by the waters that arrived from the west. The particles cross the western border of the study area, travel eastwards at distances exceeding 2700 km during the year and mix with other particles. Simultaneously, other particles travel in the opposite direction westwards, overcoming a distance of more than 1100 km (Fig. 3.19). In the north

In addition, the distance travelled by the particles during the year exceeded 2200 km and 1100 km southwards (Figure 3.20). Thus, the dominant direction of the particles involved in water mixing is the northeast.

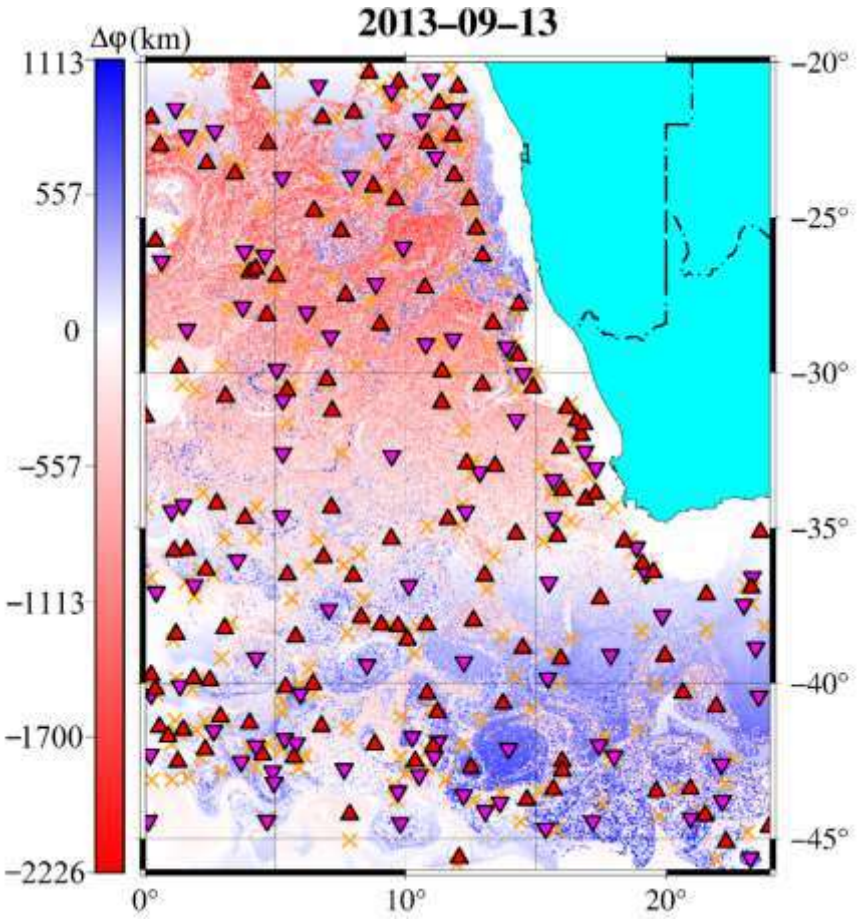

Figure 3.19. Zonal displacement of the particles on September 13, 2013, at a depth of 266 m. The scale indicates the zonal displacement (in km), which is the displacement of water particles eastwards/westwards within 365 days from this date. Red (negative values) highlights the waters that have shifted eastwards, and blue (positive values) indicates the waters that have shifted westwards. The triangles and crosses are the same as in the previous figures.

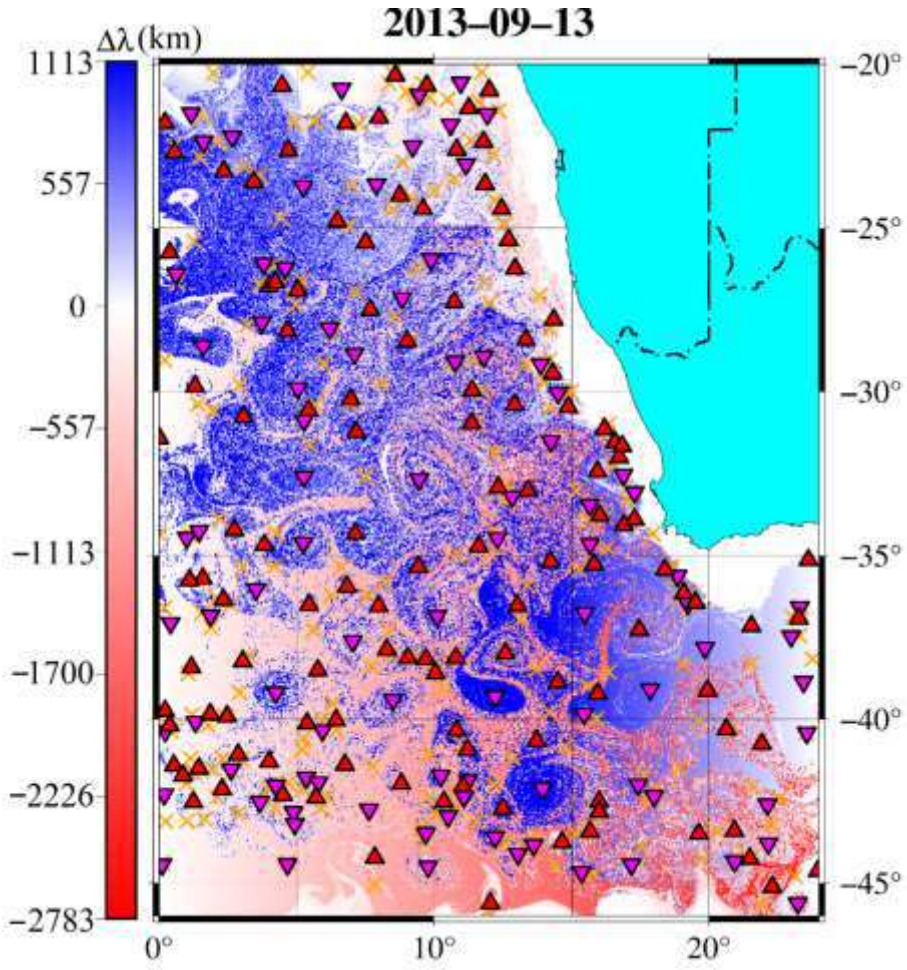

Figure 3.20. Meridional displacement of the particles on September 13, 2013, at a depth of 266 m. The scale indicates the meridional displacement (in km), which is the displacement of water particles northwards/southwards within 365 days from this date. The red color (negative values) highlights the waters that have shifted northwards, and the blue color (positive values) indicates the waters that have shifted southwards. The triangles and crosses are the same as in the previous figures.

The U-end map (Figure 3.21) complements the map with the zonal displacements (Figure 3.19). The scale indicates the latitude at which the water particles crossed the prime meridian from west to east. Figure 11 also shows how far the water particles have spread in an easterly direction. The particles that crossed the 0 meridian propagated almost zonally. These particles travel a considerable distance to the east, spreading almost to the eastern border of the basin in the latitudinal band 35–45°S. They do not cross the cores of eddies by passing them along the periphery.

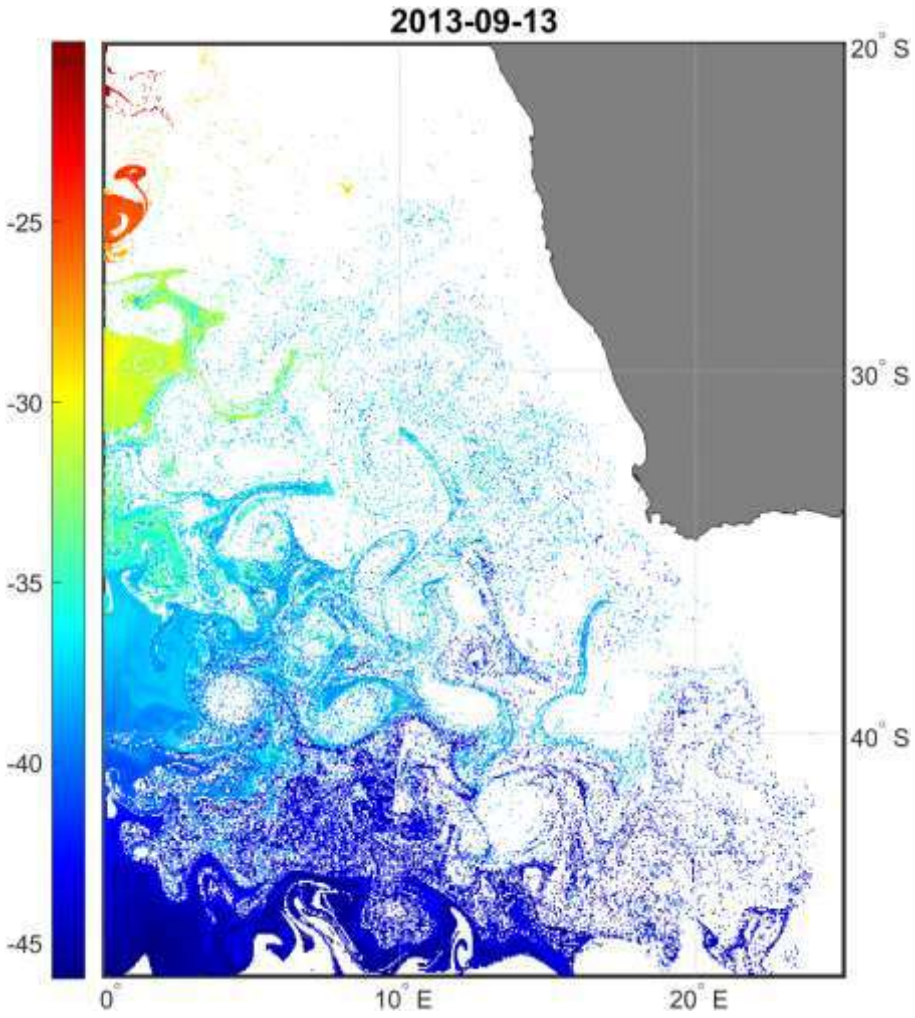

Figure 3.21. Map of determining the latitude where the particles crossed the prime meridian (Lagrangian u-end-map) on September 13, 2013, at a depth of 266 m. The color shows the value of latitude where the points (particles) cross the 0 meridian within 365 days from this date.

Thus, the analysis of Lagrangian maps (Figs. 3.16-3.21) reveals that the eddies in the study region intensely interact with the surrounding waters. This means that the eddies that formed as a result of the destruction of the Agulhas rings can change the structure of their waters while remaining in the Cape Basin. Here, the waters of the Agulhas leakage mix with the waters of the South Atlantic Gyre and the Benguela Current, and the thermohaline properties of the Agulhas eddies change as the warm and salty waters of the Indian Ocean mix with fresher and colder waters. The water particles of the South Atlantic Gyre cross the western border of the region and travel more than 500 km in an easterly direction, mixing with other particles. The Benguela Current appears in Figs. 3.16-3.20 as a line of eddies located along the coast of West Africa.

Figure 3.22 shows the salinity field at a depth of 266 m. This figure shows a visual manifestation of Agulhas leakage in the form of red spots with increased water salinity. The distribution of temperature in the water basin (not shown) is similar to the distribution of salinity. These red spots extend from the eastern border of the water basin to the northwest. The locations of these red spots correspond to the positions of the eddies in Fig. 3.16. These eddies are formed from the rings of the Agulhas Current as a result of division into eddy structures of smaller scales. The waters of Agulhas leakage extend beyond the Walvis Ridge to the northern part of the region. Benguela upwelling manifests itself in the coastal region. The upwelling process is accompanied by the formation of a significant number of mesoscale eddies, both cyclones and anticyclones, along the coastline boundary. It is important to emphasize that these eddies are stable locally and are observed on all the maps throughout the period under consideration. However, the formation of eddies from the parent rings of the Agulhas Current has already occurred in the Cape Basin (Fig. 3.8).

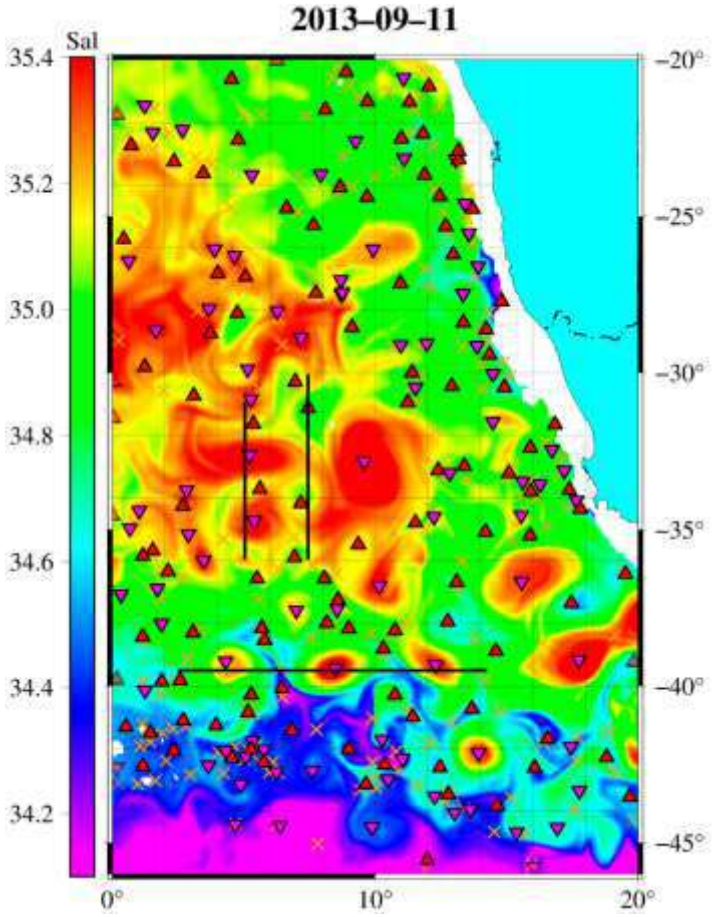

Figure 3.22. Salinity field on September 11, 2013, at a depth of 266 m. The cross-sections on which the vertical profiles of the eddies occurred are indicated by black lines. The triangles and crosses are the same as in the previous figures.

We subsequently analysed the eddies indicated in the cross-sections (Fig. 3.22). The zonal section of 39.6°S passes through the centers of three *Ac* (Figure 3.23). The meridional section at 5°E passes through the centers of two *Ac* (Fig. 3.24), and the meridional section at 7.5°E passes through the centers of two *Cyc* (Fig. 3.25). These eddies are also shown in Fig. 3.16 (S-map), Fig. 3.17 (O-map), and Fig. 3.18 (T-map). This once again emphasizes that the waters in the eddies differ from the surrounding waters both in origin and property. Figure 7 reveals that both the considered *Ac* and *Cyc* consist mainly of particles that are colored green. These waters correspond to waters that arrived from the Indian Ocean and are associated with Agulhas leakage. Figures 3.23-3.25 show the vertical cross-sections of the temperature and salinity anomalies. The anomalies are estimated relative to the mean climatic fields based on the GLORYS12V1 data for 1993–2021. The temperature and salinity anomalies in the eddies reach ± 4°C and ± 0.5–0.6 psu, respectively.

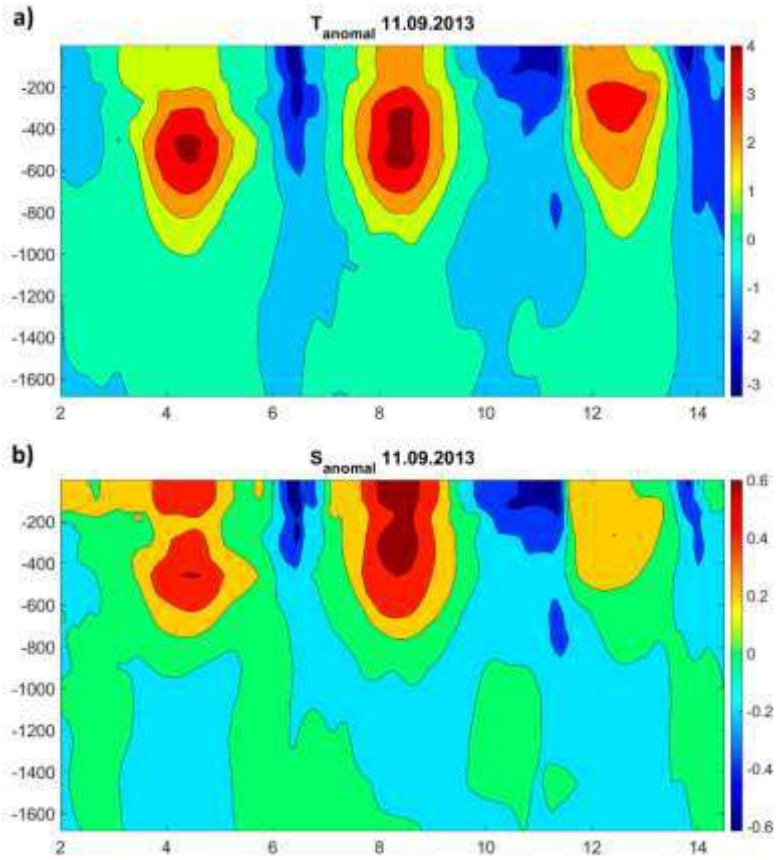

Figure 3.23. Zonal vertical cross-section of temperature (°C) and salinity anomalies for three *Ac* at 39.6°S on September 11, 2013.

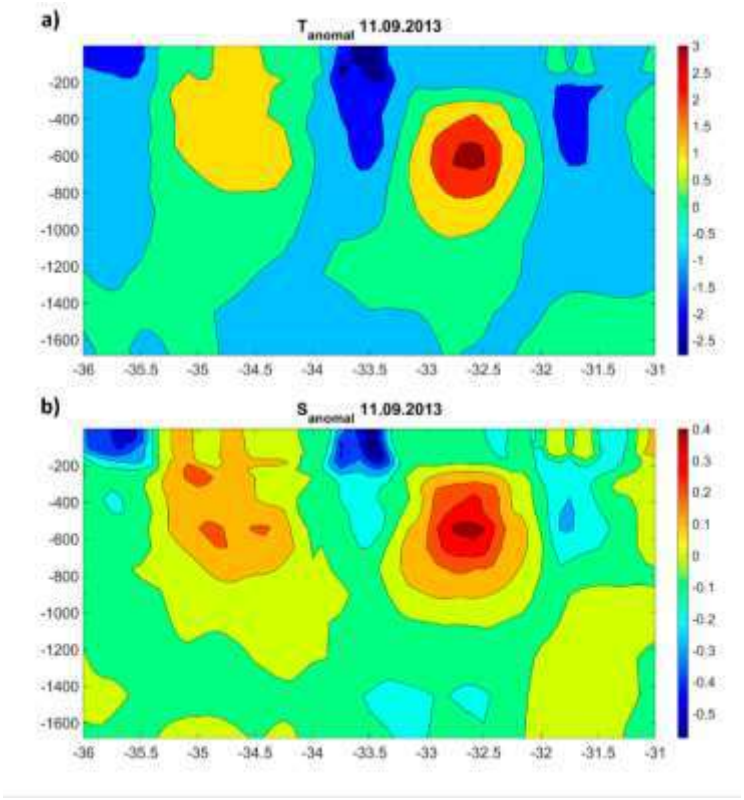

Figure 3.24. Meridional vertical cross-section of temperature (°C) and salinity anomalies for two *Ac* at 5°E on September 11, 2013.

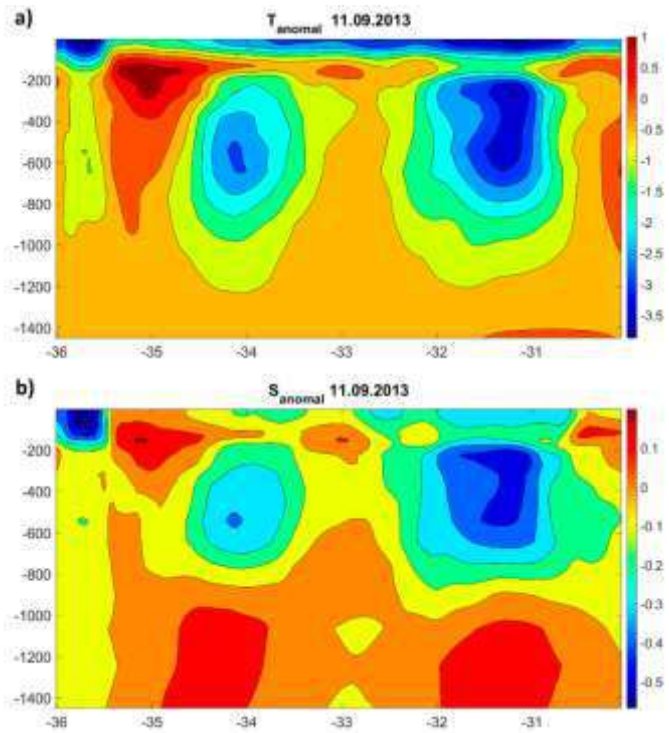

Figure 3.25. Meridional vertical cross-section of temperature (°C) and salinity anomalies for two *Cyc* at 7.5°E on September 11, 2013.

CHAPTER 4. MERIDIONAL DISPLACEMENT OF AGULHAS EDDIES

Analysis of altimetry maps of SLA (Sea Level Anomalies) shows steady westward propagation of mesoscale eddies in the World Ocean, which is explained by the existence of planetary Rossby waves. However, several researchers noticed at the same time that there is a significant meridional displacement in eddy transfer herewith cyclones tend to move poleward and anticyclones equatorward (see e.g. Cushman-Roisin, 1994; Early et al., 2011, Reznik 2010). Chelton (2011) and Morrow (2004) believe that this displacement can be explained by a modification of the potential vorticity gradient by vertically sheared mean flow. They suggest that this is an effect of the spherical geometry of the Earth on the large eddies, which cause equatorward bias because of their large latitudinal. Another explanation is the large nonlinearity of eddies. Kamenkovich et al. (1996) notice that the Agulhas eddies are nonlinear with Rossby number Ro < 0.1. Due to their nonlinearity, eddies have a meridional component to its translation velocity, thereby in the Southern Hemisphere, anticyclonic eddies tend to move to the northwest contrary to cyclones, which move to the southwest. Despite its importance, the problem of the influence of nonlinearity on moving eddies has not been sufficiently addressed. Besides, any acceptable verification of the phenomena of observations for the theories does not exist nowadays.

We believe that both of the above explanations for the meridional shift of the western propagation of eddies in the ocean do not reveal the essence of the phenomenon. The main purpose of this part of the research is to compare the existing theoretical approaches to the phenomenon. We are based on the altimetry maps of the South Atlantic. Our main interest is the meridional bias of Agulhas eddies.

In our study, only long-lived Agulhas eddies are considered, the lifespan of which exceeds 2.5 years. It turned out that only anticyclones satisfy this criterion since all formed cyclones dissipate within the first year after their generation, that is, cyclones are much less stable than anticyclones. This fact is explained in the study of Nezlin (1986) in terms of cyclone-anticyclone asymmetry. He explains more sustainability of anticyclones in comparison with cyclones by the fact that the speed rotor of a cyclone is parallel to the velocity vector of the Earth's rotation, while that of an anticyclone is antiparallel. This means that in the equation for the conservation of a potential vortex, scalar nonlinearity can balance the dispersion only in the case of an anticyclone. For a cyclone, dispersion and scalar nonlinearity have the same signs and, therefore, cannot be mutually compensated.

Thus, the observed cyclone-anticyclone asymmetry is a direct consequence of scalar nonlinearity and a dispersion-nonlinear property of Rossby vortices, which is a very fundamental law.

The presence of cyclone-anticyclonic asymmetry in the conservation laws largely determines the possibility (or impossibility) of the formation of solitary vortices of different polarities. This means that if there is a "scalar" Rossby soliton (a solitary wave in which dispersive spreading is compensated by twisting caused by scalar nonlinearity), then it can only be an anticyclone, that is, only an elevation soliton, like the classical Russell soliton. Nezlin (1986) also points out that almost all large long-lived eddies on major planets, like Jupiter's Great Red Spot, apparently are anticyclones, that is, it indicates cyclone-anticyclonic asymmetry. According to Nezlin (1986), the wave approach is more informative for the study of eddies in the ocean, that is what makes it possible to simply explain such a fundamental phenomenon as the cyclone-anticyclonic asymmetry.

Thus, according to Nezlin, anticyclones in the ocean are Rossby vortices (Rossby solitons), and its properties (dimensions, direction, and drift velocity) are well predicted and described based on wave concepts, according to which the Rossby vortex is the result of a mutual balancing of dispersion and nonlinearity. Consequently, a Rossby vortex (soliton) is an object exhibiting an explicit dualism, and therefore the frequently asked question: "Is this a vortex or a wave?", it is not quite correct. Such an object can equally well be called either a wave solitary (i.e. non-spreading) vortex or a vortex soliton, depending on which of its properties are considered.

Thus, in this paper, we analyze only anticyclones - long-lived eddies of the Agulhas current and meridional displacement of them during their moving in the South Atlantic. According to Nezlin (1986), we can also call these anticyclones as the Rossby vortices (or Rossby solitons).

Thus, the main purpose of this part of the research is to analyze the long-lived anticyclones propagating in the South Atlantic.

4.1. Analysis of Agulhas eddies tracks

An eddy identification algorithm identifies 54496 unique mesoscale eddies in the area for 1993-2017, of which 28018 are cyclones and 26478 are anticyclones. The study area is shown in Figure 4.1, which reflects the main topographic formations. The velocities of currents in the central part of the region are low and directed mainly to the northwest.

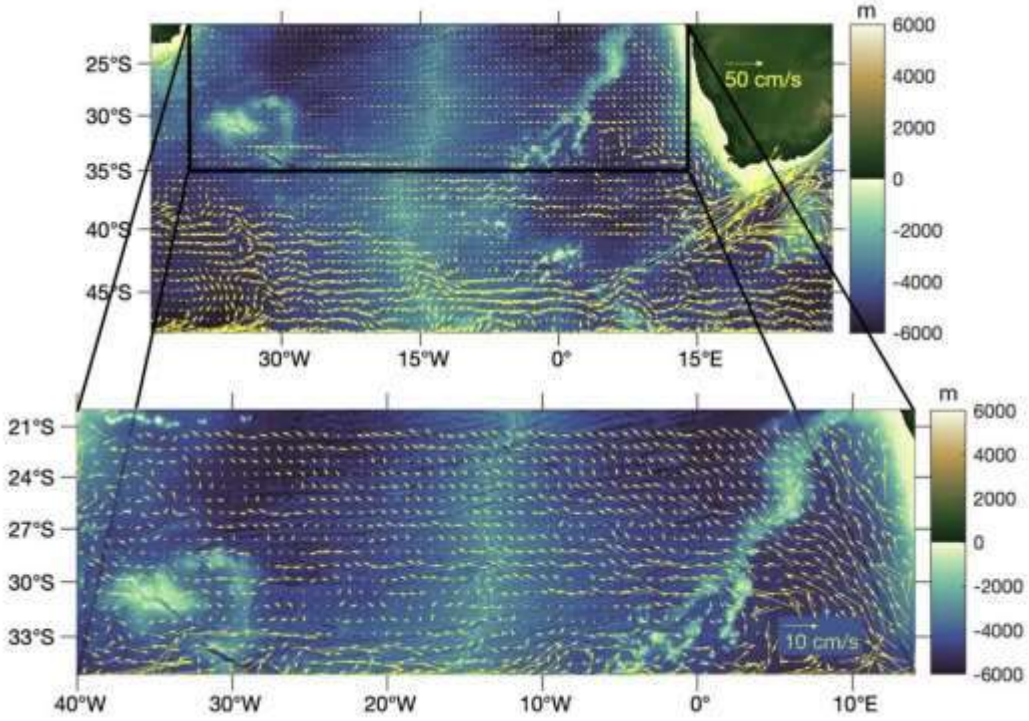

Figure 4.1. The study area. The color scale shows the depth (m). Arrows show the vectors of current velocities to the west of 30 ° E, calculated from altimetry data.

The total number of eddies identified in every bin 3.0°×3.0° is shown in Figure 2a. It can be seen that a lot of eddies have a topographic nature and are confined to the main topographic formations. It is important to note that most eddies have a short lifespan and quickly dissipate. In our study, only long-lived eddies were selected for research. These eddies move in the South Atlantic and went to extraordinary distance. Figure 4.2b shows the tracks of 15 Agulhas eddied that we selected for analysis. We note that although the total number of cyclones in the “Mesoscale Eddy Trajectory Atlas Product” exceeds the number of anticyclones, it turned out that only anticyclones are long-lived. The anticyclones in Figure 4.2b have a lifespan of more than 2.5 years. In the further

presentation, the anticyclone track numbers correspond to their numbers in the product used “Mesoscale Eddy Trajectory Atlas Product”.

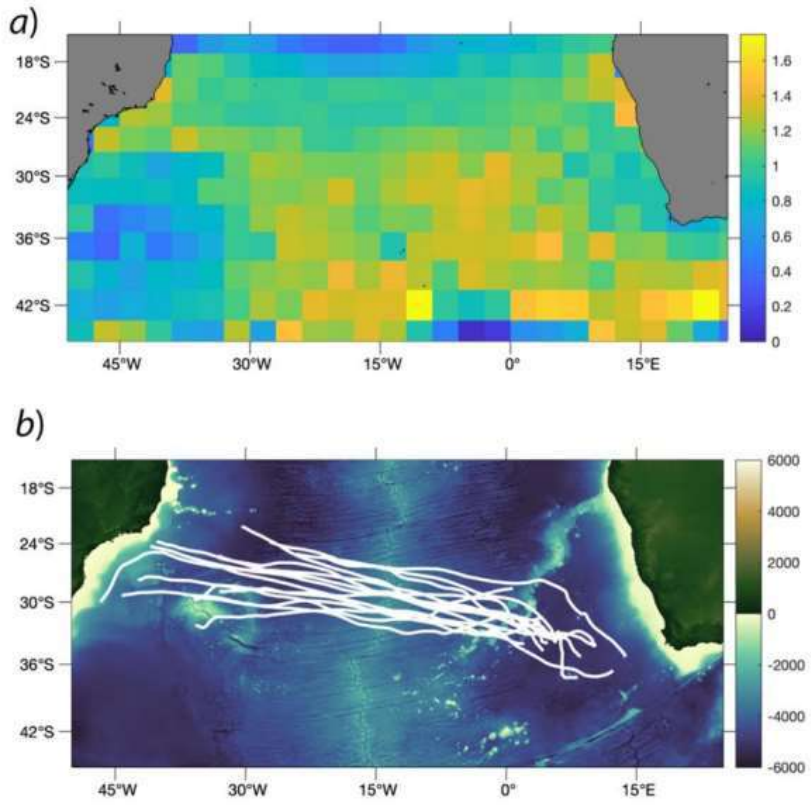

Figure 4.2. Average (1993 - 2017) daily number of mesoscale eddies identified with the automatic method by Chelton et al.(2011) in every bin 3.0°×3.0° (a); tracks (shown by white) of long-lived anticyclones crossing the South Atlantic.

We divided each track into 3-6 parts if its direction changed when the eddy moved (Table 4.1). On each part of the track, we consider the vortex characteristics to be constant. Table 4.1 shows the characteristics of these eddies on parts of the track. The zonal displacement in all cases exceeds the meridional displacement, and, in most cases, it is significant, although it should be noted that the values of them are comparable in certain parts of the track.

Table 4.1. Parameters of long-lived mesoscale eddies in the South Atlantic

Track No	Mean radius	Mean amplitude	Orbital velocity	Speed of drift	Displacement:: zonal L_x, meridional L_y; distance S				Total lifetime, days
	R, km	A, cm	V_o, cm/s	V_d, cm/s	L_x, km	L_y, km	T, days	S, km	
139147.1	86	7	74	5	558	555	220	795	1198
139147.2	87	5	70	4	1173	111	390	1377	
139147.3	95	3	65	4,3	1173	277	293	1247	
139147.4	81	6	65	3,9	1017	218	280	1248	
139147.5	71	3	55	1,2	207	118	15	69	
64204.1	89	5	65	3,3	540	331	190	572	1096
64204.2	122	3	113	5,3	1680	442	380	1812	
64204.3	60	3	75	5,5	1523	192	330	1612	
64204.4	78	3	67	6,5	1108	332	196	1139	
84755.1	72	4	61	7,5	766	221	115	770	1088
84755.2	86	6	73	4,5	466	-221	130	520	
84755.3	74	4	75	8,6	421	9,5	55	421	
84755.4	73	4	62	9,3	933	321	200	966	
84755.5	77	3	81	4,5	1906	221	480	1937	
84755.6	74	4	87	4,6	584	-9,5	108	389	
138285.1	60	10	64	5,6	280	277	70	349	1130
138285.2	60	8	91	2	187	-111	130	216	
138285.3	80	4	65	3	373	332	180	438	
138285.4	77	4	85	3,8	1264	443	380	1288	

138285.5	76	4	84	5,3	1178	442	270	1278	
138285.6	61	3	82	7,2	332	120	100	648	
78168.1	60	18	115	4,3	685	591	210	804	1057
78168.2	79	11	69	6	3606	664	690	3773	
78168.3	70	6	75	7,2	600	-120	80	515	
78168.4	67	6	73	8,7	199	-563	77	596	
61092.1	68	6	76	4,5	721	655	250	994	1045
61092.2	90	4	77	2,7	295	212	150	361	
61092.3	78	4	91	5	2900	212	645	2919	
56389.1	74	10	69	3,3	1124	221	390	1158	954
56389.2	72	7	69	4,7	1400	220	340	1446	
56389.3	65	4	68	5,2	212	111	234	1080	
44929.1	88	9	71	5,5	2230	323	460	2243	948
44929.2	85	8	68	6	2332	212	440	2364	
44929.3	75	7	58	3,6	97	-100	48	155	
83056.1	65	3	85	9,6	267	-120	50	430	936
83056.2	78	4	86	6,3	1353	656	260	1463	
83056.3	74	5	73	5,2	2900	655	626	2915	
62705.1	81	7	79	2,7	460	110	200	481	922
62705.2	94	3	71	5,4	462	101	100	484	
62705.3	162	7	55	4,7	350	-9,5	90	377	
62705.4	95	4	67	3,1	600	212	220	617	
62705.5	86	8	113	3,7	663	101	210	693	
62705.6	70	12	57	3,3	275	-12	102	299	
116552.1	71	4	64	3	115	-102	49	133	922
116552.2	76	11	88	6,4	280	101	51	292	
116552.3	59	11	72	5	483	-100	110	492	

116552.4	75	4	60	3	223	-98	90	240	
116552.5	74	4	56	5,2	2800	664	622	2870	
293011.1	61	5	90	4,5	781	-236	200	794	905
293011.2	88	4	62	5,6	1533	12	305	1533	
293011.3	56	4	66	4,7	1039	-12	250	1058	
293011.4	88	3	52	2,5	100	-9,5	50	111	
293011.5	66	3	75	1,5	92	9,5	100	137	
102254.1	57	7	94	7,1	369	323	60	381	942
102254.2	51	8	126	5,2	140	-9,5	40	185	
102254.3	62	9	78	3,2	500	453	220	641	
102254.4	115	5	86	4,8	2590	533	612	2586	
13155.1	71	11	63	4,5	1546	221	380	1545	902
13155.2	58	6	69	5,5	1619	221	340	1651	
13155.3	47	6	63	4,3	486	110	130	500	
13155.4	58	5	67	4,7	200	-101	52	218	
78132.1	70	6	98	3,1	265	9	105	267	900
78132.2	83	9	108	3,7	1	341	115	346	
78132.3	83	8	139	4,5	1902	895	515	2036	
78132.4	80	8	171	4,8	604	230	165	642	

Based on a qualitative analysis of the long-term evolution of isolated eddies, the amplitude, and radius of the eddies, it is impossible to confirm the conclusion about systematic decrease energy with time (at large times). This tendency is described by Korotaev and Fedotov (1994) and Korotaev (1997), as well as by Reznik (1994), who explains this decrease by the radiation of Rossby waves by vortices. However, the movement of eddies can be due to the absorption of Rossby waves and the fact that there is a critical value of the eddy amplitude, below which there is no radiation of Rossby waves (Korotaev 1997). On the contrary, sometimes a seemingly inexplicable short-term increase in the eddy scale occurs. This does not appear that it is related to topographic reasons (track

116552, see Fig. 4.3). Probably the enhancement is due to the baroclinic factor, which is not taken into account by the available analytical models due to the complexity of the problem statement. This is also supported by the findings of Early et al. (2011) that, possibly, the factor associated with the radiation of Rossby waves by a vortex may be strongly overestimated at long times when entering the quasi-stable state. Guerra et al. (2018) used the automatic identification method to detect mesoscale eddies in the South Atlantic. They also indicated the existence of an 'eddy corridor'. They point out that the ridges constitute obstacles to an eddy drift in the Atlantic as they usually show a deflection of trajectory and reduction of drift speed while they manage to pass through the deepest valleys. Our study confirmed the change of angles relative to latitude during eddies cross the ridges (Fig. 4.4). However, the reduction of drift speed during the eddy translation does not exist in many cases (Fig. 4.3).

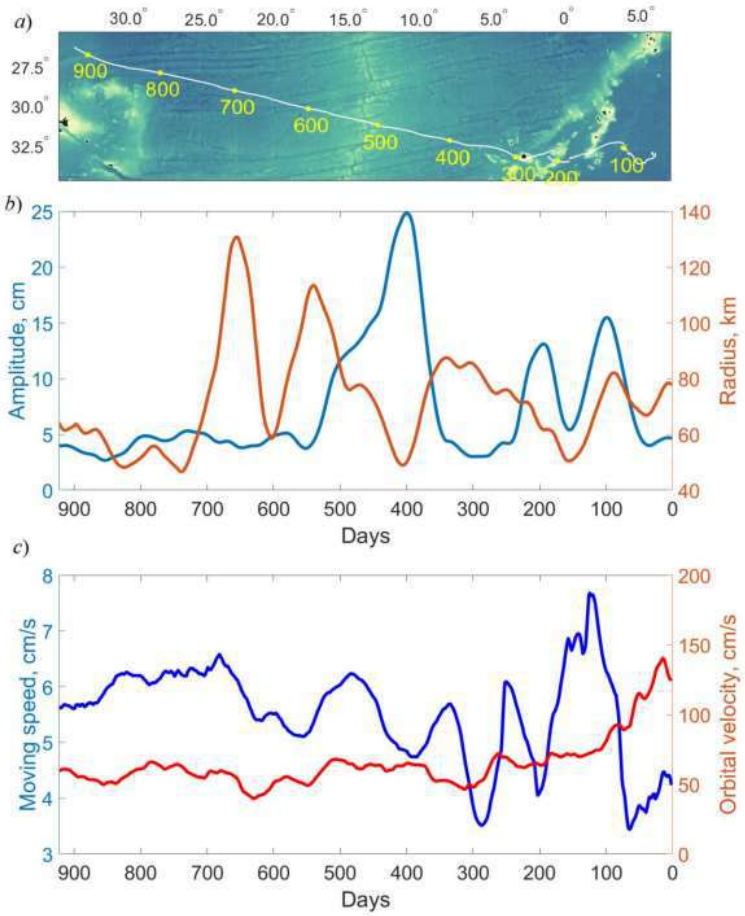

Figure 4.3. Track No 116552 (a); Time-variability of (b): amplitude and radius of the eddy, (c) moving speed and orbital velocity.

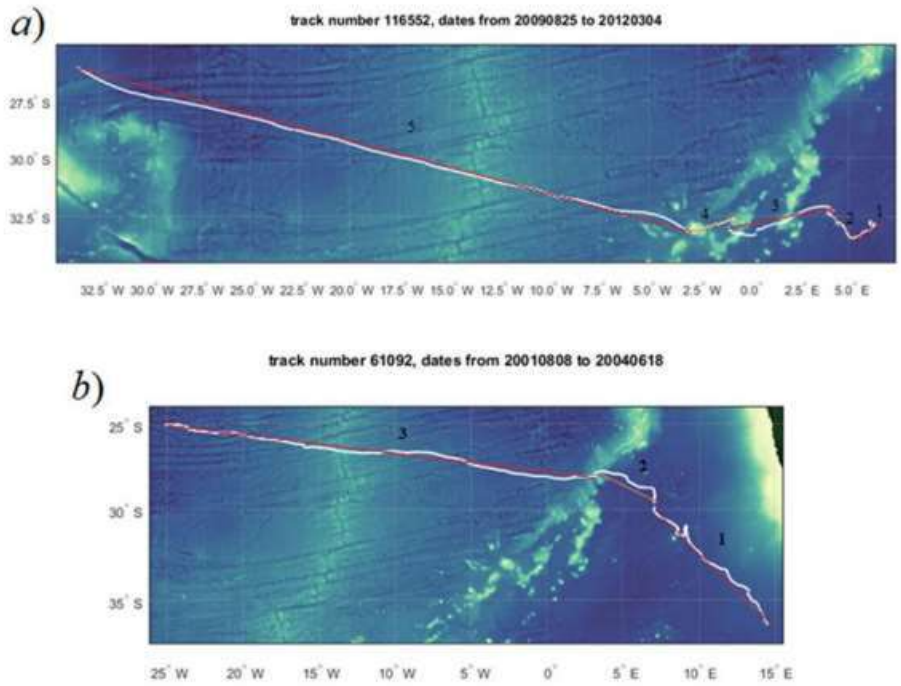

Figure 4.4. Tracks of the anticyclones crossing the South Atlantic: a) 116552 from 25.08. 2009 to 04.03. 2012; b) 61092 from 08.08.2001 to 2008 to 18.06.2004.

According to the theory of Korotaev (1997) and Reznik (1994), the trajectories of single eddies at large times propagate asymptotically to the 'repose latitude', where it disappears. This type of quasi-parabolic propagation is inherent in very strong Gaussian vortices. The observed long-lived eddies of Agulhas are most likely not of this kind. They are weaker and move more smoothly in space. The evolution of such eddies is more likely to fit the vortex model of algebraic spatial fading (see Reznik, 1994, formulas (5.9) and (5.11)). Analysis of the data from Table 1 is consistent with the results by Reznik (1994). Based on Table 4.1 two main conclusions can be drawn:

– eddy trajectories are rather quasi-linear than quasi-parabolic;

– eddies of smaller spatial sizes are more inclined to move in the meridional direction and have a greater inclination to the parallel.

Analysis of individual tracks gives the following interesting result. At the initial moment, the observed tracks of Agulhas eddies have a distinctly identified tendency towards a certain angle of propagation. The available mathematical models (Korotaev, 1997; Reznik, 2010; Early et al., 2011) proceed from the fact that, in general, the motion of eddies is highly nonlinear at large times. However, at the initial stage, at short times,

they are linear betagyres. Due to the anisotropic dispersion of Rossby waves, long Rossby waves travel to the west, short ones to the east. At the initial stage, the localized axisymmetric formation stretches in the zonal direction, forming the so-called beta-gyres. This is kind of the zero stage of vortex development on the β-plane. Further, this gyre is already controlled by nonlinearity and leads to a purely meridional displacement, depending on the polarity of the eddy. The principal point of analytical approaches is that linearity is considered unable to give a meridional asymmetry of motion (due to the meridional symmetry of the dispersion relation of linear Rossby waves).

4.2. Analysis of the main theoretical approaches to meridional eddies displacement

It is believed that linear Rossby waves can explain the East-West asymmetry, but not North-South. However, at the subsequent time stage, it is the nonlinearity that leads to the western displacement of eddies, which is accompanied by the meridional anisotropy. Perhaps this time, when a strictly meridional displacement occurs, is too short, and in Table 4.1 we are already observing the stage of the so-called adjustment. However, it is possible to give another explanation for this fact.

The existing analytical models of the dynamics of single vortices on the β-plane have one significant drawback. Discussing and recognizing certain resonant interactions of a nonlinear vortex and linear Rossby waves emitted or absorbed by it, the authors break the process of vortex initiation and its further evolution.

According to Korotaev (1997), ‘An interesting problem is the entire life cycle of a vortex, starting from its birth due to flow instability or other reasons. Unfortunately, this problem is too complex to be solved now. Instead, we'll focus on the problem of initial values. Although the formation process usually is not considered, the problem of initial values provides a physical understanding of the strong vortex dynamics on the β-plane’. Thus, it is logical to expect that these reasons (of initial values) should play a significant role, at least at the initial stages of eddy evolution. The reasons and methods of eddy generation can be different, but this is not reflected in any way in existing models.

We propose the following alternative version of the evolution of the eddy initial stage and do not reject other possible scenarios for mesoscale eddies in other regions. We

rely on the statement that eddy dynamics, at large times, is highly nonlinear. We propose to explain the first stage of eddy nucleation and evolution by the stage of narrowly directed long Rossby wave emission under the combined influence of topography and large-scale non-zonal flow. This can be qualitatively explained as follows.

The Agulhas current, being a strong jet flow, carries with it weak captured wave and vortex disturbances, which initially have a small amplitude. In this case, the orbital velocities of the eddies do not differ much from the forward speed, and the nonlinearity parameter (the ratio of the orbital velocity to the forward speed) is approximately equal to one. Colliding with strong topographic changes in the form of a sharp increase in depth, there is a double effect of transforming these disturbances.

The Agulhas current, being a strong jet flow, carries with it weak captured wave and vortex disturbances, which initially have a small amplitude. In this case, the orbital velocities of the eddies do not differ much from the forward speed, and the nonlinearity parameter (the ratio of the orbital velocity to the forward speed) is approximately equal to one. Colliding with strong topographic changes in the form of a sharp increase in depth, there is a double effect of transforming these disturbances.

Secondly, the current slows down significantly, on the contrary, and it is due to the law of conservation of mass, encountering a sharp increase in depth. Consequently, the nonlinearity parameter sharply increases both due to the numerator, the swirling of the eddies, and due to the denominator, the deceleration of the forward motion of the flow. In this sense, the influence of topography can be characterized as a kind of separator separating the forward motion of the current and eddy formations. Figuratively, the influence of topography can be described as throwing in pair figure skating. When the partner (current), slowing down, throws out the female partner (eddy), and she greatly increases her rotational movement, then the usual conservation of angular momentum law works. Compressing to the center of her axis of rotation, she (female partner) decreases her moment of inertia but increases the speed of rotation. (The moment of impulse is equal to the product of the speed of rotation and the moment of inertia, and it is constant. When the moment of inertia decreases, the rotation speed increases automatically). In this case, the analogue of the conservation law of the inertia moment is the conservation law of potential vorticity.

The scenario described above suggests that at the moment of generation, vortex not only captures the water mass, but also acquires a certain translational and rotational moment, which is a function of the velocity and direction of the large-scale current, as well as topography at a point of the vortex generation, and, as it will be shown below, it also depends on the baroclinic flow parameters in the form of the first baroclinic Rossby radius. This can explain the observed practically rectilinear motion of long-lived eddies of the Agulhas.

Contrary to the model of Korotaev (1997), where the motion of a vortex at the initial stage is determined by some isotropic radiation of Rossby waves, and due to this radiation, the vortex adapts to a hostile environment, we assert the opposite. At the moment of generation, the vortex cannot be coming out of anywhere. The vortex, at the moment of its generation, is a consequence of narrowly directed angular (at an angle to latitude) radiation by the current. At the initial moment, the vortex not only captures a certain volume of water mass but also acquires a certain initial translational and rotational angular momentum, which determines all of its further behavior until the moment of disappearance. This is the scenario we are offered by the empirical data obtained in Table 4.1.

The importance of the long-wave approximation gives in the linear formulation the following formula for the radiation of Rossby waves by a non-zonal baroclinic flow

$$\Psi = \Psi_0(x,y) + \varepsilon\varphi_1(x,y,z,t), \quad \varepsilon << 1, \tag{4.1}$$

here Ψ is the quasi-geostrophic stream function, x, y, z – axes of a rectangular coordinate system, t – time. Here $U(x,y) = -\left(\Psi_0(y)\right)_y'$ is a zonal component of the background current velocity, $V(x,y) = \left(\Psi_0\right)_x'$ is a meridional component of it. The first term is the background stationary flow, the second term in the equation (4.1) is linear waves, which can be searched in the form $\varphi_1 = \varphi_1(z)\exp\left(i\left(k\,x + l\,y - \omega t\right)\right)$, where *k*, *l* are zonal and meridional wavenumbers, ω is a frequency, $\varphi_1(z)$ is a depth-dependent wave amplitude. The effects associated with the nonlinear long-wavelength approximation are outlined in Gnevyshev et al. (2019). A mathematical model that explains the narrowly directed angular radiation of long Rossby waves by non-zonal currents was formulated by Lighthill (1967). He used the idea to describe the resonance between the flow and the linear divergence-free Rossby waves radiated by the flow. The formula (26) from his paper is

$$U\left(k\cos\alpha + l\sin\alpha\right)\left(k^2 + l^2\right) + \beta k = 0, \tag{4.2}$$

where β is a meridional variation of the Coriolis parameter, and velocity of flow is $\vec{U} = U(\cos\alpha, \sin\alpha)$. If we draw the radiation indicatrix (see Figure 2 of Lighthill 1967), corresponding to Eq. (4.2), we get the radiation of waves in a purely westerly direction. This is part of the scenario of the formation of the β-gyre, which again leads us to the statement that in the linear divergence-free problem, it is impossible to obtain the meridional asymmetry.

For a better understanding, let us explain the transition from formula (26) in Lighthill's paper (in our article, this is formula (4.2)) to formula (38) in Lighthill's paper. This formula is the resonance condition for the flow and generated waves. This term is associated with the name of Kelvin, whose ideas were later be developed by Lighthill. Sometimes this formula is called the condition for the stationary of waves in the system associated with their generation source, taking into account the Doppler shift $\Omega = \omega - \vec{k}\,\vec{U} = 0$.

Further, Lighthill assesses how the divergence factor affects the radiation of long Rossby waves. Considering the calculations trivial, he answers immediately in the form of the classical formula (38), which is probably the most physically successful one for representing the widespread idea of the resonance between the motion of the radiator and the waves radiated by it. A similar formula for resonance was used by Kelvin to construct a picture of ship waves (Lord Kelvin, 1906).

Let us explain how it turns out. For this, we must modify equation (4.2) as follows:

$$U\left(k\cos\alpha + l\sin\alpha\right)\left(k^2 + l^2 + R_d^{-2}\right) + \beta k = 0, \tag{4.3}$$

here *Rd* is the baroclinic Rossby radius of deformation. In a long-wavelength limit at $k^2 + l^2 \ll R_d^{-2}$ and taking into account the fact that the direction of wave radiation (the direction of the normal) at zero frequency will be perpendicular to the quasi-plane term near the origin, we obtain a modified formula which is an analogue of formula (38) in the form

$$\Theta = \arctan\left(\frac{\sin\alpha}{\frac{\beta \cdot R_d^2}{U} + \cos\alpha}\right), \tag{4.4}$$

here Θ is the angle of the direction of wave radiation from the western direction and an angle α is measured in the positive sense from the same (westward) direction. The difference between formula (4) and Lighthill's formula (38) is that Lighthill used a barotropic radius of deformation while we use baroclinic one. If we also used a barotropic radius we would not get any difference from the purely zonal wave direction using this formula. Lighthill concluded that for both nondivergent and divergent Rossby waves, when using the barotropic Rossby radius, the results are practically the same. However, if we use the first baroclinic radius instead of the barotropic one, then the meridional displacement of the waves is observed, and we see a good correspondence of the directions of movement of the tracks of the Agulhas eddies in the South Atlantic with the modified Lighthill formula. Perhaps the first baroclinic radius was not yet known in 1967.

The resonance is also mentioned in the model by Korotaev (1997) and Reznik (2010) in a quasi-stationary regime. But it is used there to describe the resonance between a vortex and Rossby waves radiated or absorbed by a vortex. For example, Korotaev (1997) writes that a moving vortex on a rotating sphere or the β -plane excites Rossby waves, just as a moving ship causes ship waves; Rossby waves are observed during the entire period of vortex evolution, but they are very weak for short periods (Reznik, 1992). It is easy to see that this condition of linear resonance is in harmony with the nonlinear condition of stationarity if we take the purely zonal case and go from wave motions to localized ones:

$$p^2 = \frac{\beta}{U} + R_d^{-2}, \tag{4.5}$$

here p is a parameter, that sets space scales of the vortex velocity fields can, in principle, depends on time (Reznik, 1992). Non-zonal currents, regardless of the angle of their propagation, radiate long Rossby waves almost only in the westerly direction. And in this case, we again obtain the classical result of the linear problem, that is, no anisotropy in the north-south direction can be obtained in the linear formulation. However, the fact, that the angle of the radiation of Rossby waves almost does not depend on the angle of direction of the flow, does not physically look quite logical and can only be explained by the long-wave approximation.

Thus, if we use not the barotropic, but the first baroclinic deformation radius R_d, we get a completely different result. In this case, the spread in values depending on the first baroclinic radius at the place of radiation will be extremely small. It is this fact that we use as the basis for the idea of the radiation of the Agulhas eddies by a non-zonal current taking

into account the bottom topography and baroclinicity of the current. Since the flow velocities at the generation places have approximately the same direction, all the tracks propagate along the same path (Fig. 4.2b).

Thus, after analyzing the main theoretical approaches (Korotaev, 1997; Reznik, 2010; Early et al., 2011), in which the meridional displacement of eddies is discussed, we conclude that no one concept can fully explain this phenomenon since the resulting displacement estimates do not correspond to theoretical formulas. This allows us to conclude that the mechanisms responsible for the meridional displacement of vortices should be different from them. Based on the Lighthill's approach and using his modified formula, we obtain an acceptable comparison of the empirical and theoretical parameters of the meridional displacement of moving eddies: at a 36° inclination angle of the track, we obtain by formula (4.4) Θ = 32-40°, and at a 64° inclination angle, we obtain at the initial stage of the eddy motion Θ = 49-58°. The calculations used the values of the deformation radius R_d = 30-35 km (Chelton et al., 1998), current velocity U = 5-10 cm/s, $\beta = 1{,}9\times 10^{-11}$ m^{-1} s^{-1}. Thus, the observed meridional displacement of eddies in the South Atlantic may be a consequence of the emerging resonance between the non-zonal flow and the wavefield generated by the flow, which manifests in the form of narrowly directed radiation of Rossby waves. Perhaps the proposed interpretation is not universal for the entire World Ocean, but its application for the South Atlantic has shown its viability.

4.3. Analysis of Rossby wave transformation on a non-zonal flow

Based on two different approaches (the WKB-approximation and the Cauchy problem), the transformation of Rossby waves on a non-zonal flow is studied (Gnevyshev et al., 2020). Figure 4.1 demonstrates that currents in the South Atlantic, where the tracks of eddies are located, are mostly non-zonal. Therefore, the main conclusion of this research is appropriate for the tracks of the Agulhas eddies propagating northwest. Non-zonal flows lead to the splitting of such a concept as a critical layer (Gnevyshev and Shrira, 1989a,b,c,d, 1990). Along with the classical concept of the critical layer, when the waves asymptotically approach slowly the critical layer and the intrinsic frequency is positive, there is another regime of Rossby wave propagation. In the case of non-zonal flow, the wave action (eddy) undergoes a discontinuous jump and the critical layer is crossed twice. Duba et al. (2014), called this regime as “overshooting”. At first, an intrinsic frequency becomes equal to zero

for the finite values of the time and the wavenumber components. In this case, the wave action does undergo a discontinuous jump (Duba et al., 2014), and the intrinsic frequency becomes negative which corresponds to Rossby waves of negative energy. Only after that, the reflected wave is approaching again the critical layer asymptotically for a long time. Hence, the effect of the short-wave transformation of Rossby waves near the so-called critical layer exists in two forms: (1) as an adhering, which is a monotonic approaching of wave packets to the critical layer for an infinitely long time. The sign of the intrinsic frequency of the packet remains the same all the time; (2) as an adhering after overshooting when the wave packet, first, crosses its critical layer at finite wavenumber. The wave changes the sign of the intrinsic frequency when overshooting the critical layer and then keeps the sign when it is adhering to this layer asymptotically similar to the previous scenario (Gnevyshev et al., 2020). The latter regime does not exist for zonal flows. Figure 4.5 shows examples of these two regimes for the eddies propagating in the South Atlantic.

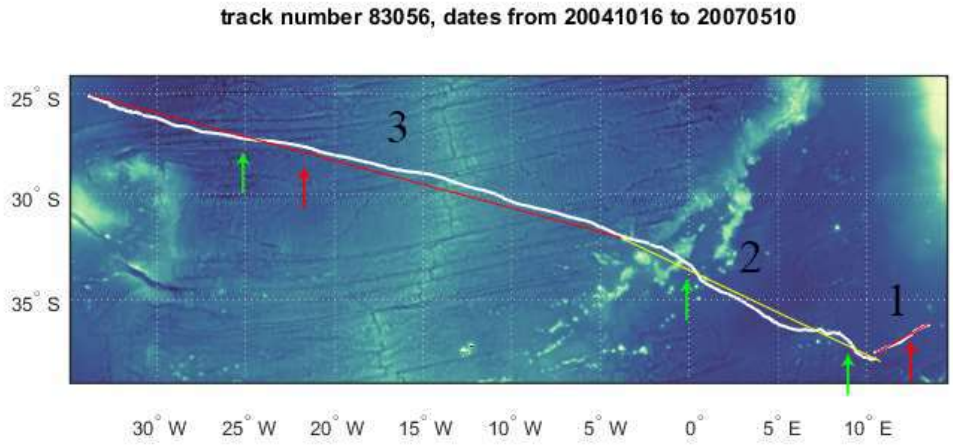

Figure 4.5. Two regimes of Rossby wave propagation: adhering (red arrows) and overshooting (green arrows).

The finding of this paragraph can be extremely useful and significant in the study of the baroclinicity of Rossby waves. It will lead to a splitting of the spectrum of the vertical Rossby wave problem. Such a scenario has not been previously considered yet some related ideas (multi-level waveguides) have long been known for internal waves (see, for example, Shrira & Townsend, 2010). However, the application of these ideas to Rossby waves requires development.

CHAPTER 5. KINEMATIC AND DYNAMIC CHARACTERISTICS OF THE CAPE-BASIN EDDIES

The purpose of this part of the research is to analyse the vertical structure and estimate the potential vorticity of two long-lived Agulhas eddies—cyclones and anticyclones—and to analyse the evolution of the kinetic and available potential energy of the eddies located in the Cape Basin during the process of stretching. The analysis of kinematic and dynamic characteristics of multipolar eddies will provide an adequate understanding of the structure and dynamic parameters of the mesoscale eddy dynamics of the water area.

5.1. Dynamic characteristics of eddies

To analyse the main dynamic characteristics among all the eddies of the Agulhas Current, we needed eddies satisfying the following conditions:

- the eddies are formed by the Agulhas Current;
- the eddies are identified throughout their entire cycle of existence using the "Mesoscale Eddy Trajectory Atlas Product" database;
- eddies of different polarities;
- eddies are located at a minimum distance from each other.

We were able to find several pairs of Agulhas cyclones and anticyclones that satisfy the selected conditions during the period from 1993 to 2022. One pair of vortices particularly attracted our attention, as the anticyclone was one of the longest-lived Agulhas eddies and existed for almost 3 years. This pair of eddies was selected for further analysis. The vertical structure and potential vorticity of the cyclone (*Cyc*) and anticyclone (*Ac*) were analysed. At the time of the meeting (13.12.2012), these two eddies were located west of the African coast at the same latitude, Sus was west of *Ac*, and the vortices practically formed a dipole. Figure 5.1 shows the sea level anomalies, where *Cyc* is characterized by negative anomalies up to -0.4 m and *Ac* by positive anomalies reaching 0.6 m at its center. During the observation period and at the time of the meeting (13.12.2012), the eddies had already left the area of formation and began moving westwards.

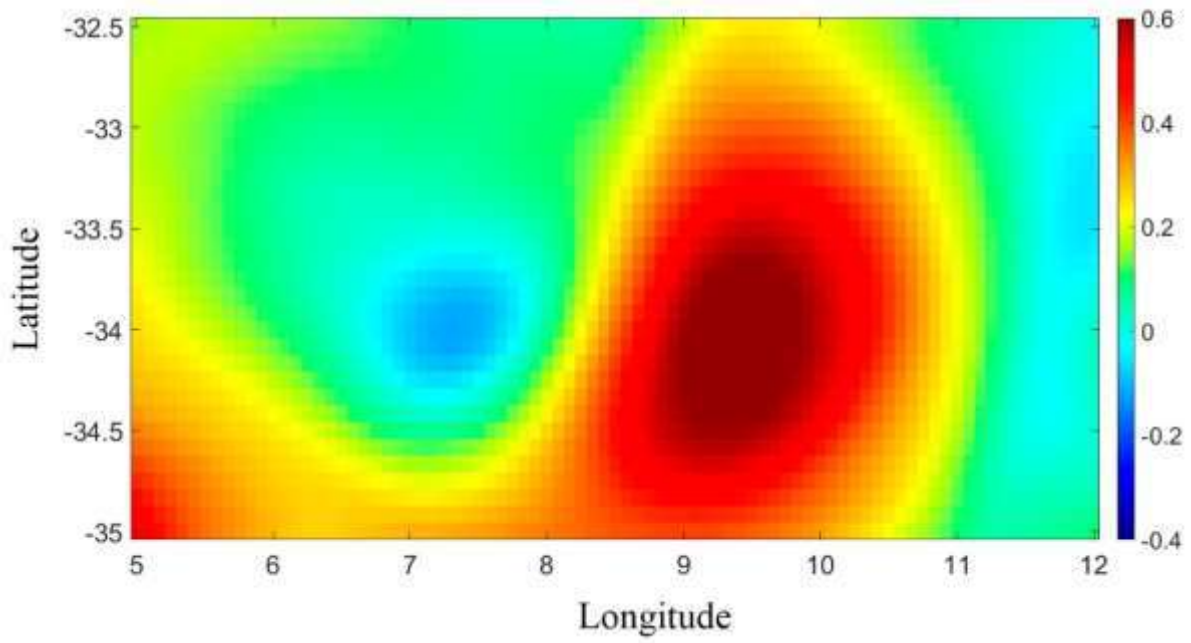

Figure 5.1. Sea level anomalies (m) from GLORYS data for 13.12.2012.

On the basis of the "Mesoscale Eddies..." data, the average parameters of vortices and their life periods were estimated. If long-lived *Ac* existed for 1065 days—from 30.10.2012 to 29.09.2015—then *Cyc* had a lifetime of 123 days—from 2.12.2012 to 3.04.2013. The life cycle of *Ac* exceeds that of *Cyc* by an order of magnitude. The reason that anticyclones are more stable structures than cyclones lies in the so-called cyclone-anticyclone vortex asymmetry, which follows from the nonlinear properties of cyclones and anticyclones. In a cyclone, the velocity rotor is parallel to the vector of the vertical component of the Earth's rotation, while in an anticyclone, it is antiparallel. This leads to the fact that the scalar nonlinearity balances the dispersion only in the anticyclone. In a cyclone, however, the dispersion and scalar nonlinearity have the same signs and therefore cannot be mutually compensated (Nezlin, 1986). This feature, demonstrating the cyclone-anticyclone asymmetry of vortices, has been proven both theoretically and experimentally: anticyclones are stable and characterized by a relatively long lifetime; additionally, cyclones decay (disperse) relatively quickly. This feature also characterizes the vortices presented in Figure 5.1. The mean eddy parameters obtained from the "Mesoscale Eddies..." array are presented in Table 5.1.

Table 5.1. Characteristics of Agulhas eddies

Eddy polarity	Mean radius of the eddy	Mean amplitude	Mean orbital velocity	Path	Movement time	Average speed movements
	R , km	A, cm	V_0, cm/sec	S, km	t, days	V_d, cm/sec
Ac	74	5	79	4217	1065	5,8
Cyc	72	6	107	438	123	5,7

It can be seen that the mean values of the orbital velocity are significantly larger than the mean values of the eddy displacement velocity. Such eddies can be considered axisymmetric (Korotayev, 2020).

Figure 5.2 shows the eddy motion tracks based on the "Mesoscale Eddies..." data.

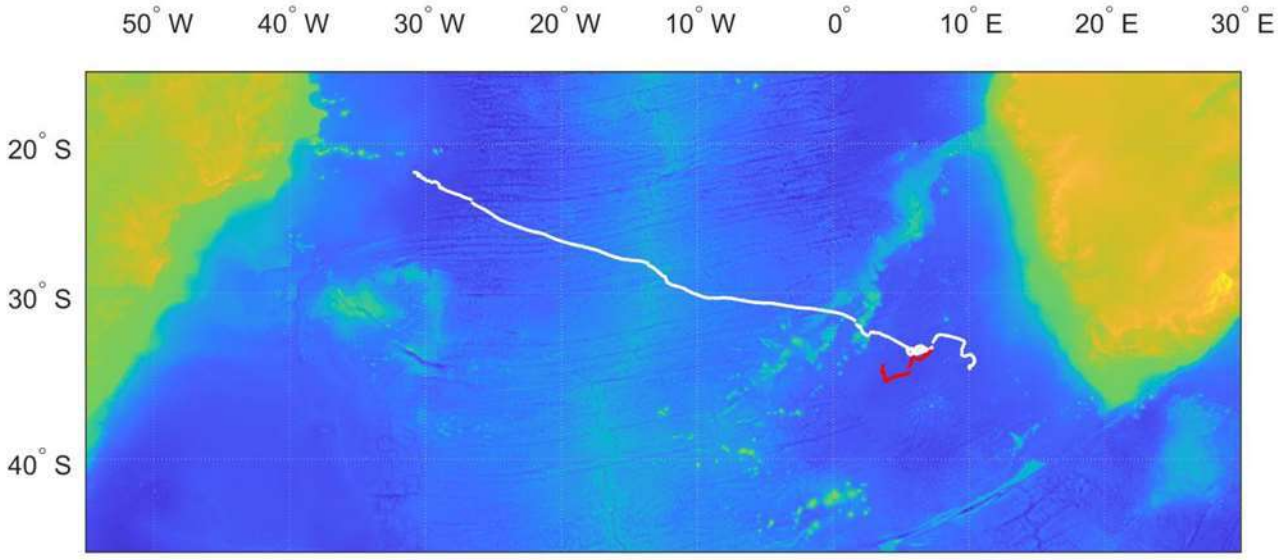

Figure 5.2. Tracks of the anticyclone (white) and cyclone (red) from the moments of their generation to dissipation. The intersection of the tracks corresponds to the observation date 13.12.2012 (see Fig. 5.1).

We note that at the dominating motion of vortices in the western direction, a meridian deviation is observed, with *Ac* deviating toward the equator and *Cyc* toward the pole. The theoretical justification for this phenomenon is discussed in Chapter 4. However, as shown in Figure 5.3, for the anticyclone under consideration, this fact is not confirmed;

i.e., there is no decrease in the eddy velocity or radius with time. Obviously, eddy motion is influenced by many external factors when eddies periodically lose or gain additional energy.

Figure 5.3a shows that the displacement rate *Ac* varies from 3 to 10 cm/s. The eddy motion does not slow during evolution. Moreover, toward the end of the eddy life cycle, the displacement velocity reaches a maximum value of 10 cm/s and then decreases to 0.065 cm/s, after which the eddy dissipates. An increase in the displacement velocity is sometimes correlated with an increase in the eddy radius, but this dependence is observed only at certain moments in time. Obviously, the variability of the *Ac*-eddy parameters is determined by a complex complex of different dynamic conditions—interaction with background currents, changes in the thermohaline structure of the medium, merging with other eddies, atmospheric influences, etc.

For the *Cyc* (Fig. 5.3b), an increase in the displacement velocity before eddy dissipation is also noted. The velocities vary between 0.045 and 0.072 cm/s. However, the radius of the eddy gradually decreases from 115 to 57 km by the end of the life cycle.

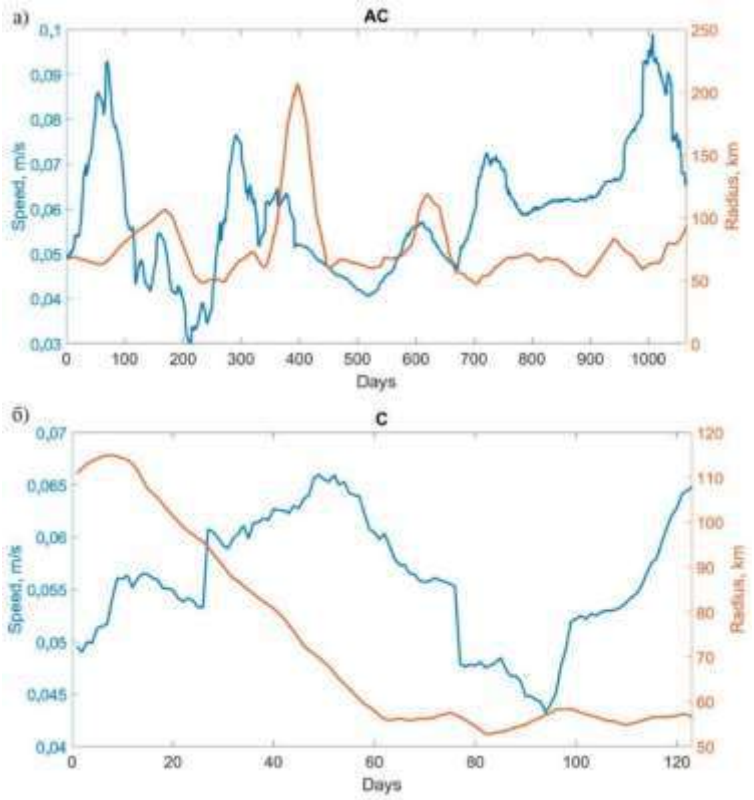

Figure 5.3. Temporal variability in the displacement velocity (in blue) and radius (in red) of the anticyclone (a) and cyclone (b).

Relative vorticity

One of the main parameters of vortices is the relative vorticity. In addition to the cyclone and anticyclone shown in Figure 5.1, other dynamic structures are distinguished in the field of relative vorticity (Figure 5.4). The maximum modulus values of ζ ($4 \cdot 10^{-6}$ s^{-1}) are located in the eastern part of *Cyc*, while in its northern part, the values are close to zero or even negative. This means that the vorticity is a dynamic feature, while the level anomalies shown in Figure 5.1 are kinematic. In addition to eddies, the vorticity field displays shear currents, which also have positive or negative vorticity. For *Ac*, the maximum negative values of ζ ($-2 \cdot 10^{-6}$ s^{-1}) are located in the central and southern parts of the eddy.

The Rossby number $Ro = \left|\frac{\zeta}{f}\right|$ (*f*- Coriolis parameter) varies from 0.03 to 0.05 and is rather small, indicating a large nonlinearity of the eddies, which is one of the reasons for the meridional displacement as they move westwards (Le Blon, 1981).

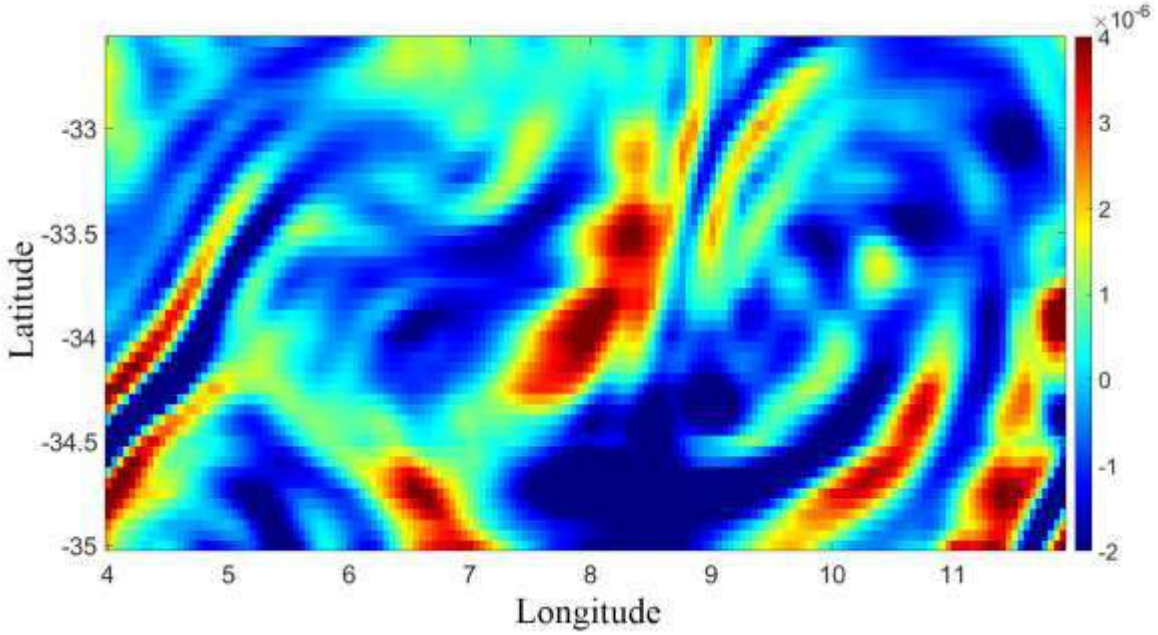

Figure 5.4. Spatial distribution of relative vorticity (s-1) at the surface on 13.12.2012.

Potential vortex vorticity determined by the formula of Ertel and Rossby

On the vertical section of the PV by Ertel (Fig. 5.5), the *Cyc* and *Ac* cores surrounded by isopycnies are well distinguished. In a cyclone, the isopycnies are compressed, and in an anticyclone, they are pushed apart. In the whole study area, PV > 0; however, in the *Ac* core, it has zero values, which is favoured by the absence of stratification. The minimum values ($0.6 \cdot 10^{-10}$—$0.8 \cdot 10^{-10}$ $m^{-1} \cdot s^{-1}$) are located at the periphery of the *Ac* core, and the maximum values ($1.8 \cdot 10^{-10}$—$2 \cdot 10^{-10}$ $m^{-1} \cdot s^{-1}$) are located in the region of the cyclone core.

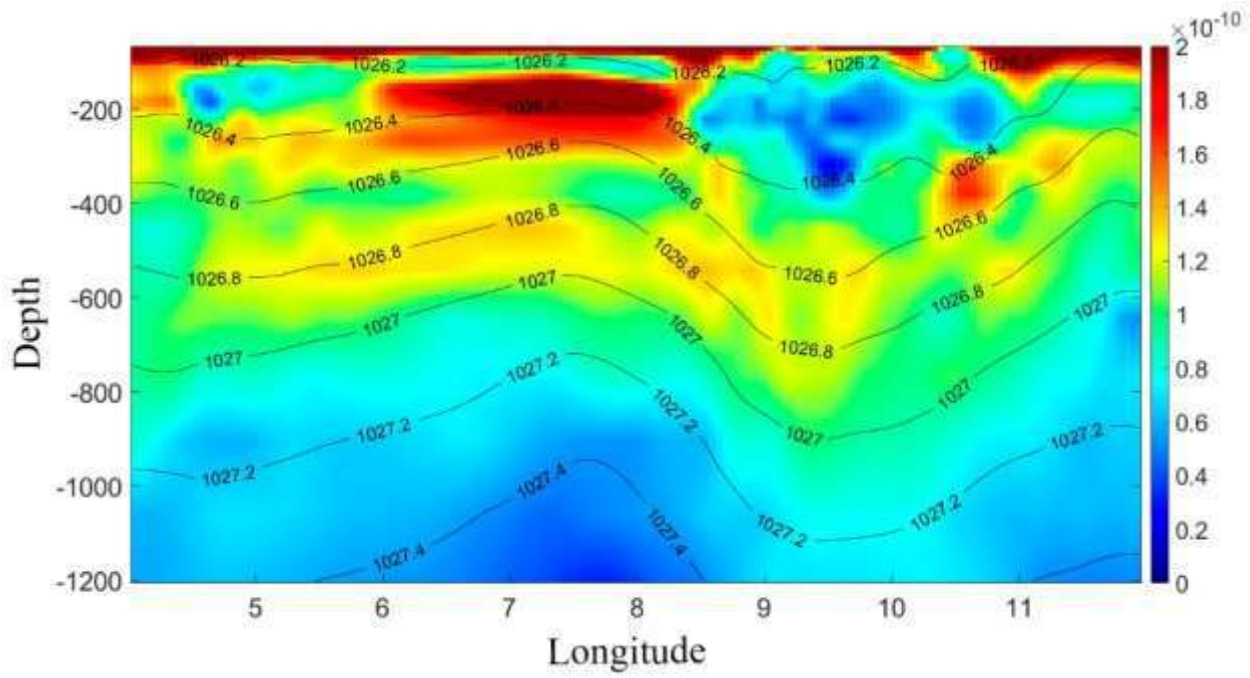

Figure 5.5. The PV was estimated via Ertel's formula ($m^{-1} \cdot s^{-1}$) for 12/13/2012 on a transect at 33.5ºS. The black lines show isopycnies.

The potential vorticity σ calculated by the Rossby formula (Fig. 5.6) differs in dimension from that calculated by the Ertel formula. In contrast to the PV estimates, the values of σ in the anticyclone core are negative and reach a minimum of $-2 \cdot 10^{-5}$ s^{-1}. In the cyclone, σ values are positive in the *Cyc* core and reach a maximum of $8 \cdot 10^{-5}$ s^{-1} at the 200 m horizon. A comparison of Figures 5.5 and 5.6 shows that the core of the anticyclone in the Rossby plot of potential vorticity has a larger vertical extent than according to the Ertel formula. The core is divided into two parts by an insignificant region with positive σ values at a depth of approximately 500 m, which is caused by an insignificant increase in isopycn in this part of the core. In the layer below 500 m to 900 m, the PV values are again negative and reach $-2 \cdot 10^{-5}$ s^{-1}. The cyclone core with positive values is also divided into two parts:

the layer up to 200 m with positive values. Figure 5.6 shows that the cyclone and anticyclone interact with each other, the exchange potential vorticity increases, and the areas of positive and negative σ values extend to the depths where the cyclone is located.

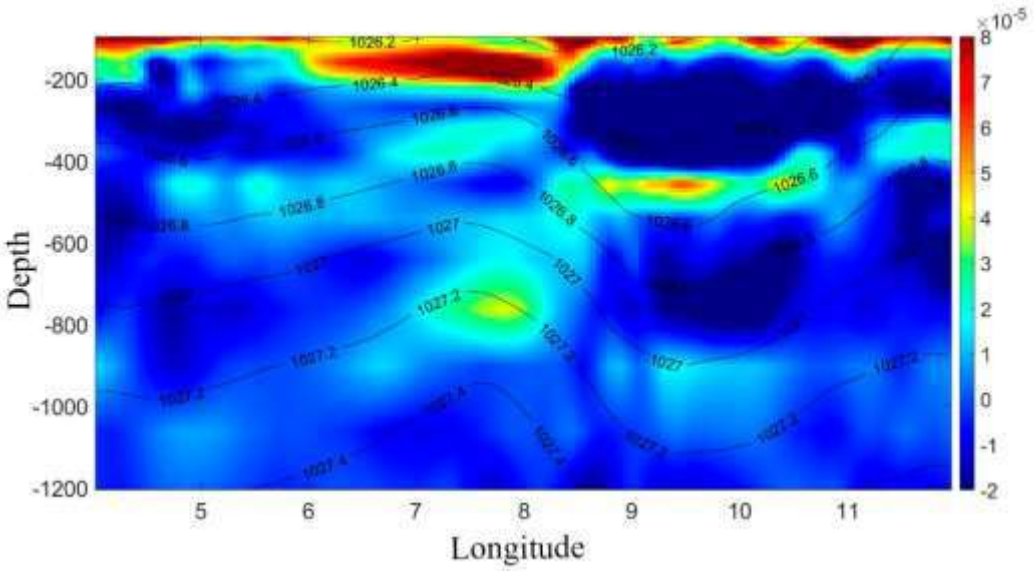

Figure 5.6. Estimated PV using the Rossby formula (s^{-1}) as of 12/13/2012 on the 33.5°S transect. The black lines show isopycnies.

5.2. Thermohaline characteristics of vortices

Anomalies of thermohaline characteristics were calculated relative to the mean annual values at the corresponding points (see vertical sections at 33.5°S in Fig. 5.7).

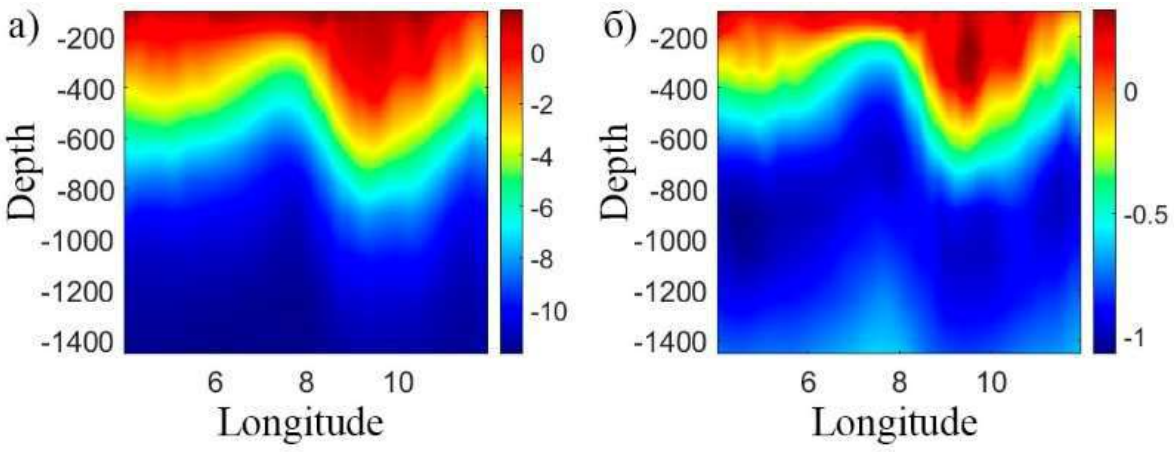

Figure 5.7. Anomalies in temperature (°C) (a) and salinity (psu) (b) at transect 33.5°S on 12/13/2012.

The vertical sections of temperature and salinity (Fig. 5.7) clearly show both eddy types. The center of the cyclone is located at 7.5° E, and the center of the anticyclone is located at 9° E. Both vortices are subsurface. The isotherm and isohaline anomalies of the cyclone extend to 1000 m and to approximately 1200 m, respectively, for the anticyclone. *Ac* is a subsurface eddy in the shape of a semiellipsoid with a core to a depth of 800 m and elevated temperature and salinity values. The temperature and salinity in the core of the anticyclone are higher than the mean background values by 2 °C and 0.3, respectively. The cyclone core is located at a depth of approximately 200 meters, and the temperature and salinity in the cyclone core are below the background values by 1°C and 0.2, respectively.

The Brunt–Vaisala frequency was calculated using the thermodynamic equation TEOS-10 (http://www.teos-10.org/) implemented in the MATLAB environment. The eddy cores are well distinguished on the vertical section of the Brunt–Vaisala frequency (Fig. 5.8). The maximum Brunt–Vaisala frequency is observed in the region of the *Cyc* core and is $4 \cdot 10^{-5}$ s^{-1}, while in the *Ac* core, there is no stratification, and the Brunt–Vaisala frequency values are zero. The cyclone core with homogeneous stratification is located at approximately 100-200 m, and the anticyclone core is located at horizons of 200-400 m. At the same time, isopycn troughs extend at least to a depth of 1200 m.

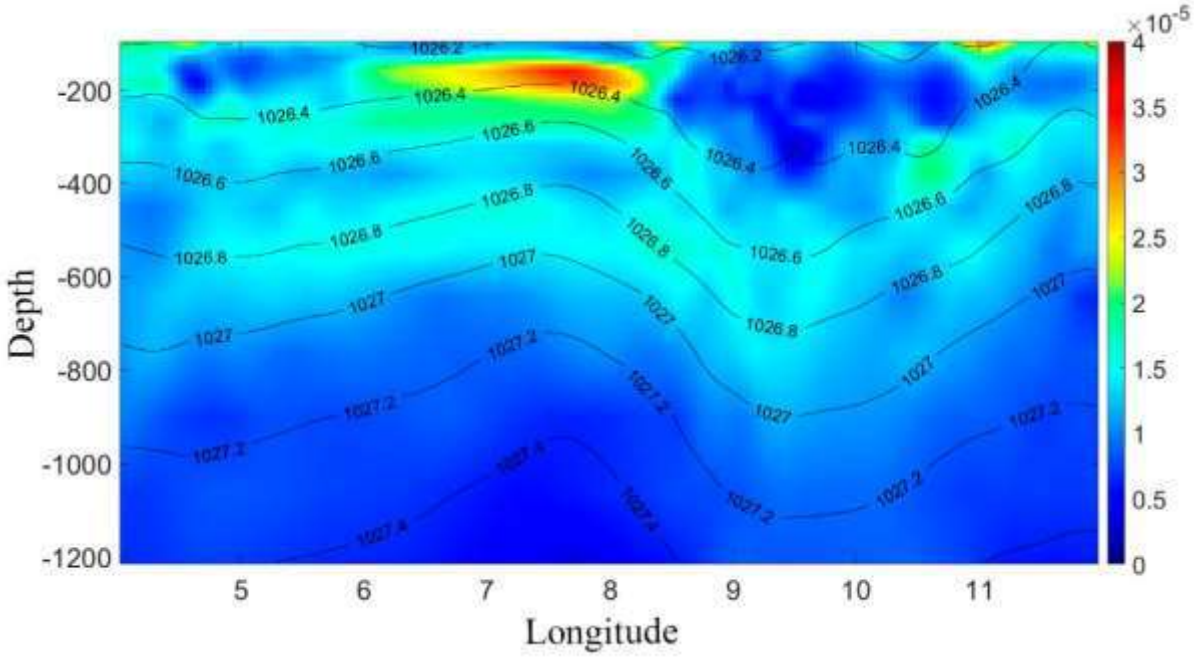

Figure 5.8. The Brunt–Vaisala frequency (s^{-1}) at transect 33.5°S. 13.12.2012. The black lines show isopycnies.

5.3. Kinematic characteristics of eddies

5.3.1. Interaction of eddies with barotropic flow

Theoretical studies have shown that there are three variants of the behavior of mesoscale eddies during the interaction of vortices with barotropic flow: rotation, nutation oscillations, and unrestricted stretching (Malysheva et al., 2020). The evolution of eddies by stretching is accompanied by the loss of kinetic and available potential energy (Zhmur, 2023). A stretched eddy is called an eddy filament in theoretical studies and a filament when analysing satellite or in situ data. The term “filament” is widely used in oceanological studies (Malysheva et al., 2020).

The mechanisms of filament formation are known and have been described in many works: Zhmur (Zhmur, 2011), Kida (Kida et al., 1981), Zhmur and Pankratov (Zhmur et al., 1990), and Travkin (Travkin et al., 2022). Zhmur (Zhmur et al., 2022) considered the evolution of a mesoscale anticyclonic уввн located in the Lofoten Basin, which was initially circular in the horizontal plane and gradually transformed into a filament. The authors observed the evolution process on successive maps constructed from reanalysis data over a period of three weeks. The authors noted an almost linear decrease in energy as the уввн stretched out.

The following question arises: is it possible to observe eddy stretching in the Cape Basin region, which is located southwest of Africa where eddies are more stable and long-lived? Gnevyshev et al. (2022) analysed 28018 cyclones and 26478 anticyclones and showed that Agulhas transports anticyclones, which are longer lived than cyclones, move northwestward in an almost straight line and cross the South Atlantic after crossing thousands of kilometers. The following regularity is noted: when moving westwards under the action of the beta effect, anticyclones are deflected toward the equator, while cyclones are deflected toward the south pole. Various physical mechanisms for this phenomenon have been proposed, and a discussion of these mechanisms can be found in Gnevyshev et al. (2022).

Zhmur (Zhmur et al., 2023b; Zhmur et al., 2023c) theoretically showed that there are regions in the ocean where eddy stretching is forbidden and where eddy stretching has potential. If ocean current data are available, it is possible to plot the geographical

distributions of these regions on maps and calculate their areas. The authors constructed such distributions for different regions of the world ocean and showed that the integral area of areas where eddies can be stretched exceeds the areas where eddies are not stretched.

By analysing radar images of the ocean surface, one can observe many filaments. There are reasons to suppose that some of these faults may have formed during the process of stretching mesoscale eddies (see the example (Zhmur et al., 2023b)). However, the task of analysing eddy transformations on the basis of in situ observations is practically intractable and is hampered by the lack of relevant information on currents with the necessary spatial resolution. Zhmur et al. (2022) considered eddy evolution by stretching using GLORYS12V1 reanalysis data and analysed the changes in kinetic and available potential energy. In this part of the paper, two new examples demonstrating eddy stretching are considered. Thus, the aim of this part of the paper is to analyse the evolution of the kinetic and available potential energy of vortices located in the Cape Basin during the pulling process.

5.3.2. Pulling behavior of the vortices in the Cape Basin

Recent studies related to vortex deformation during interactions with background flow (e.g., Zhmur et al., 2022; Zhmur and Pankratov, 1990) have shown that mesoscale vortices can be stretched into filaments in certain cases and that by stretching, vortices redistribute energy from the mesoscale to the submesoscale. Mesoscale and submesoscale processes are known to have different spatial sizes. The baroclinic Rossby deformation radius is used as a criterion for estimating the scale of the phenomenon:

$$R_d = \frac{N^*}{f} H \,, \tag{5.1}$$

where f is Coriolis parameter, N^* - characteristic value of the Brunt–Vaisala frequency, and H - vertical size of the phenomenon. If the horizontal size of the phenomenon (L) < Rd, the phenomenon is considered submesoscale; if L > Rd, the phenomenon is considered mesoscale. The Rossby number, which is the ratio of the inertia force to the Coriolis force, is also used to describe the scales:

$$R_0 = \frac{U}{fL}, \tag{5.2}$$

where U is the horizontal component of the velocity and L is the horizontal dimension.

For large scales L, the Rossby number is small: Ro < 1. It also follows from the formula that the Rossby number increases as the horizontal size decreases. The transition of this phenomenon to the submesoscale leads to large Rossby numbers and ageostrophic acceleration.

To evaluate the stretching behavior of the eddies in the Cape Basin, two main dynamic characteristics of the eddies were calculated: relative (ζ) and potential vorticity (PV):

$$\zeta = \frac{\partial v}{\partial x} - \frac{\partial u}{\partial y}\ , \tag{5.3}$$

where *u* and *v* are the zonal and meridional components of the flow velocity, respectively; the coordinate axis is right-handed; the x-axis is eastwards; the y-axis is northwards; and z is the vertical axis.

$$PV = \frac{(\zeta + f)\frac{\partial \rho}{\partial z}}{\rho_0}, \tag{5.4}$$

where ρ is the density of water and ρ_0 is the reference density of water; here, ρ_0 = 1027 kg/m^3. A direct difference scheme was used to calculate the derivatives. One of the key properties of potential vorticity is the fulfilment of the permeability theorem (Zhmur and Harutyunyan, 2023a): there is no net PV transport across isopycnic surfaces; hence, the law of conservation of potential vorticity is satisfied, which is analogous to the law of conservation of quantity of motion. However, since ocean systems are not closed, the potential vorticity changes during the process of eddy evolution along with changes in other dynamic and kinematic characteristics.

For this study, many potential vorticity fields were constructed and analysed by Ertel for the presence of eddies capable of stretching. Among others, two eddies of different polarities were found, one located at the smallest distance from each other and one stretching almost simultaneously; these two eddies are representative of each other. Figs. 5.9 and 5.10 show the two eddies at the initial and final moments of their evolution by

stretching. One of the eddies is an anticyclone, and the other is a cyclone. These two eddies of different polarities could be pulled into filaments within 7 days and were chosen for further analysis as an example. The eddy centers at the initial time points are located at 9°E and 39.2°S (anticyclone) and at 12°E and 36.5°S (cyclone). Notably, for the selected vortices, the Rossby number values range from 0.03 to 0.05, which is a rather small value; this indicates the large nonlinearity of the vortices. In Figs. 5.9 and 5.10, one can see that there is a change in the shape of these eddies: if at the initial observation date (19.12.2001), the eddies have the form of ellipses; at the end of the observation period (25.12.2001), the eddies are stretched so that the length exceeds the width 4.5 times for an anticyclone and 3.5 times for a cyclone.

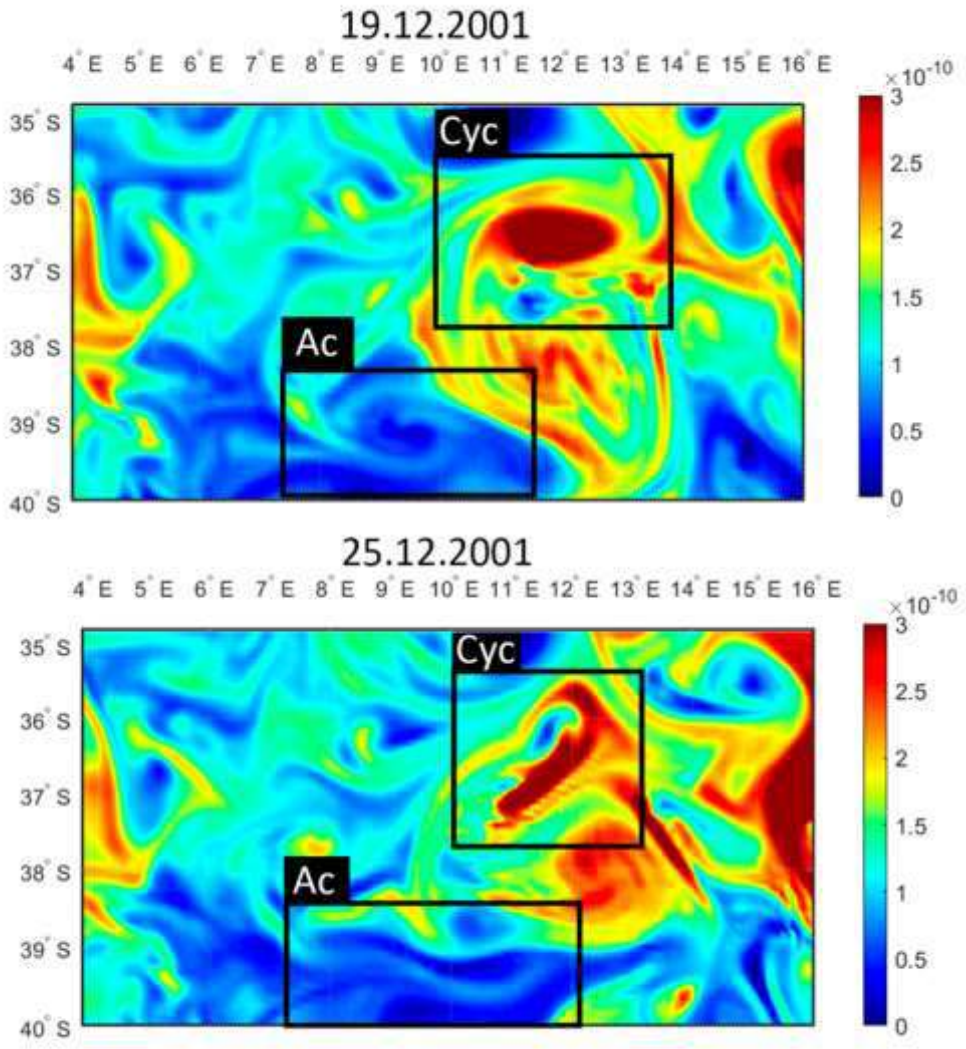

Figure. 5.9. Ertel potential vorticity ($m^{-1} \cdot s^{-1}$) at the initial (19.12.2001) and final (25.12.2001) moments of the evolution of initially horizontally circular eddies into

filaments. The black rectangles indicate anticyclones (*Ac*) and cyclones (*Cyc*). The observation horizon is 200 m long.

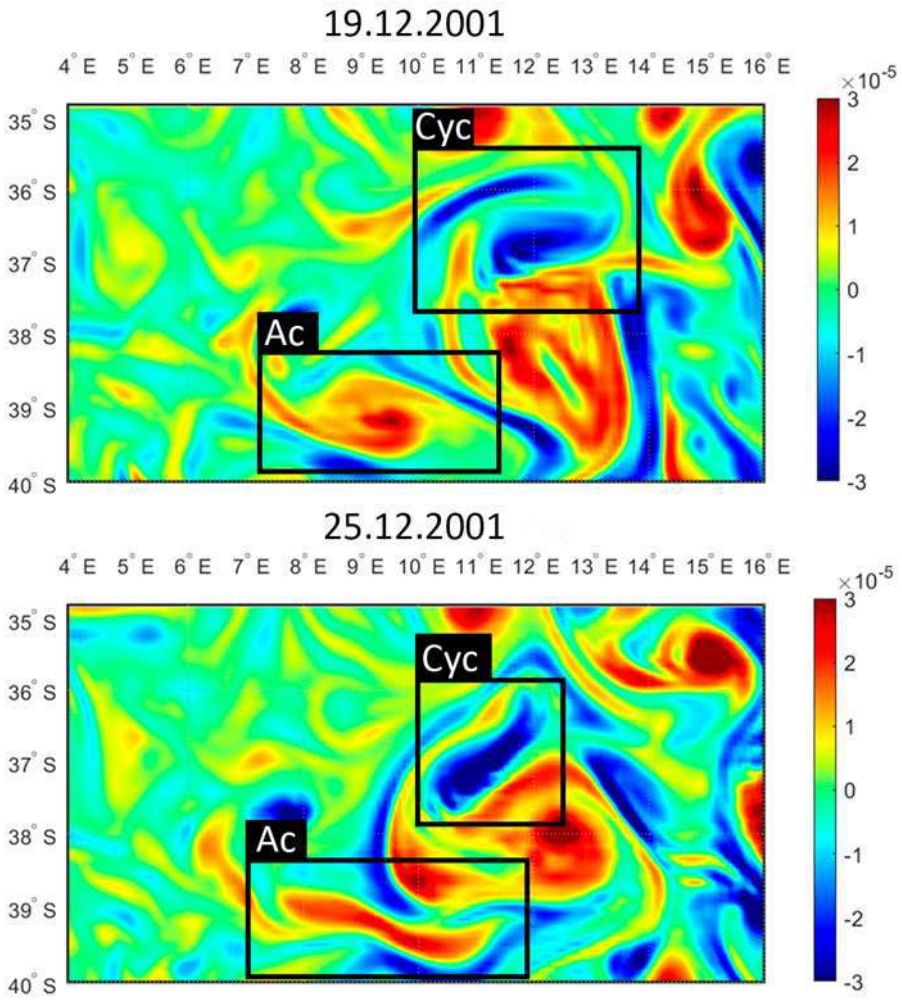

Figure 5.10. Relative vorticity (s^{-1}) at the initial (19.12.2001) and final moments (25.12.2001) of the evolution of initially horizontally circular eddies into filaments. The black rectangles indicate anticyclone *Ac* (positive values) and cyclone *Cyc* (negative values of relative vorticity). The observation horizon is 200 m long.

Zhmur et al. (Zhmur et al., 2023c) considered the different behaviors of mesoscale eddies during their interaction with barotropic flow. Using ocean reanalysis data and parameters that describe the spatial variability of the background flow, namely, the angular velocity of rotation of liquid particles in the background flow (γ) and the background flow deformation coefficient (e), the authors analysed the dependence of γ on e (γ/e). This relationship is used to determine the regions where vortices are allowed to stretch into

filaments and where such stretching does not occur. The application of this theory to different regions of the World Ocean is presented in Zhmur et al. (2023c).

Fig. 5.11 shows the distribution of the γ/e ratios in the area of the Cape Basin as of 25.12.2001, which corresponds to the final date of observation of eddies and their maximum stretching. If the ratio $|\gamma/e| \leq 1$ is valid in a region, then unlimited eddy stretching is allowed in this region. In the other case, when $|\gamma/e| > 1$, pulling is forbidden. If unrestricted vortex stretching is allowed in the area, some of the existing eddies will stretch into filaments. In Fig. 5.11, the red color corresponds to the areas where eddies pulling into filaments are forbidden, and the blue color corresponds to the areas where unrestricted vortex pulling is allowed. The black rectangles denote the regions where the eddies selected for analysis are located (see Figs. 5.9 and 5.10). It can be seen that where the anticyclonic eddy is stretched (eddy center), the area is colored blue, i.e., stretching is allowed. In contrast, both parts into which the eddy has separated are colored red and are not stretched. In the cyclone area, the same situation is observed: the center of the eddy, which is being pulled out, is colored blue, while the parts of the eddy that eventually separate from the parent vortex during pulling out are marked in red. Thus, we observe eddy stretching and further transformation of eddies into eddies on smaller scales. In this case, energy redistribution from the mesoscale to the submesoscale occurs.

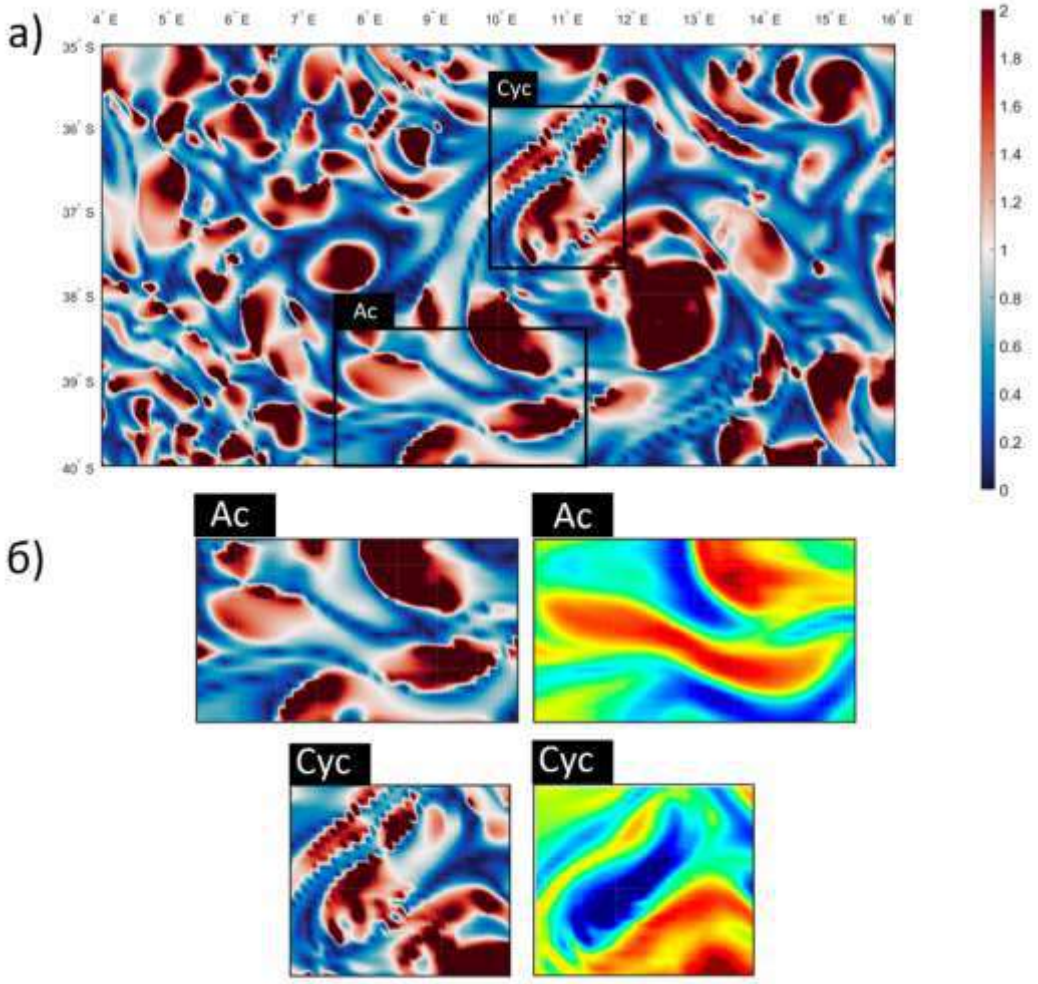

Figure 5.11. Distribution of γ/e coefficients (s^{-1}) in the Cape Basin on 25.12.2001. Horizon 200 m. The black rectangles indicate the areas of vortices selected for analysis. *Ac* - anticyclone, *Cyc* - cyclone (a); b) - approximate fragments of eddies in the field of γ/e coefficients (left) in comparison with the same eddies in the field of relative vorticity (right).

The main parameter characterizing eddy elongation is the dimensionless elongation parameter $\varepsilon = \frac{a}{b} \geq 1$ and effective radius $r_0 = \sqrt{ab}$, where a is the large horizontal semiaxis of the eddy and b is the small horizontal semiaxis. Figure 5.12 shows a plot of the variation in ε and r_0 as the eddies are stretched. At the initial time instant, ε = 1 for *Ac* and 1.2 for *Cyc* since the eddies are nearly circular. As the eddies are stretched, the elongation parameter increases as the length significantly exceeds the width, and the effective radius in turn increases by 17% for the anticyclone and by 6% for the cyclone.

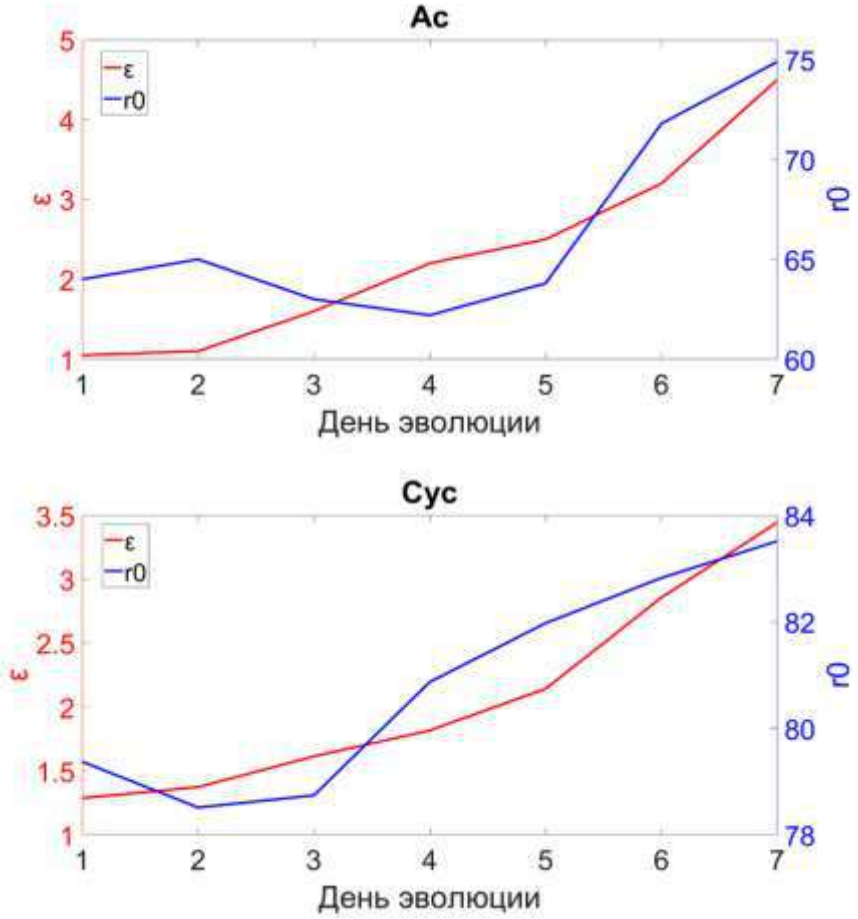

Figure 5.12. Dimensionless eddy elongation parameter (horizontal) ε (red) and the effective radius (blue). The anticyclone is *Ac*, and *Cyc* is a cyclone. The x-axis shows the days of eddy evolution from the beginning of the observation period from 19.12.2001 to 25.12.2001.

Fig. 5.13 shows plots of the dimensionless parameter of the vertical flattening of the vortex core $K = \frac{N}{f}\frac{c}{r_0}$, where c is the vertical semiaxis of the vortex and the Brunt–Vaisala frequency (*N*). The parameter *K* is consistent with the Brunt–Vaisala frequency. During eddy evolution, the parameters increase proportionally. The increase in the the Brunt–Vaisala frequency is associated with the strengthening of water stratification.

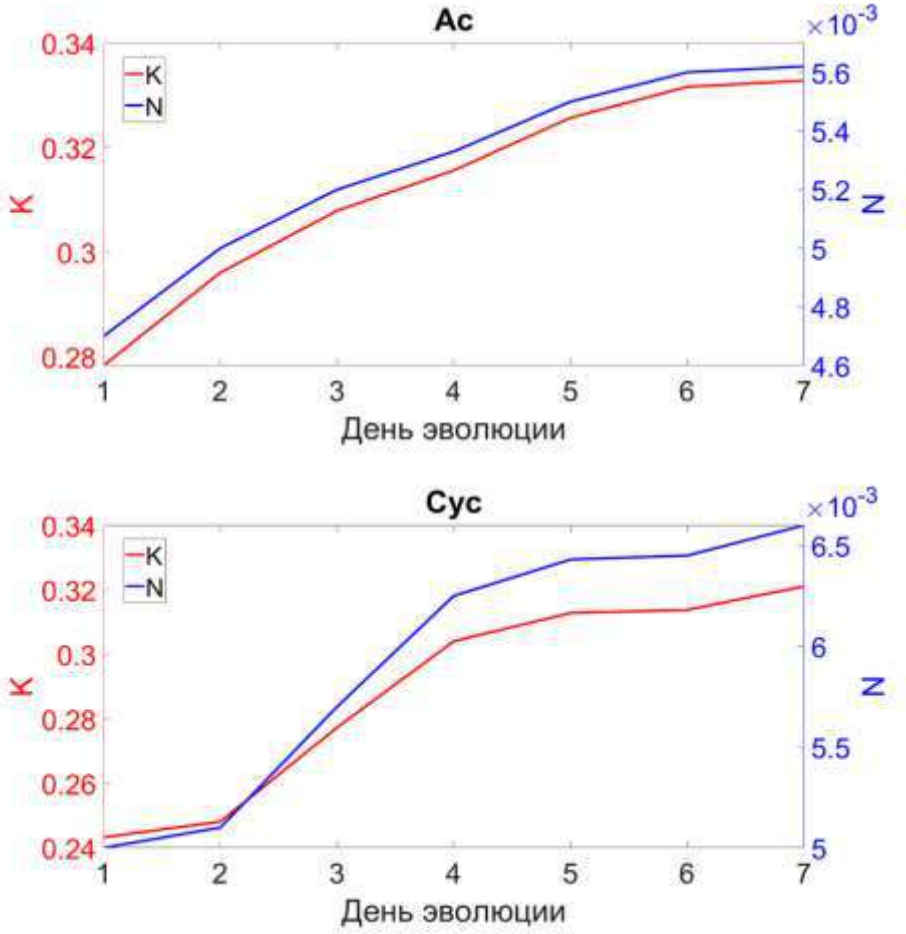

Figure 5.13. Dimensionless parameters of the vertical flattening of the eddy core (K) (red) and the Brunt–Vaisala frequency (N) (blue) of the eddies (anticyclone *Ac* and cyclone *Cyc*). The x-axis shows the days of eddy evolution from 12/19/2001 to 12/25/2001.

Furthermore, we estimated the potential and kinetic energies of the two eddies separately. The potential energy was calculated by the following formula:

$$EP = 0,5 \iiint \left[\frac{g^2}{\rho_0(z)} \frac{\rho^2(x,y,z)}{N^2(x,y,z)} dx\ dy\ dz \right], \tag{5.5}$$

where g is the free-fall acceleration and $\rho = (\rho_\Sigma - \rho_0)$ is the deviation of the current density ρ_Σ from ρ_0. The eddy scale defines the integration boundaries, the isolines of zero relative vorticity define the horizontal boundaries, and the vertical boundaries range from 0 to 1000 m.

For the kinetic energy, the following formula was used:

$$EK = 0,5\iiint\left[\rho_{\Sigma}(x,y,z)\left(u^2(x,y,z)+v^2(x,y,z)\right)\right]dx\ dy\ dz\ .$$

(5.6)

Fig. 5.14 shows that the potential energy of the anticyclonic eddy is 3 orders of magnitude greater than its kinetic energy. As time passes and the shape of the anticyclonic eddy stretches, the energy decreases. The cyclonic eddy has the same situation: the potential energy decreases as the eddy is stretched out, with the kinetic energy being 1 order of magnitude less than the potential energy. It is important to clarify that the last day of observation was not the day of eddy dissipation but was the day of maximum shape stretching. Thus, as the shape of the cyclonic and anticyclonic eddy changes, the kinetic and potential energy decreases. The maximum energy values correspond to the circular shape of eddies of both polarities, and the minimum values correspond to the elongated shape, which is consistent with theory (e.g., Zhmur et al., 2022).

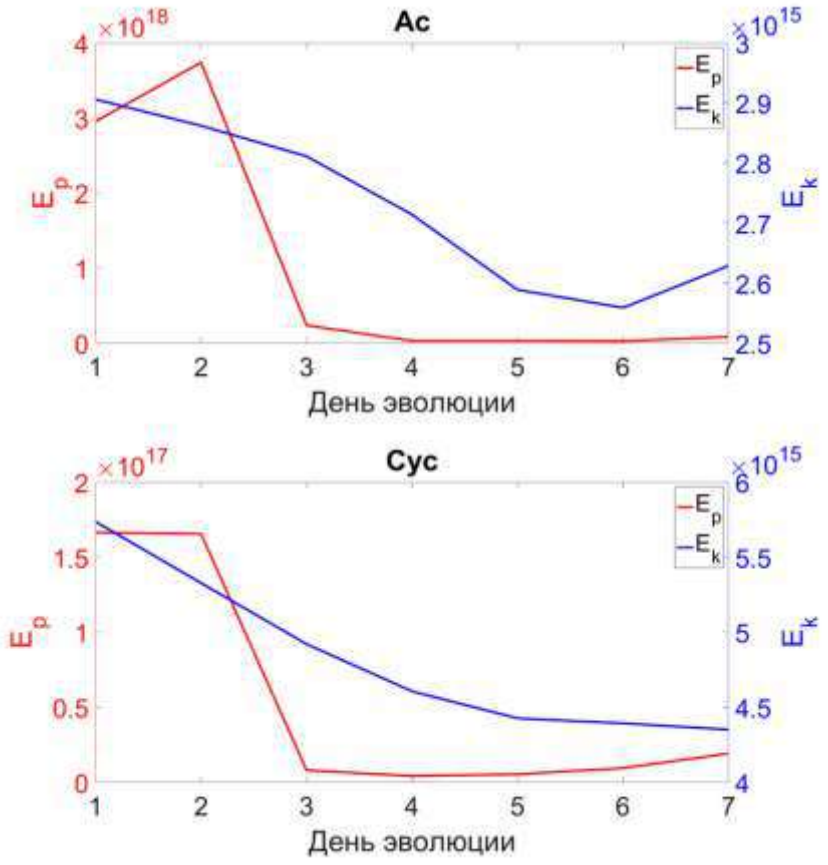

Figure. 5.14. Available potential (red) and kinetic (blue) energy of eddies (J). The x-axis shows the days of eddy evolution in the period from 19.12.2001 to 25.12.2001.

CONCLUSION

In the present work, the eddy dynamics of the South Atlantic Ocean were comprehensively analysed. This study presents quantitative estimates and statistical and Lagrangian analyses of the eddies involved in Agulhas transport and in the Cape Basin. The following dynamic and kinematic parameters of the eddies were also calculated: relative and potential vorticity, the Brunt–Vaisala frequency, spatial dimensions, available potential and kinetic energy, and thermohaline characteristics. An alternative version of the evolution of the initial stage of Agulhas eddy nucleation is proposed, which allows us to explain the almost rectilinear motion of Agulhas eddies. Let us turn to the main results.

1. The vertical structure of the Agulhas transport eddy was analysed. Based on Argo floats data, the temperature and salinity in the eddy waters are 5°C and 0.8-1 greater than the average values in the South Atlantic, respectively. The eddy, which moves considerable distances westwards, retains its unique thermohaline characteristics for a long time. The estimate of Agulhas leakage (flow rate) by a single mesoscale eddy averages 8.5 Sv. The obtained estimate is somewhat lower than that reported in the literature; however, we emphasize that this estimate refers to a single eddy. The heat and salt transport capacities of the single mesoscale Agulhas leakage eddy are $2.25 \cdot 10^9$ W and $5.36 \cdot 10^5$ kg·s^{-1}, respectively. The heat and salt contents in one Agulhas leakage eddy are $2.03 \cdot 10^{15}$ J and $4.83 \cdot 10^{11}$ kg, respectively.

2. Lagrangian analysis of water particles was performed based on GLORYS12V1 reanalysis data and the AMEDA algorithm. The main feature of the study area is the mixing of water particles of different origins. The waters of the South Atlantic circulation interact with the waters of the Agulhas Current more actively than previously thought. This mixing effect of different water types may influence the formation of the two-mode eddy structure previously described by Guerra et al. (2022). The waters carried by the Agulhas leakage eddies originate not only from the Agulhas Current itself but also from the South Atlantic circulation and the Benguela Current. Particles of waters propagating from the west and southwest of the highlighted area travel hundreds of kilometers and fill the study region. We have shown that the influence of the South Atlantic circulation is much more significant than previously thought. Particles of the South Atlantic Gyre waters propagate in the eastwards direction and travel a distance exceeding 2700 km, while in the opposite direction (westwards), this distance is less than half. Most eddies in the study region have

a radius of 40-50 km. We also show that the integral area of anticyclones is much larger than the integral area of cyclones, although the number of individual cyclones with a lifetime of more than 60 days exceeds the number of long-lived anticyclones. The distribution of eddy lifetimes confirms that anticyclones have longer lifetimes than cyclones. The lifetime of most eddies is less than 100 days. However, some eddies with the longest trajectory lengths have lifetimes of more than 500 days. We also show that thermohaline anomalies in eddy characteristics can reach ±4°C and ± 0.5-0.6 psu. This effect may influence the formation of two-mode eddy structures, which has been described but unexplained in other studies.

3. The following is shown on the basis of data from the array of automatic identification and tracking of eddies (META3.2):

- Only anticyclones are long-lived Agulhas eddies. They move northwestward in a nearly straight line, travelling thousands of kilometers and crossing the South Atlantic;

- The characteristics of the eddies (amplitude, radius, orbital velocity, and travel speed) change significantly during their lifetime. We found no clear dependence on the topography or weakening of eddies over time. In contrast, there is sometimes a seemingly unexplained short-term strengthening of the eddy, which seems to be due to a baroclinic factor. The possibility of amplification is also supported by the findings of Early et al. (2011), where the emission of Rossby waves by the eddy was analysed;

- Estimates of the zonal and meridional biases of the Agulhas eddies are given. The zonal displacement, and hence the zonal component of the displacement velocity, dominates, but in some parts of the track, the displacement of the eddy toward the equator is comparable to the zonal displacement. The meridional displacement varies between 9 and 895 km;

- We found that the greater the eddy velocity is, the greater the meridional displacement per unit time;

- The eddies propagate almost rectilinearly. Under the influence of topography, especially when crossing ridges, vortices change azimuth, after which they again propagate rectilinearly;

- The current theories about Rossby eddies (Korotaev, 1997; Reznik, 2010; Early et al., 2011) do not adequately explain the phenomenon of meridional displacement of

Agulhas eddies. In our opinion, the main problem of inapplicability of these models to the description of the phenomenon is the neglect of initial values. Although we do not consider the formation process, the problem of initial values provides a physical understanding of the dynamics of a strong eddy on the β-plane. These causes should play a significant role, at least in the initial stages of vortex evolution;

- The only theory that agrees with observations is that of Lighthill (1967). This allows us to explain the narrowly directed angular emission of long Rossby waves by nonzonal currents;

We propose an alternative version of the evolution of the initial stage of the Agulhas eddy origin without rejecting other scenarios for eddies in other regions of the World Ocean. We propose to explain the first stage of eddy nucleation and evolution by the stage of narrowly directed emission of long Rossby waves under the combined influence of topography and a large-scale nonzonal current. The subsequent eddy dynamics, at large times, are strongly nonlinear, but the law of conservation of potential vorticity is satisfied. At the moment of vortex nucleation, the eddy not only captures the water mass but also acquires translational and rotational momentums, which are functions of the velocity and direction of the large-scale flow and the topography at the point of vortex formation. This can explain the almost rectilinear movement of Agulhas eddies to the northwest.

4. On the basis of the META3.2 automatic eddy identification dataset and GLORYS12V1 ocean reanalysis data, we analysed the dynamic characteristics of the eddies in the Cape Basin. Using the example of two multipolar eddies of the Agulhas Current, it is shown that the eddies propagate westwards, with the anticyclone being more stable and almost crossing the Atlantic Ocean within 1065 days, while the cyclone dissipates 123 days after onset. Accordingly, the anticyclone travelled a distance of 4217 km, and the cyclone travelled 438 km. The drift velocity values differ insignificantly (5.8 and 5.7 cm/s), as do the radii (74 and 72 km).

The vertical structure of eddies is also analysed. For *Cyc*, the anomalies of isotherms and isohalines extend up to 1000 m, and for *Ac*, they extend up to 1200 m. The core of *Ac* extends to a depth of 800 m. The eddy cores are clearly distinguished on the section of the Brunt–Vaisala frequency. The cyclone core, which is characterized by homogeneous stratification, is characterized by the maximum values of the Brunt–Vaisala frequency ($4 \cdot 10^{-5}$ s^{-1}), in contrast to the anticyclone core, in which the Brunt–Vaisala frequency values

are equal to zero; hence, stratification is absent. The relative vorticity is also clearly visible in the eddy cores, with maximum positive values ($4 \cdot 10^{-6}$ s^{-1}) observed in the cyclone region and maximum negative values ($-2 \cdot 10^{-6}$ s^{-1}) in the anticyclone region. An estimation of the potential of eddies based on two approaches is presented: by the Ertel formula and by the Rossby formula. In the anticyclone center, there is practically no stratification, which contributes to small values of potential vorticity according to Ertel ($0.6 \cdot 10^{-10}$-$0.8 \cdot 10^{-10}$ $m^{-1} \cdot s^{-1}$). In addition, in the center of the cyclone, large buoyancy frequencies contributed to large PVs ($1.8 \cdot 10^{-10}$-$2 \cdot 10^{-10}$ $m^{-1} \cdot s^{-1}$). In addition, in the center of an anticyclone, where the negative relative vorticity is large, the PV is close to zero. The minimum (negative) values of the potential Rossby curl reach $-2 \cdot 10^{-5}$ s^{-1} and are observed in the region of the *Ac* core. The maximum values of $8 \cdot 10^{-5}$ s^{-1} are located in the region of the *Cyc* core. The exchange of potential vorticity between eddies upon interaction with each other is also observed.

The kinematic characteristics of the eddies were investigated. The mesoscale eddies of the Cape Basin of different polarities, which change shape over 7 days and transform into filaments during evolution, are considered. It was found that during the process of eddy deformation by barotropic flow, the horizontal semimajor axes of eddies change: the large semimajor axis *a* an increases unlimitedly, and the small semimajor axis *b* decreases significantly. The vertical size of the eddies remains unchanged. The horizontally stretched eddy–filament structure is well observed in the field of relative vorticity since, in the stretched core, the values of relative vorticity are maximal in modulus. During 7 days of evolution, the eddies stretch so that the longitudinal scale is 4.5 times larger than the transverse scale for an anticyclone and 3.5 times larger than that for a cyclone. Extending into filaments, eddies lose energy: the maximum values of all types of energy correspond to the circular form of eddies, and the minimum values correspond to the elongated form. Thus, as the elongation parameter ε increases, the energy decreases: during 7 days of eddy elongation, the potential energy decreases 3 times for an anticyclone and 1.5 times for a cyclone, while the kinetic energy decreases 1.3 times on average. Additionally, at eddy deformation, the vertical flattening parameter grows in proportion to the Brunt–Vaisala frequency, which is connected with the intensification of water stratification.

REFERENCES

1. Arhan M., Mercier H., Lutjeharms J. R. E. The disparate evolution of three Agulhas rings in the South Atlantic Ocean // J. Geophys. Res. 1999. № 104. P. 20987–21005. https://doi.org/ 10.1029/1998jc900047
2. Beal L.M., and Bryden H.L. The velocity and vorticity structure of the Agulhas Current at 32°S // J. Geophys. Res. 1999. № 104 (C3). P. 5151-5176. https://doi.org/10.1029/1998JC900056
3. Beismann J.-O., Kase R.H., Lutjeharms J.R.E. On the influence of submarine ridges on translation and stability of Agulhas rings // J. Geophys. Res. 1999. № 104 (C4). P. 7897–7906. https://doi.org/10.1029/1998JC900127.
4. Belonenko T.V., Budyansky M. V., Malysheva A. A., Udalov A. A. Observing the Agulhas Leakage Source in the Water Mixing Area // Pure Appl. Geophys. 2023. № 180. P. 3401–3421. https://doi.org/10.1007/s00024-023-03331-w
5. Belonenko T. V., Zinchenko V.A., Gordeeva S.M., Raj R.P. Evaluation of heat and salt transports by mesoscale eddies in the Lofoten Basin // Russian Journal of Earth Sciences. 2020. № 20. P. ES6011. https://doi.org/10.2205/2020ES000720.
6. Belonenko T.V., Kubryakov A.A. Temporal variability of phase velocity of Rossby waves in the North Pacific Ocean // Current problems in remote sensing of the Earth from space. 2014. № 3 (11). P. 9–18. [In Russian].
7. Belonenko T.V., Kubryakov A.A., Stanichnyj S.V. Spectral characteristics of Rossby waves of the Northwestern Pacific Ocean // Earth Observation and Remote Sensing. 2016. № 1–2. P. 43–52. [In Russian].
8. Belonenko T.V., Zaharchuk E.A., Fuks V.R. Gradient eddy waves in the ocean. SPb: UDB-SPU, 2004. 215 p. [In Russian].
9. Belonenko T.V., Zaharchuk E.A., Fuks V.R. Waves or vortices? // Vestnik SPbSU. 1998. № 21. P. 37–44. [In Russian].
10. Belyakov L.N., Volkov V.A. Mesoscale subsurface currents in the Arctic Basin // Proceedings of AARI. 1985. № 389. P. 46–51. [In Russian].
11. Benilov E.S. Stability of a Two-Layer Quasigeostrophic Vortex over Axisymmetric Localized Topography // Journal of Physical Oceanography. 2005. № 35 (1). P. 123–130. https://doi.org/10.1175/JPO-2660.1.

12. Biastoch A., Boning C.W., Lutjeharms J.R.E. Agulhas leakage dynamics affects decadal variability in Atlantic overturning circulation // Nature. 2008. № 456. P. 489–492. https://doi.org/10.1038/nature07426.
13. Biastoch A., Böning C.W., Schwarzkopf F.U., Lutjeharms J. R. E. Increase in Agulhas leakage due to poleward shift of southern hemisphere westerlies // Nature. 2009. № 462 (7272). P. 495–498. https://doi.org/10.1038/nature08519
14. Boebel O., Rae C.D., Garzoli S., Lutjeharms J., Richardson P., Rossby T., Schmid C. and Zenk W. Float experiment studies interocean exchanges at the tip of Africa // Trans. Amer. Geophys. Union. 1998. № 79. P. 1–8. https://doi.org/10.1029/98EO00001
15. Boebel O., Rossby T., Lutjeharms J.R.E., Zenk, Walter and Barron C. Path and variability of the Agulhas Return Current // Deep Sea Research. Part II. 2003. № 50. P.35—56. https://doi.org/10.1016/S0967-0645(02)00377-6.
16. Borisov A.V., Mamaev I.S. and Sokolovskij M.A. (ed.) Fundamental and applied problems of vortex theory. Izhevsk: Institute for Computer Research, 2003. 704 p. [In Russian].
17. Bryden H.L., Beal L.M., Duncan L.M. Structure and transport of the Agulhas Current and its temporal variability // J. Oceanography. 2005. № 61. P. 479–492. https://doi.org/10.1007/s10872–005–0057–8.
18. Budyansky M.V., Prants S.V., Uleysky M.Y. Odyssey of Aleutian eddies // Ocean Dynamics. 2022. № 72. P. 455–476. https://doi.org/10.1007/s10236-022-01508-w.
19. Bunker A.F. Surface energy fluxes of the South Atlantic Ocean // Mon. Weather Rev. 1988. № 116. P. 809–823. https://doi.org/10.1175/1520-0493(1988)116<0809:SEFOTS>2.0.CO;2
20. Byrne D.A., Gordon A.L., Haxby W.F. Agulhas eddies: A synoptic view using geosat ERM data // J. Phys. Oceanogr. 1995. № 25, P. 902–917. https://doi.org/10.1175/1520-0485(1995)025<0902:AEASVU>2.0.CO;2
21. Caley T., Giraudeau J., Malaizé B., Rossignol L., Pierre C. Agulhas leakage as a key process in the modes of Quaternary climate changes // Proc. Natl. Acad. Sci. USA. 2012. № 109. P.6835–6839. https://doi.org/10.1073/pnas.1115545109
22. Casanova -Masjoan M., Pelegrí JL, Sangrà P., Martínez A, Grisolía-Santos D., Pérez-Hernández M. D., Hernández-Guerra A. Characteristics and evolution of an Agulhas ring // Journal of Geophysical Research: Oceans. 2017. № 122 (9). P.7049-7065. https://doi.org/10.1002/2017JC012969

23. Chaigneau A., Le Texier M., Eldin G., Grados C., Pizarro O. Vertical structure of mesoscale eddies in the eastern South Pacific Ocean: A composite analysis from altimetry and Argo profiling floats // J. Geophys. Res. 2011. C11025. https://doi.org/10.1029/2011JC007134.
24. Chelton D.B., Schlax M.G., Samelson R.M. Global observations of nonlinear mesoscale eddies // Progress in Oceanography. 2011. № 91 (2). P. 167–216. https://doi.org/10.1016/j.pocean.2011.01.002.
25. Chelton D.B., Schlax M.G., Samelson R.M., de Szoeke R.A. Global observations of large oceanic eddies // Geophys. Res. Lett. 2007. № 34. L15606. https://doi.org/10.1029/2007GL030812.
26. Cheng Yu., Putrasahan D., Beal L., Kirtman B. Quantifying Agulhas leakage in a high-resolution climate model // Journal of Climate. 2016. № 29 (19). P. 6881–6892. https://doi.org/10.1175/ JCLI-D-15-0568.1.
27. Curry J.A., and Webster P. J. Thermodynamics of Atmospheres and Oceans. Academic Press, 1999. 467p.
28. Cushman-Roisin B. Introduction to Geophysical Fluid Dynamics. N. J.: Prentice-Hall, Upper Saddle River, 1994. 313 p.
29. Danabasoglu G., McWilliams J. C., Gent P. R. The role of mesoscale tracer transports in the global ocean circulation // Science. 1994. № 264 (5162). P. 1123–1126. https://doi.org/10.1126/science.264.5162.1123
30. de Ruijter W. P. M., Ridderinkhof H., Lutjeharms J. R. E., Schouten M. W. Direct observations of the flow in the Mozambique channel // Geophysical Research Letters. 2002. № 29 (10). P. 140-1–140-3. https://doi.org/10.1029/2001GL013714.
31. De Steur L., Van Leeuwen P. J., Drijfhout S. S. Tracer leakage from modeled Agulhas rings // Journal of Physical Oceanography. 2004. № 34(6). P. 1387–1399. https://doi.org/10.1175/1520- 0485(2004)034%3c1387:TLFMAR%3e2.0.CO;2.
32. Dencausse G., Arhan M., Speich S. Routes of Agulhas rings in the southeastern Cape Basin // Deep-Sea Res. Part I: Oceanographic Res. Papers. 2010. № 57 (11). P. 1406–1421. https://doi.org/10.1016/j.dsr.2010.07.008
33. Dijkstra H. A. and de Ruijter W. P. M. On the Physics of the Agulhas Current: Steady Retroflection Regimes // J. Phys. Oceanogr. 2001. № 31. P.2971–2985. https://doi.org/10.1175/1520-0485(2001)031<2971:OTPOTA>2.0.CO;2

34. Doglioli A. M., Blanke B., Speich S., Lapeyre G. Tracking coherent structures in a regional ocean model with wavelet analysis: Application to Cape Basin eddies // J. Geophys. Res. 2007. № 112. C05043. https://doi.org/10.1029/2006JC003952.
35. Doglioli A. M., Veneziani M., Blanke B., Speich S., Griffa A. Lagrangian analysis of the Indian-Atlantic interocean exchange in a regional model // Geophysical Research Letters. 2006. № 33. L14611. https://doi.org/10.1029/2006GL026498.
36. Dong C., McWilliams J. C., Liu Y., Chen D. Global heat and salt transports by eddy movement // Nat. Commun. 2014. № 5. P. 1–6. https://doi.org/10.1038/ncomms4294
37. Donners J., Drijfhout S. S., Coward A. C. Impact of cooling on the water mass exchange of Agulhas rings in a high resolution ocean model // Geophysical Research Letters. 2004. № 31 (16). L16312. https://doi.org/10.1029/2004GL020644.
38. Donohue E.A., Firing E., Beal L. Comparison of the three velocity sections of the Agulhas Current and the Agulhas Undercurrent // Journal of Geophysical Research. 2000. № 105 (C12). P.28585 – 28593. https://doi.org/10.1029/1999JC000201.
39. Drijfhout S. S., de Vries P. Impact of eddy-induced transport on the Lagrangian structure of the upper branch of the thermohaline circulation // Journal of Physical Oceanography. 2003. № 33 (10). P. 2141–2155. https://doi.org/10.1175/1520-0485(2003)033%3c2141:IOETOT%3e2.0.CO;2.
40. Duba C.T., Doyle T.B., McKenzie J.F. Rossby wave patterns in zonal and meridional winds // Geophysical & Astrophysical Fluid Dynamics. 2014. № 108 (3). P. 237–257. https://doi.org/10.1080/03091929.2013.867604.
41. Duncombe Rae C. M. Agulhas retroflection rings in the South Atlantic Ocean: An overview // South African Journal of Marine Science. 1991. № 11 (1). P. 327–344. https://doi.org/10.2989/ 025776191784287574.
42. Duncombe Rae C. M., Garzoli S. L., Gordon A. L. The eddy field of the southeast Atlantic Ocean: A statistical census from the Benguela sources and transports project. Journal of Geophysical Research, 1996. № 101(11). P. 949–964. https://doi.org/10. 1029/95JC03360.
43. Durgadoo J. V., Ruhs S., Biastoch A., Boning C. W. B. Indian Ocean sources of Agulhas leakage // Journal of Geophysical Research: Oceans. 2017. № 122. P. 3481–3499. https://doi.org/ 10.1002/2016JC012676.
44. Early J. J., Samelson R. M., Chelton D. B. The Evolution and Propagation of Quasigeostrophic Ocean Eddies // J. Phys. Oceanogr. 2011. № 41. P. 1535–1555. https://doi.org/10.1175/2011JPO4601.1.

45. Fedorov K.N. (ed.) Collection of articles “Intrathermocline eddies in the ocean.” M: Academy of Sciences of the USSR, 1986. 142 p. [In Russian].
46. Garzoli S. L., Gordon A. L. Origins and variability of the Benguela current // Journal of Geophysical Research. 1996. № 101 (C1). P. 897–906. https://doi.org/10.1029/95JC03221.
47. Garzoli S. L., Richardson P. L., Duncombe Rae C. M., Fratantoni D. M., Goñi G. J., Roubicek A. J. Three Agulhas rings observed during the Benguela Current experiment // J. Geophys. Res. 1999. № 104. P. 20971–20986. https://doi.org/10.1029/1999JC900060
48. Garzoli S.L., Goni G.J. Combining altimeter observations and oceanographic data for ocean circulation and climate studies // Elsevier Oceanographic Series. 2000. № 63. P. 79–95. https://doi.org/10.1016/S0422–9894(00)80006–9.
49. Gill A.E. Atmosphere-Ocean Dynamics. AcademicPress, 1982. 662p.
50. Giulivi C.F., Gordon A.L. Isopycnal displacements within the Cape Basin thermocline as revealed by the hydrographic data archive // Deep Sea Res. Part I. 2006. № 53. P. 1285– 1300. https://doi.org/10.1016/j.dsr.2006.05.011.
51. Gnevyshev V. G., Malysheva A. A., Belonenko T. V., Koldunov A.V. On Agulhas eddies and Rossby waves travelling by forcing effects // Russian Journal of Earth Sciences. 2021. № 21. ES5003. https://doi.org/10.2205/2021ES000773
52. Gnevyshev V.G., Badulin S.I., Belonenko T.V. Rossby waves on non-zonal currents: structural stability of critical layer effects // Pure Appl. Geophys. 2020. № 177. P. 5585–5598. https://doi.org/10.1007/s00024-020-02567-0.
53. Gnevyshev V.G., Frolova A.V., Kubryakov A.A., Sobko Y.V., Belonenko T.V. Interaction of Rossby waves with the jet stream: basic equations and their verification for the Antarctic Circumpolar Current // Izvestiya, Atmospheric and Oceanic Physics. 2019. № 5 (55). P. 39–50. https://doi.org/10.1134/S0001433819050074. [In Russian].
54. Gnevyshev V.G., Frolova A.V., Kubryakov A.A., Sobko Yu.V., Belonenko T.V. Interaction of Rossby waves with a jet stream: basic equations and their verification for the Antarctic circumpolar current // Izv. Atmos. Ocean. Phys. 2019. № 55 (5). P. 412–422. https://doi.org/10.1134/S0001433819050074.
55. Gnevyshev V.G., Shrira V.I. Dynamics of Rossby wave packets in the vicinity of the zonal critical layer taking into account viscosity // Izv. Akad. Nauk SSSR, Fiz. Atmos. Okeana. 1989a. № 25 (10). P. 1064–1074.

56. Gnevyshev V.G., Shrira V.I. Kinematics of rossby waves on non-uniform meridional current // Okeanologiya. 1989b. № 29 (4). P. 543–548.
57. Gnevyshev V.G., Shrira V.I. On the evaluation of barotropic-baroclinic instability parameters of the zonal flows in beta-plane // Dokl. Akad. Nauk SSSR. 1989c. № 306 (2). P. 305–309.
58. Gnevyshev V.G., Shrira V.I. On the evaluation of barotropic-baroclinic instability parameters of zonal flows on a beta-plane // J Fluid Mech. 1990. № 221. P. 161–181. https://doi.org/10.1017/S0022112090003524.
59. Gnevyshev V.G., Shrira V.I. Transformation of monochromatic Rossby waves in the critical layer of the zonal current // Izv. Akad. Nauk SSSR, Fiz Atmos Okeana. 1989d. № 25 (8). P. 852–862.
60. Goni G. J., Garzoli S. L., Roubicek A. J., Olson D. B., Brown O. B. Agulhas ring dynamics from TOPEX/POSEIDON satellite altimeter data // Journal of Marine Research. 1997. № 55(5). P. 861–883. https://doi.org/10.1357/0022240973224175.
61. Gordon A. L. Indian—Atlantic transfer of thermocline water at the Agulhas Retroflection // Science. 1985. № 227. P. 1030—1033. https://doi.org/10.1126/science.227.4690.1030.
62. Gordon A. L., Weiss R. F., Smethie W. M., Warner M. J. Thermocline and intermediate water communication between the South Atlantic and Indian Ocean // Journal of Geophysical Research. 1992. № 97 (C5). P. 7223—7240. https://doi.org/10.1029/92JC00485.
63. Gordon A.L., Haxby W.F. Agulhas eddies invade the south Atlantic: Evidence From Geosat altimeter and shipboard conductivity-temperature-depth survey // Journal of Geophysical Research: Oceans. 1990. № 5 (C3). P. 3117—3125. https://doi.org/10.1029/JC095iC03p03117.
64. Gordon A.L., Lutjeharms J.R.E., Grundlingh M.L. Stratification and circulation at the Agulhas retroflection // Deep Sea Res. Part A. 1987. № 34. P. 565–599. https://doi.org/10.1016/0198–0149(87)90006–9.
65. Guerra L. A. A., Mill G. N., Paiva A. M. Observing the spread of Agulhas leakage into the Western South Atlantic by tracking mode waters within ocean rings // Frontiers in Marine Science. 2022. № 9. 958733. https://doi.org/10.3389/fmars.2022.958733.
66. Guerra L. A. A., Paiva A. M., Chassignet E. P. On the translation of Agulhas rings to the western South Atlantic Ocean // Deep Sea Research Part I: Oceanographic

Research Papers. 2018. № 139. P. 104—113. https://doi.org/10.1016/j.dsr.2018.08.005.

67. Hall C., Lutjeharms J.R.E. Cyclonic eddies identified in the Cape Basin of the South Atlantic Ocean // Journal of Marine Systems. 2011. № 85. P. 1–10. https://doi.org/10.1016/j.jmarsys.2010.10.003.
68. Hall M. M, Bryden H. L. Direct estimates and mechanisms of ocean heat transport // Deep Sea Res. 1982. № 29. P. 339 – 359. https://doi.org/10.1016/0198-0149(82)90099-1
69. Haynes P., McIntyre M. On the conservation and impermeability theorems for potential vorticity // J. Atmos. Sci. 1990. № 47 (16). P. 2021—2031. https://doi.org/10.1175/1520-0469(1990)047<2021:OTCAIT>2.0.CO;2.
70. Haynes P., McIntyre M. On the evolution of vorticity and potential vorticity in the presence of diabatic heating and frictional or other forces // J. Atmos. Sci. 1987. № 44 (5). P. 828—841.
71. Hermes, J.C., Reason, C.J.C., Lutjeharms, J.R.E. Modeling the variability of the Greater Agulhas Current System // J. Climate. 2007. № 20. P.3131–3146. https://doi.org/10.1175/JCLI4154.1
72. Hutchings L., van der Lingen C. D., Shannon L. J., Crawford R. J. M., Verheye H. M. S., Bartholomae C. H., van der Plas A. K., Louw D., Kreiner A., Ostrowski M., Fidel Q., Barlow R. G., Lamont T., Coetzee J., Shillington F., Veitch J., Currie J. C., Monteiro P. M. S. The Benguela Current: An ecosystem of four components // Progress in Oceanography. 2009. № 83 (1–4). P. 15–32. https://doi.org/10.1016/j.pocean.2009.07.046.
73. Jayne S. R., Marotzke J. The Oceanic Eddy Heat Transport // J. Phys. Oceanogr. 2001. № 32. P. 3328 – 3345. https://doi.org/10.1175/1520-0485(2002)032<3328:TOEHT>2.0.CO;2
74. Kamenkovich V. M., Leonov Y. P., Nechaev D. A., Byrne D. A., Gordon A. L. On the influence of bottom topography on the Agulhas eddy. Journal of Physical Oceanography. 1996. № 26 (6). P. 892–912. https://doi.org/10.1175/1520-0485(1996)026%3c0892: OTIOBT%3e2.0.CO;2.
75. Kamenkovich V.M., Koshlyakov M.N., Monin A.S. Synoptic eddies in the ocean. L: Gidrometeoizdat, 1987. 512 p. [In Russian].

76. Kida S. Motion of an Elliptic Vortex in a Uniform Shear Flow // Journal of the Physical Society of Japan. 1981. № 50 (10). P. 35173520. https://doi.org/10.1143/JPSJ.50.3517.
77. Korotaev G., Fedotov A. Dynamics of an isolated barotropic eddy on a beta-plane // Journal of Fluid Mechanics. 1994. № 264. P. 277–301. https://doi.org/10.1017/S0022112094000662.
78. Korotaev G.K. Structure and kinematics of synoptic eddies in the ocean: theory and modern observations // Marine Hydrophysical Journal. 2020. № 36 (6). P. 757–780. https://doi.org/10.22449/0233-7584-2020-6-757-780. [In Russian].
79. Korotaev G.K., Dorofeev V. L., Fedotov A.B. Dynamics of an intensive isolated barotropic eddy in the presence of background vorticity // Physical Oceanography. 1997. № 8 (1). P. 1–8. https://doi.org/10.1007/BF02522560.
80. Koshlyakov M. N., Belokopytov V. N. Synoptic eddies of the open ocean: a review of experimental studies // Marine Hydrophysical Journal. 2020. № 36 (6). P. 613–627. https://doi.org/10.22449/0233-7584-2020-6-613-627. [In Russian].
81. Laxenaire R., Speich S., Alexandre S. Evolution of the thermohaline structure of one Agulhas Ring reconstructed from satellite altimetry and Argo floats // J. Geophys. Res: Oceans. 2019. № 124. https://doi.org/10.1029/2019JC015210
82. Laxenaire R., Speich S., Stegner A. Agulhas ring heat content and transport in the South Atlantic estimated by combining satellite altimetry and Argo profiling floats data // J. Geophys. Res: Oceans 2020. № 125 (e2019JC015511). https://doi.org/10.1029/2019JC015511
83. LeBlond P.H., Mysak L.A. Waves in the ocean. Amsterdam: Elsevier Scientific Publishing Company, 1981. 602 p.
84. LeBlond P.H., Mysak L.A. Waves in the ocean in 2 volumes. M.: Mir, 1981. 846 p. [In Russian].
85. Leonov Y.P. The influence of topography on the eddies of the Agulhas Current: abstract of the dissertation of a candidate of physical and mathematical sciences. Shirshov Institute of Oceanology of the Russian Academy of Sciences. 1995. [In Russian].
86. Lighthill M. J. On waves generated in dispersive systems by travelling forcing effects, with applications to the dynamics of rotating fluids // Journal of Fluid Mechanics. 1967. № 27 (04). P. 725—752. https://doi.org/10.1017/S0022112067002563.

87. Lord Kelvin. Deep Sea Ship-Waves // Proc. R. Soc. Edinburgh. 1906. № 25 (2). P. 1060—1084. https://doi.org/10.1017/S0370164600016771.
88. Lutjeharms J. R. E. Three decades of research on the greater Agulhas Current // Ocean Science. 2007. №3. P. 129—147. https://doi.org/10.5194/os-3-129-2007.
89. Lutjeharms J. R. E. The Agulhas Current. Berlin: Springer-Verlag, 2006. 329 p.
90. Lutjeharms J. R. E., & van Ballegooyen R. C. The retroflection of the Agulhas Current // Journal of Physical Oceanography. 1988. № 18. P. 1570–1583. https://doi.org/10.1175/1520- 0485(1988)018%3c1570:TROTAC%3e2.0.CO;2.
91. Lutjeharms J. R. E., Valentine H.R. Eddies at the SubTropical Convergence south of Africa // Journal of Physical Oceanography. 1988. № 18. P. 761—774.
92. Lutjeharms J.R.E., Gordon A.L. Shedding of an Agulhas Ring observed at sea // Nature 1987. № 325 (6100). P. 138–140. https://doi.org/10.1038/325138a0
93. Lutjeharms J.R.E., Valentine H.R. Evidence for persistent Agulhas rings southwest of Cape Town // S. Afr. J. Sci. 1988. № 84. P. 781–783.
94. Malysheva A. A., Belonenko, T. V. Changes in available potential and kinetic energy of mesoscale eddies in the Cape Basin // Hydrometeorology and ecology. 2023. № 73. P. 684–699. https://doi.org/10.33933/2713-3001-2023-73-684-698
95. Malysheva A. A., Belonenko, T. V., Budyansky M. V. Lagrangian Method for Studying Agulhas Leakage in the Water Mixing Area // Complex Investigation of the World Ocean (CIWO-2023). 2023. P. 111–117. https://doi.org/10.1007/978-3-031-47851-2_18
96. Malysheva A.A., Kubryakov A.A., Koldunov A.V., Belonenko T.V. Estimation of Agulhas leakage based on satellite altimetry and Argo floats data // Earth Observation and Remote Sensing. 2020a. № 2. P. 24—34. https://doi.org/10.31857/S0205961420020049. [In Russian].
97. Malysheva A. A., Kubryakov A. A., Koldunov A. V., Belonenko, T. V. Estimating Agulhas leakage by means of satellite altimetry and argo data // Izvestiya, Atmospheric and Oceanic Physics. 2020b. № 56. P. 1581–1589. https://doi.org/10.1134/ S0001433820120476.
98. Malysheva A.A., Belonenko T.V., Yakovleva D.A. Characteristics of two eddies of different polarity in the Agulhas Current // Hydrometeorology and ecology. 2022. № 68. P. 478—493. https://doi.org/10.33933/2713-3001-2022-68-478-493. [In Russian].

99. Malysheva A.A., Koldunov A.V., Belonenko T.V., Sandalyuk N.V. Agulhas leakage eddies according to satellite altimetry data // Scientific notes of the RSHU. 2018. №52. P. 154—170. [In Russian].
100. Marcos M., Pascual A., Pujol I. Improved satellite altimeter mapped sea level anomalies in the Mediterranean Sea: A comparison with tide gauges // Advances in Space Research. 2015. № 56 (4). P. 596–604. https://doi.org/10.1016/j.asr.2015.04.027.
101. Matano R. P., Beier E. J. A kinematic analysis of the Indian/Atlantic inter-ocean exchange // Deep-Sea Research II. 2003. № 50. P. 229–250. https://doi.org/10.1016/S0967-0645(02)00395-8.
102. McDonagh E.L., Heywood K.J., Meredith M.P. On the structure, paths, and fluxes associated with Agulhas Rings // J. Geophysical Research: Oceans 1999. № 104 (C9). P. 21007–21020. https://doi.org/10.1029/1998JC900131
103. Monin A.S., Krasickij V.P. Phenomena on the surface of the ocean. L: Gidrometeoizdat, 1985. 376 p. [In Russian].
104. Monin A. S., Zhikharev G. M. Ocean vortices // Physics–Uspekhi. 1990. №33 (5). P. 313-339. https://doi.org/10.1070/PU1990v033n05ABEH002569.
105. Morrow R., Birol F., Griffin D., Sudre J. Divergent pathways of cyclonic and anti-cyclonic ocean eddies // Geophys. Res. Lett. 2004. № 31. L24311. https://doi.org/10.1029/2004GL020974.
106. Munk W. Achievements in Physical Oceanography. 50 Years of Ocean Discovery. Washington, DC: National Academic Press. 2000, 300 p.
107. Nencioli F., Dall'Olmo G., Quartly G.D. Agulhas ring transport efficiency from combined satellite altimetry and argo profiles // J. Geophysical Research: Oceans. 2018. № 123. P. 5874–5888. https://doi.org/10.1029/2018JC013909
108. Nezlin M. V. Rossby solitons (Experimental investigations and laboratory model of natural vortices of the Jovian Great Red Spot type) // Sov. Phys. Usp. 1986. № 29. P. 807-849.
109. Nezlin M.V. Rossby solitons // Advances in Physical Sciences. 1986. № 150 (1). P. 1–58. [In Russian].
110. Nof D. Strange encounters of eddies with walls // J. Mar. Res. 1999. № 57. P. 739–761.

111. Olson D.B., Evans R.H. Rings of the Agulhas current // Deep Sea Research Part A: Oceanographic Research Papers. 1986. № 33 (1). P. 27—42. https://doi.org/10.1016/0198-0149(86)90106-8.
112. Pedlosky J. Geophysical Fluid Dynamics. New York: Springer Verlag, 1984. 624 p.
113. Pegliasco C., Delepoulle A., Mason E., Morrow R., Faugère Y., Dibarboure G. META3.1exp: a new global mesoscale eddy trajectory atlas derived from altimetry // Earth Syst. Sci. Data. 2022. № 14. P. 1087–1107. https://doi.org/10.5194/essd-14-1087-2022.
114. Prants S. V., Uleysky M.Y., Budyansky M.V. Lagrangian oceanography: Large-scale transport and mixing in the ocean. Springer-Verlag, 2017. 273 p.
115. Prants S.V., Budyansky M.V., Lobanov V.B., Sergeev A.F., Uleysky, M.Y. Observation and Lagrangian analysis of quasistationary Kamchatka trench eddies // Journal of Geophysical Research: Oceans. 2020. № 125 (6). e2020JC016187. https://doi.org/ 10.1029/2020jc016187.
116. Prants S.V., Budyansky M.V., Uleysky M.Y. How eddies gain, retain, and release water: A case study of a Hokkaido anticyclone // Geophysical Research Letters. 2018. № 123 (3). P. 2081–2096. https://doi.org/10.1002/2017jc013610.
117. Prants S.V., Budyansky M.V., Uleysky M.Y. Identifying Lagrangian fronts with favourable fishery conditions // Deep Sea Research Part i: Oceanographic Research Papers. 2014. № 90. P. 27–35. https://doi.org/10.1016/j.dsr.2014.04.012.
118. Reason C. J. C., Lutjeharms J. R. E., Hermes J., Biastoch A., Roman R. E. Inter-ocean fluxes south of Africa in an eddy permitting model // Deep Sea Research Part II. 2003. № 50. P. 281–298. https://doi.org/10.1016/S0967-0645(02)00385-5.
119. Reznik G. M., Dewar W. K. An analytical theory of distributed axisymmetric barotropic vortices on the β-plane // Journal of Fluid Mechanics. 1994. № 69. P. 301–321. https://doi.org/10.1017/S0022112094001576.
120. Reznik G. M. Dynamics of localized vortices on the beta plane // Izvestiya, Atmospheric and Oceanic Physics. 2010. № 46 (6). P. 846-860. [In Russian].
121. Reznik G.M. Dynamics of singular vortices on a beta-plane // Journal of Fluid Mechanics. 1992. № 240. P. 405-432. https://doi.org/10.1017/S0022112092000144.
122. Reznik G.M., Dewar W.K. An analytical theory of distributed axisymmetric barotropic vortices on the β –plane // Journal of Fluid Mechanics. 1994a. № 269. P. 301-321. https://doi.org/10.1017/S0022112094001576.

123. Reznik G.M., Kizner Z. SINGULAR VORTICES IN REGULAR FLOWS // Theoretical and Computational Fluid Dynamics. 2010. № 24 (1-4). P. 65–75. https://doi.org/10.1007/s00162-009-0150-5.
124. Reznik G.M., Tsybaneva T.B. The effect of topography and stratification on planetary waves in the ocean // Okeanologiya. 1994b. № 34 (1) P. 1–9.
125. Richardson P.L. Agulhas leakage into the Atlantic estimated with subsurface floats and surface drifters // Deep-Sea Res. Part I. 2007. № 54 (8). P. 1361–1389. https://doi.org/10.1016/j.dsr. 2007.04.010.
126. Ruijter W.P.M., van Leeuwen P. J., Lutjeharms J. R. E. Generation and evolution of Natal Pulses, solitary meanders in the Agulhas Current // Journal of Physical Oceanography. 1999. № 29 (12). P. 3043–3055. https://doi.org/10.1175/1520-0485(1999)029<3043:GAEONP>2.0.CO;2.
127. Sandalyuk N. V., Belonenko T. V. Three-Dimensional Structure of the mesoscale eddies in the Agulhas Current region from hydrological and altimetry data // Russian Journal of Earth Sciences. 2021. № 21. ES4005. https://doi.org/10.2205/2021ES000764.
128. Sandalyuk N.V., Belonenko T.V. Mesoscale eddy dynamics in the Agulhas Current region according to satellite altimetry data // Current problems in remote sensing of the Earth from space. 2018. № 15 (5). P. 179–190. https://doi.org/10.21046/2070-7401-2018-15-5-179-190. [In Russian].
129. Schmid C., Boebel O., Zenk W., Lutjeharms J. R. E., Garzoli S. L., Richardson P. L., Barron C. Early evolution of an Agulhas Ring // Deep Sea Research Part II: Topical Studies in Oceanography. 2003. № 50 (1). P. 141–166. https://doi.org/10.1016/S0967- 0645(02)00382-X.
130. Schmitz W. J. On the interbasin-scale thermohaline circulation // Reviews of Geophysics. 1995. № 33 (2). P. 151–173. https://doi.org/ 10.1029/95RG00879.
131. Schouten M.W., De Ruijter W.P.M., Van Leeuwen P.J., Lutjeharms J.R.E. Translation, decay and splitting of Agulhas rings in the southeastern Atlantic Ocean // J. Geophysical Research. 2000. № 105 (C9). P. 21913–21925. https://doi.org/10.1029/1999JC000046.
132. Shakina N.P. Hydrodynamic instability in the atmosphere. L: Gidrometeoizdat, 1990. 312 p. [In Russian].

133. Shrira V.I., Townsend W.A. Inertia-gravity waves beyond the inertial latitude. Part 1. Inviscid singular focusing // J. Fluid Mech. 2010. № 664. P. 478–509. https://doi.org/10.1017/S0022112010003812.
134. Stewart R.H. Introduction To Physical Oceanography. Department of Oceanography, Texas A & M University, 2006. 352 p.
135. Stocker T. F. Climate changes: from the past to the future — a review // Int. J. Earth Sci. 1999. № 88. P. 365–374. https://doi.org/10.1007/s005310050271.
136. Stommel H. The Gulf Stream. A physical and Dynamical Description. Univ. of California, 1965. 248 p.
137. Stramma L. and Lutjeharms J.R.E. The flow field of the subtropical gyre in the South Indian Ocean into the Southeast Atlantic Ocean: a case study // Journal of Geophysical Research. 1997. № 102 (C3). P.5513-5530. https://doi.org/10.1029/96JC03455
138. Travkin V.S., Zhmur V.V., Belonenko T.V. Contribution of mesoscale eddies of the Lofoten Basin to its energetics // Russian Journal of Earth Sciences. 2022. № 22. ES4002. https://doi.org/10.2205/2022ES000802. [In Russian].
139. Treguier A.M., Boebel O., Barnier C., Madec G. Agulhas eddy fluxes in a 1/6° Atlantic model // Deep Sea Research Part II: Topical Studies in Oceanography. 2003. № 50 (1). P. 251-280. https://doi.org/10.1016/S0967-0645(02)00396-X
140. van Sebille E., van Leeuwen P. J., Biastoch A., Barron C. N., de Ruijter W. P. M. Lagrangian validation of numerical drifter trajectories using drifting buoys: Application to the Agulhas system // Ocean Modelling. 2009. № 29. P. 269–276. https://doi.org/ 10.1016/j.ocemod.2009.05.005.
141. van Sebille E., van Leeuwen P.J. Fast Northward Energy Transfer in the Atlantic due to Agulhas Rings // J. Physical Oceanography. 2007. № 37. P. 2305–2315. https://doi.org/10.1175/JPO3108.1.
142. Walker N.D., Mey R.D. Ocean/atmosphere heat fluxes within the Agulhas Retroflection region // J. Geophysical Research: Oceans. 1988. № 93. P. 15473–15483. https://doi.org/10.1029/JC093iC12p15473
143. Wang Y., Olascoaga M. J., Beron-Vera F. J. Coherent water transport across the South Atlantic // Geophysical Res. Lett. 2015. № 42 (10). P. 4072–4079. https://doi.org/10.1002/2015GL064089

144. Weijer W., Sebille E. Impact of Agulhas Leakage on the Atlantic Overturning Circulation in the CCSM4 // J. Climate. 2014. № 27. P. 101–110. https://doi.org/10.1175/JCLI-D-12-00714.1.

145. Williams S., Petersen M., Bremer P.-T., Hecht M., Pascucci V., Ahrens J., Hlawitschka M., Hamann B. Adaptive extraction and quantification of geophysical vortices // IEEE Transactions On Visualization and Computer Graphics. 2011. № 17 (12). P. 2088–2095. https://doi.org/10.1109/TVCG.2011.162.

146. Yari S., Kovačević V., Cardin V., Gačić M., Bryden H. L. Direct estimate of water, heat, and salt transport through the Strait of Otranto // J. geophysical research. 2012. № 117. C09009. https://doi.org/10.1029/2012JC007936.

147. ys B., Stegner A., Arsouze T. Angular Momentum Eddy Detection and Tracking Algorithm (AMEDA) and Its Application to Coastal Eddy Formation // J. Atmos. Oceanic Technol. 2018. № 35 (4). P. 739–762. https://doi.org/10.1175/JTECH-D-17-0010.1

148. Zhmur V.V. Mesoscale vortices of the ocean. Moscow: GEOS, 2011. 384 p. [In Russian].

149. Zhmur V.V., Arutyunyan D.A. Redistribution of energy during horizontal pulling of ocean vortices by barotropic currents // Oceanology. 2023. № 63 (1). P. 3–19. https://doi.org/10.31857/S0030157423010185. [In Russian].

150. Zhmur V.V., Belonenko T.V., Novoselova E.V., Suetin B.P. Conditions for the transformation of a mesoscale vortex into a submesoscale vortex thread when the vortex elongates by an inhomogeneous barotropic flow // Oceanology. 2023a. № 63 (2). P. 200—210. https://doi.org/10.31857/S0030157423020144. [In Russian].

151. Zhmur V.V., Belonenko T.V., Novoselova E.V., Suetin B.P. Direct and Inverse Energy Cascades in the Ocean during Vortex Elongation // Doklady Earth Sciences. 2023c. № 508 (2). C. 270–274. https://doi.org/10.1134/S1028334X22601675. [In Russian].

152. Zhmur V.V., Belonenko T.V., Novoselova E.V., Suetin B.P. On the stretching of mesoscale vortices into filaments and their distribution on the ocean surface // Radiophysics and Quantum Electronics. 2023b. № 66 (2—3). [In Russian].

153. Zhmur V.V., Novoselova E.V., Belonenko T.V. Potential vorticity in the ocean: Ertel and Rossby approaches with estimates for the Lofoten vortex // Izvestiya, Atmospheric and Oceanic Physics. 2021b. № 57 (6). P. 632–641. https://doi.org/10.1134/S0001433821050157. [In Russian].

154. Zhmur V.V., Pankratov K.K. Dynamics of an ellipsoidal near-surface vortex in an inhomogeneous flow // Oceanology. 1989. № 29 (2). P. 205–211 [In Russian].
155. Zhmur V.V., Travkin V.S., Belonenko T.V., Arutyunyan D.A. Transformation of Kinetic and Potential Energy during Elongation of a Mesoscale Vortex // Physical Oceanography. 2022. № 38 (5). P. 466–480. https://doi.org/10.22449/0233- 7584-2022-5-466-480. [In Russian].